University of Alberta

Layer-by-Layer Assembly of Multilayers on Carbon Surfaces and Molecular Electronic Junctions

by

Xiao Xing

A thesis submitted to the Faculty of Graduate Studies and Research
in partial fulfillment of the requirements for the degree of

Master of Science

Department of Chemistry

Spring 2010
Edmonton, Alberta

Examining Committee

Prof. Richard L. McCreery, Chemistry

Prof. Jillian M. Buriak, Chemistry

Prof. Karthik Shankar, Electrical and Computer Engineering

Dedicated to those I most beloved

Father: Xing, Lanping

Mother: Lu, Yanhua

Fiance: Liu, Yang

Abstract

In the research described in this thesis, two molecular layers were successfully anchored on carbon surfaces (pyrolyzed photoresist films, PPFs) sequentially through two independent approaches. The first molecular layer, styrene, was covalently bonded on PPF surfaces via the method of reduction of *in situ* generated diazonium ions. The resulting molecular films were characterized by AFM measurements, and catechol and ferrocyanide voltammetry. The second molecular layer, ferrocene-thiol, was anchored on top of the first molecular layer through the method of thiol-ene reaction, which is an effective method for building up multilayers through layer-by-layer assembly. As ferrocene is an electrochemically active species, quantitative surface coverage was calculated according to the amount of surface-bound ferrocene through electrochemical measurements. Finally, molecular junctions were fabricated by depositing metal top contacts based on the molecular layers through electron-beam evaporation and the electronic characteristics of these molecular junctions were investigated.

Acknowledgements

First and foremost, I would like to express my deep and sincere gratitude to my supervisors, Dr. Richard L. McCreery and Dr. Jillian M. Buriak, for their guidance and encouragement during my Masters studies. I still clearly remember the first scientific talk with them in Dr. McCreery's chemistry office. Their patience, wide knowledge, logic way of thinking, and detailed and constructive comments, have made my research work smooth and rewarding.

I would like to show my warm thanks to the present and former group members in both the McCreery group and the Buriak group. So lucky am I that I could share friendship and communications with people from both of the groups. It is really a memorable experience for working with them. In particular, I want to thank Dr. Haijun Yan and Dr. Yunhui Li, for their mentoring on operation of research procedures and instruments at the beginning stage of my research and for their scientific discussion and involvement. I thank Jie Ru for training me on "e-beam deposition" and for her valuable friendship. I would also like to thank Andrew Bonifas and Dr. Adam Johan Bergren for always willing to answer my scientific questions.

I am greatly indebted to my parents for their encouragement, understanding and endless love throughout my life. Thank them for providing me an unrestricted growth environment and supporting me for whatever I want to achieve. I owe my

loving thanks to my fiance for his absolute support and understanding; it would have been impossible for me to finish this thesis without him.

Table of Contents

List of Tables

List of Figures

Chapter 1. Introduction

Molecular electronics is a research topic referring to an electron transfer system, which involves organic molecules as active electronic components in electric contact with two or more conductors. A wide variety of molecular structures, such as Au/thiol self-assembled monolayer,[1] Langmuir-Blodgett structures,[2] Si-C and Si-O-C bonds,[3] and C-C bonds,[4] have been employed in molecular electronic junctions. Electron transport in molecular junctions has been demonstrated to highly depend on the length, conformation and structure of the "bridging" molecule between two conductors. However, in most cases, only one kind of molecule is involved in the molecular junctions, which limits the range of available junction structures. Recently, Frisbie et al.[5] incorporated more than one kind of molecule in a single molecular junction, which resulted in some intriguing electronic effects. However, in that report, the bonding between the bottom contact, Au, and the molecular layer was a Au-S bond, which is relatively weak and thermally unstable. The Au-S bond needs to undergo repeated breaking and re-forming processes in order to achieve high packing density. The primary motivation for the current work is to establish a molecular junction, which involves an irreversible and strong surface bond between the molecular layer and the substrate, and meanwhile, incorporates more than one kind of molecule

through construction of covalent bonded multilayers. The general approach involves layer-by-layer assembly of a covalent multilayer on a flat carbon surface, followed by metal deposition to form a complete molecular junction.

In the first part of this chapter, pyrolyzed photoresist film (PPF), which is one type of carbon surfaces and is used as the substrate in this research, is introduced. The second part describes a diversity of approaches for surface modification of carbon surfaces. The third part presents the thiol-ene reaction, which is utilized for layer-by-layer assembly of multilayers on solid substrates. The fourth section of this chapter provides a brief review of molecular electronic junctions and in the last part, the research objective of this work is outlined.

1.1 Introduction to Pyrolyzed Photoresist Film (PPF)

Pyrolyzed photoresist film (PPF) is basically a conducting carbon surface, which is comprised of sp^2 hybridized graphitic carbon. It is made from pyrolyzing a commercially available photoresist, which is uniformly spin-coated onto a cleaned Si wafer, at the temperature of 1000℃ in a reducing atmosphere (forming gas, composed of 5% hydrogen and 95% nitrogen). With its smooth and robust properties, as well as its advantages of low cost, versatility, easy handling and disposability, PPF has numerous potential applications in electrochemical sensors, energy conversion and microelectromechanical systems.[6-8] The

root-mean-square (rms) roughness of PPF surface determined by AFM (atomic force microscopy) measurements is typically less than 0.5nm, which is nearly atomically smooth. An AFM image of PPF surface is shown in Figure 1.1. The features of exceptional smoothness and low background current of PPF surface result in excellent electrochemical properties and suitability for high resolution patterning and thin molecular layer imaging.[9]

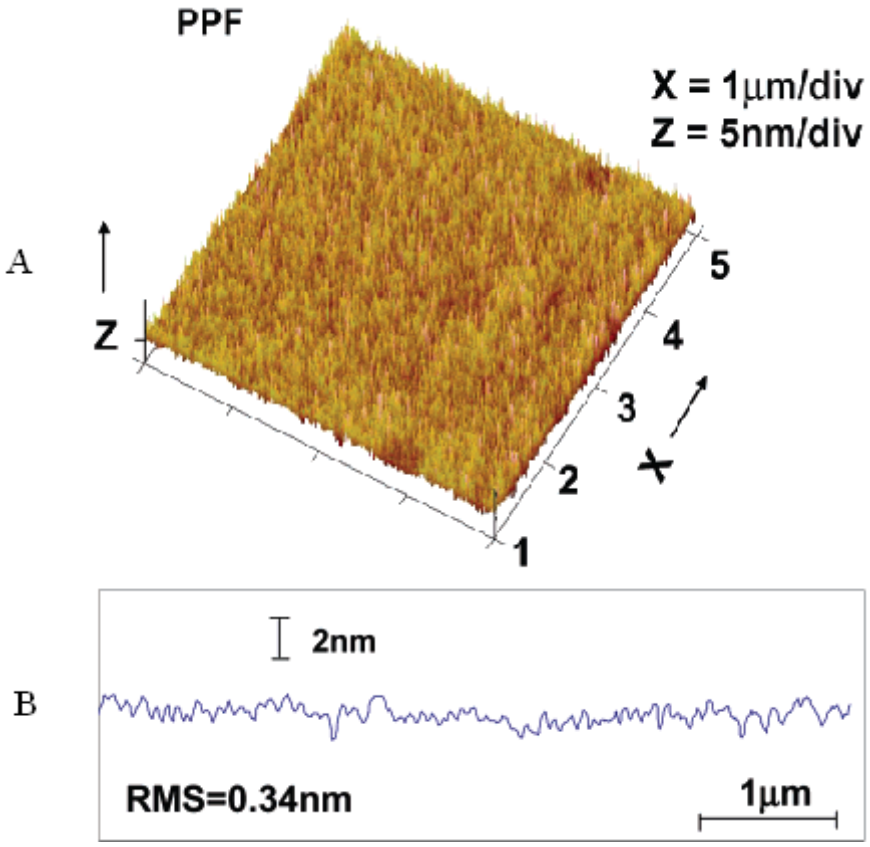

Figure 1.1 (A) Tapping mode AFM image of 5 μm × 5 μm area of a PPF sample; (B) Line profile showing the variation in z-axis height illustrates an rms roughness of 0.34nm (Figure adapted from ref.[10]).

1.2 Modification Methods on Carbon Surfaces

A variety of modification methods applied on carbon surfaces have been broadly investigated during the past decades. The versatility of modification methods provides a way of grafting diverse organic molecules on carbon surfaces, controlling interfacial structures, altering surface properties and immobilizing specific functionalities for various applications, such as electrocatalysis and electroanalytical selectivity.[11,12] The first paper concerning electrochemically assisted covalent modification of carbon surfaces was reported by Pinson and coworkers.[13] The paper described oxidation of primary amines to radicals, which could couple with the carbon surface to form covalent bonds. Later, Pinson et al. introduced another important method for molecular modification of carbon surfaces in 1992.[14] Target molecules were attached on the carbon surface through a strong covalent bond between the carbon surface and an aryl radical generated from reduction of the corresponding aryl diazonium cation. In addition to the above two methods, there are other instrumental approaches available for modification of carbon surfaces, including electrochemical oxidation of carboxylates, thermal reactions and photochemical reactions. All of the methods and procedures which result in stable surface coatings and high surface coverage will be discussed in detail in the following sections.

1.2.1 Electrochemical Reduction of Aryl Diazonium Salts

Modification of carbon surfaces through electrochemical reduction of phenyl diazonium salts has been extensively and thoroughly investigated since this technique was first introduced by Pinson and coworkers.[14] Generally, diazonium salts are synthesized from the corresponding aromatic amines; and the resultant diazonium cations are stored at low temperature after isolation and purification. A fresh solution of the diazonium salt is prepared in an electrolyte solution immediately before carbon surface modification.

However, not all the desired diazonium salts can be synthesized readily, and some of the diazonium salts cannot be easily isolated from impurities. Consequently, another approach, known as reduction of *in situ* generated aryl diazonium cations, was proposed recently.[15-17] In this procedure, modification was carried out directly in the reaction solution without separation and purification of the synthesized phenyl diazonium salts. Examples include reduction of *in situ* generated nitrophenyl diazonium salts,[18,19] bromophenyl diazonium salts[20] and anthraquinone diazonium salts[21] either in acetonitrile or in aqueous acid solution.

1.2.1.1 Reduction of Isolated Aryl Diazonium Salts

The methods and procedures for synthesis of phenyl diazonium salts are well established and standardized. Typically, a primary aromatic amine is selected as

the precursor. After reacting with nitrous acid, generated from the reaction of tetrafluoroboric acid with sodium nitrite; the aromatic amine is transformed to its corresponding aromatic diazonium salt. The entire process of synthesis should be maintained at low temperature (below 4℃) to prevent decomposition of the generated diazonium salt. After recrystallization and separation steps, very pure diazonium tetrafluoroborate salts could be obtained and they are usually stored at low temperature for further use. Diazonium compounds are routinely isolated as tetrafluoroborate salts, in the form of which diazonium reagents are stable for a long period of time.[14,22]

The process of preparation of diazonium salts and electrochemical reduction of phenyl diazonium ions is depicted in Figure 1.2. By transferring one electron from the carbon electrode and cleavage of N_2, the diazonium cation is reduced to a phenyl radical; then the generated phenyl radical bonds to the carbon surface, forming a strong covalent bond. The modification is implemented either in an organic solvent with a supporting electrolyte (such as acetonitrile, ACN with 0.1M tetrabutylammonium tetrafluoroborate, $TBABF_4$) or in an acidic aqueous medium with a low pH value (for example, 0.1M H_2SO_4).

Figure 1.3 shows the cyclic voltammogram of electrochemical reduction of 4-nitrophenyl diazonium ion in ACN + 0.1M $TBABF_4$ solution on a freshly polished glassy carbon electrode. A broad, chemically irreversible cathodic peak

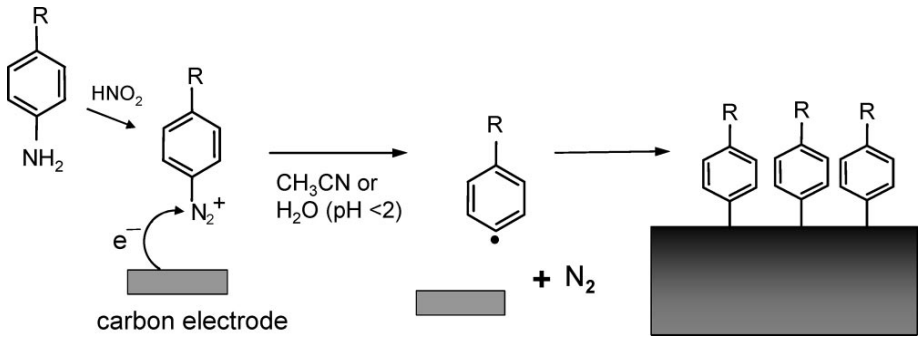

Figure 1.2 Synthesis of phenyl diazonium ions from aromatic amines and modification of carbon electrodes through electrochemical reduction of aryl diazonium salts (Figure adapted from ref.[12]).

is observed for the first scan, which is attributed to the formation of phenyl radicals generated from the reduction of diazonium ions. The voltammetric reduction peaks decrease rapidly during subsequent scans, indicating that the carbon surface is passivated by an organic layer and therefore less able to reduce additional diazonium ions. Diazonium cations are reduced readily due to the strong electron-withdrawing effect of the diazonium group.[23]

The reactions of electrogenerated phenyl radicals are quite aggressive, which consequently lead to the formation of multilayers on carbon surfaces.[22] A proposed mechanism is shown schematically in Figure 1.4. For the first step, a molecular layer is formed on the carbon surface through the reaction of phenyl radicals with the carbon electrode. Additional generated phenyl radicals in solution may then attack the first grafted molecules instead of the carbon surface;

in such a way, two molecular layers are bonded on the surface. With the repetition of this reaction, multilayers are eventually immobilized on the carbon electrode. Based on a wide variety of experiments, several factors are found to be responsible for the formation and thickness of grafted multilayers. The factors include the property of the surface, the specific diazonium salt involved and its corresponding concentration, potential range, scan rate and number of voltammetric scans.[24-26]

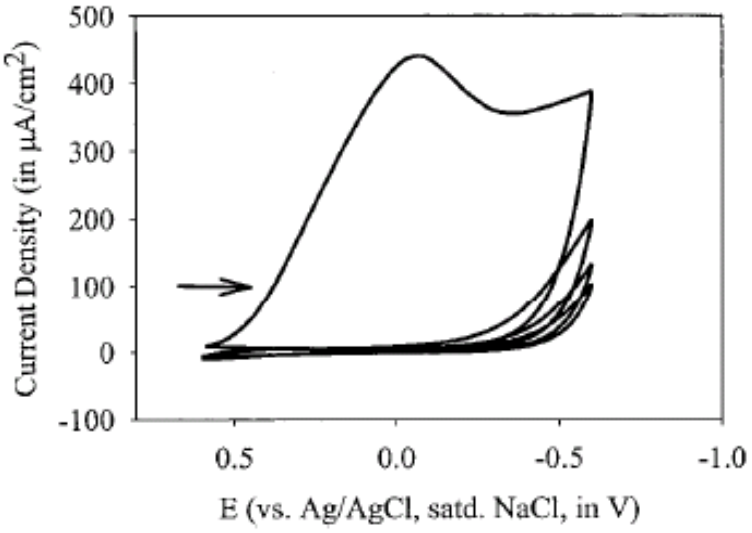

Figure 1.3 Cyclic voltammogram of reduction of 10mM $NO_2C_6H_4N_2^+ BF_4^-$ at a freshly polished glassy carbon electrode. Medium, 0.1M $TBABF_4$ in ACN; Scan rate = 200mV/s (Figure adapted from ref.[27]).

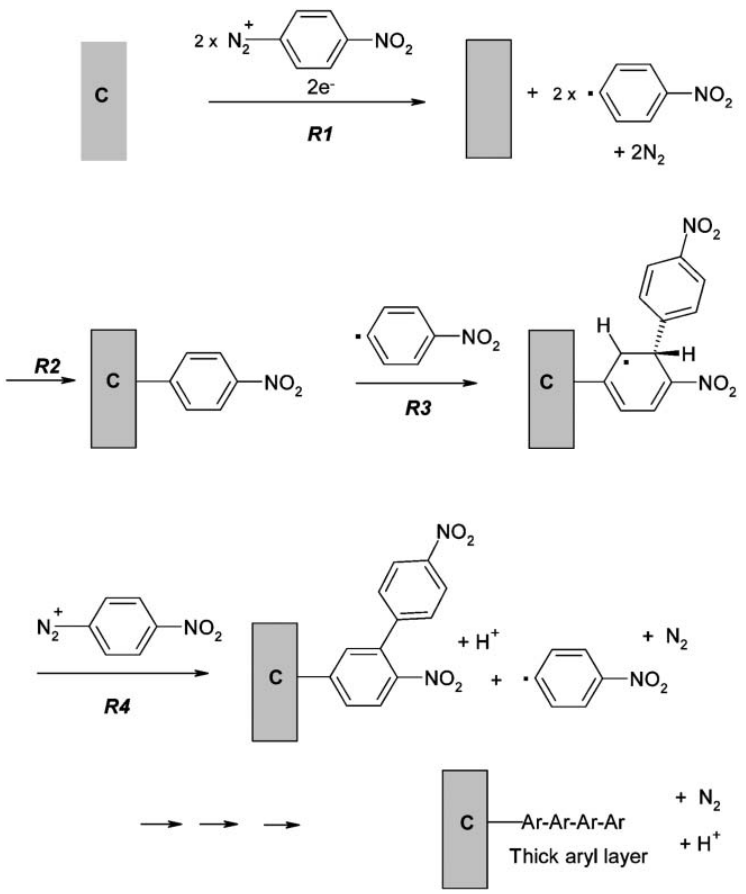

Figure 1.4 Proposed mechanism of the formation of multilayers during electrochemical reduction of diazonium reagents on carbon surfaces (Adapted from ref.[22]).

1.2.1.2 Reduction of *in situ* Generated Aryl Diazonium Salts

Derivatization by electrochemical reduction of dissolved phenyl diazonium salts has been broadly utilized during the past years and a wide range of functional groups have been immobilized on carbon surfaces through this approach. However, a major disadvantage of this modification method is that it is difficult to

isolate certain diazonium salts after synthesis, or they tend to be unstable after being prepared. In order to compensate for this shortcoming, electrochemical reduction of *in situ* generated aryl diazonium salts was investigated.[15-17] For the *in situ* procedure, modification of electrode surfaces is accomplished directly in the reaction solution; in this way, the separation and purification steps are avoided. This *in situ* derivatization method has been successfully applied on a variety of electrode surfaces, including carbon, gold and copper in the medium of either acetonitrile or acidic aqueous solution.[16,20,28,29] This method has also been used to modify single-walled carbon nanotubes spontaneously without applying an external potential.[30]

There are two ways to generate diazonium salts using this *in situ* procedure. The surface modification is carried out either in acetonitrile containing the target aromatic amine, 0.1M $TBABF_4$ and *tert*-butylnitrite or in an acidic aqueous medium with the target phenyl amine and sodium nitrite, $NaNO_2$. These two diazotization procedures are depicted in Figure 1.5, using the synthesis of anthraquinone diazonium salts as the example. The electrochemical reduction of *in situ* generated diazonium salts results in the same electrografting behavior as that of isolated diazonium cations in 0.1M $TBABF_4$ + ACN solution. As shown in Figure 1.6, the first potential scan for the reduction of *in situ* generated aminoanthraquinone diazonium cations exhibits a broad electrochemically

irreversible wave and the consecutive scans rapidly decrease to near-background levels for modifications carried out in both acetonitrile and acidic aqueous solutions.

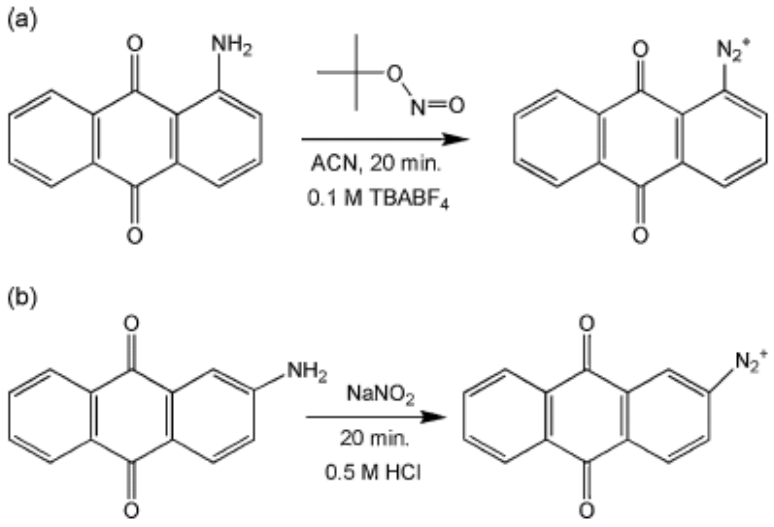

Figure 1.5 Diazotization procedures of aminoanthraquinones (a) with *tert*-butylnitrite and 0.1M $TBABF_4$ in ACN and (b) with $NaNO_2$ in 0.5M HCl (Figure taken from ref.[21]).

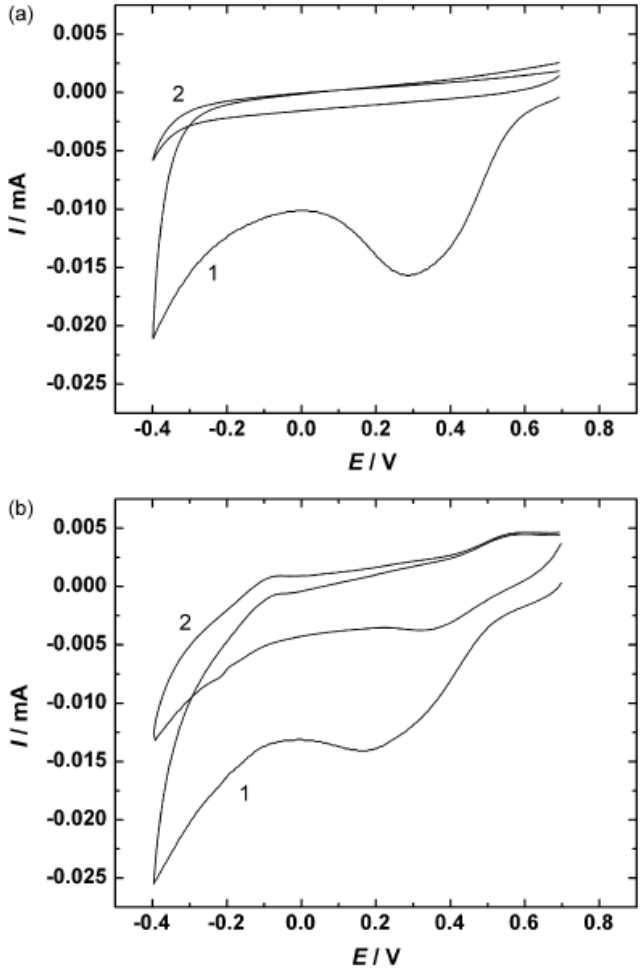

Figure 1.6 Electrochemical grafting of anthraquinone groups to glassy carbon using *in situ* generated diazonium derivatives. Electrode modified in: (a) ACN containing 1mM of 2-aminoanthraquinone and 3mM tert-butylnitrite and (b) 0.5M HCl containing 2mM of 2-aminoanthraquinone and 4mM $NaNO_2$. Trace (1) corresponds to the first and trace (2) to the fifth scan (Figure taken from ref.[21]).

1.2.2 Electrochemical Oxidation of Amines

The early reports with regard to electrochemical oxidation of amines on carbon surfaces, including modification of carbon fibers[13] and glassy carbon electrodes,[31] appeared in the early 1990s. The modification process is based on one-electron oxidation of an aliphatic amine to its corresponding amine cation radical, which then couples to an unsatisfied valence or double bond on the carbon surface to form a strong carbon-nitrogen covalent bond. This electrochemically assisted method is illustrated in Scheme 1.1. In some cases, primary amines could be grafted to carbon surfaces through spontaneous adsorption.[32]

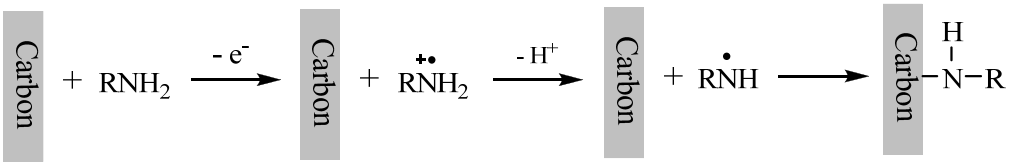

Scheme 1.1 The route for electrogeneration of amine cation radicals through one-electron oxidation of amine functionalities and coupling of the generated radicals to the carbon surface.

The electrografting of aliphatic amines to carbon electrodes could be achieved by cyclic voltammetric scans or controlled potential electrolysis in both anhydrous and acetonitrile solutions. An example of electrochemical grafting of ethylenediamine (ED) on a glassy carbon (GC) electrode through voltammetric scans is shown in Figure 1.7(a). The irreversible oxidation peak in the first

voltammetric scan indicates the transformation of amine to its corresponding cation radical and the diminishing peak currents with successive scans gives a hint of the formation of an organic layer on the GC surface, which prevents further oxidation reactions on the surface.

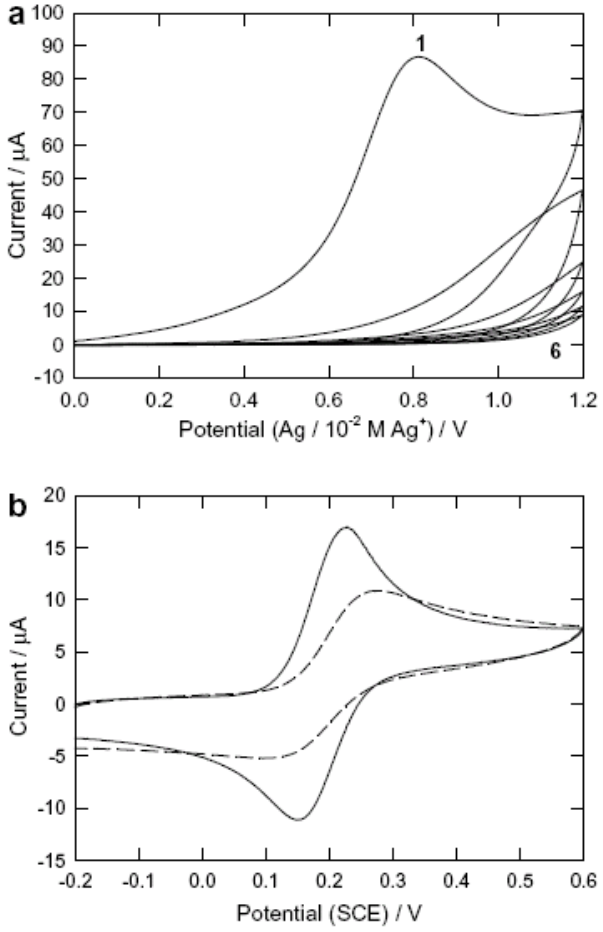

Figure 1.7 Cyclic voltammograms at GC of: (a) 5 mM ethylenediamine (ED) in $TBABF_4$–ACN solution, showing first 6 scans, and (b) FcOH (1 mM in phosphate buffer) before (—) and after (---) grafting ED (Figure taken from ref.[33]).

The presence of a molecular layer on the GC surface can also be proved by comparing the voltammetry of a probe redox species on unmodified and modified GC electrodes. As denoted in Figure 1.7(b), the voltammogram of FcOH (hydroxymethyl ferrocene, 1mM in phosphate buffer) is electrochemically reversible on the unmodified GC electrode; but for the modified electrode, the peak potentials for the anodic and cathodic waves separate, indicating the formation of a blocking film on the GC surface.

The modification of primary, secondary and tertiary amines on carbon surfaces has all been investigated previously.[31,33,34] It was discovered that surface binding was the most effective for primary amines; lower surface coverage was obtained for secondary amines; and there was almost no grafting for tertiary amines. The phenomena above could be attributed to the following two aspects: (a) steric effects prevent secondary and tertiary amines from approaching the surface; and (b) the process of surface modification by amine functionalities requires loss of a proton from the amine radical cation, which is not available for tertiary amines.

1.2.3 Electrochemical Oxidation of Carboxylates

By means of electrochemical oxidation of carboxylates, molecular species can be attached to carbon electrodes via covalent C–C bonding. The oxidation of

carboxylates results in formation of carbon radicals, together with elimination of CO_2; and then the generated carbon radicals react with the carbon surface to form strong covalent bonds (Scheme 1.2).

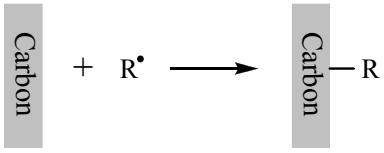

(Scheme 1.2)

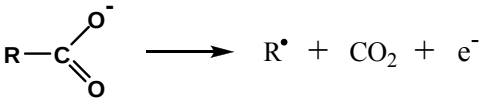

(Scheme 1.3)

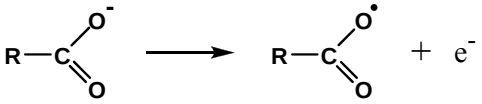

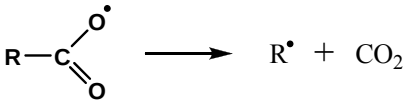

(Scheme 1.4)

During the process, a carboxylate ion transfers an electron to the carbon electrode, causing cleavage of the R–C bond, generating carbon radicals and carbon dioxide. The mechanism of how carbon radicals are produced has been long debated since the early 1960s.[35-37] The main focus is on whether electron transfer and bond breaking are taking place simultaneously (Scheme 1.3) or these two processes undergo successive pathways accompanied by generation of acyloxy radicals as the intermediate products (Scheme 1.4). There is as yet no

definite conclusion for the mechanism of carbon radical formation. In some cases, the formation of carbon radicals undergoes the concerted mechanism; under other circumstances, the process performs the stepwise mechanism.

The cyclic voltammetry of electrochemical oxidation of carboxylates ions shows that the oxidation peak keeps decreasing with the number of cycles until it completely disappears, which is indicative of the formation of a passivating film

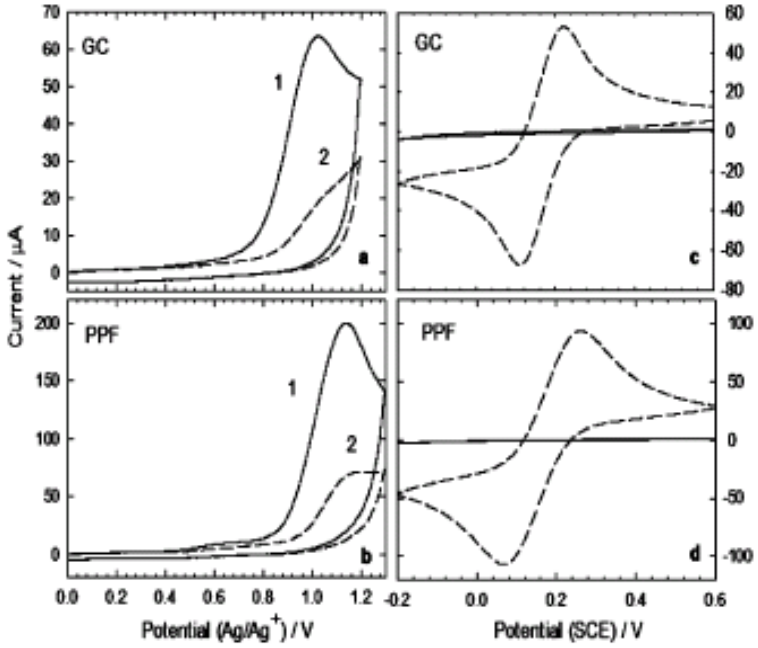

Figure 1.8 Comparison of cyclic voltammetry at GC (a and c) and PPF (b and d) surfaces. (a and b) First scan (—) and second scan (---) (200 mV s^{-1}) with stirring between scans, of 5.2mM NM-COO^- (NM: naphthyl-methyl) in 0.1M $TBABF_4$-acetonitrile solution. (c and d) Scans of 3.1mM $Fe(CN)_6^{3-}$ in aqueous 0.2M KCl at bare (---) and NM-modified (—) surfaces (Figure adapted from ref.[38])

on the carbon surface (Figure 1.8a and Figure 1.8b). Furthermore, the derivatized carbon electrode can effectively inhibit electron transfer to a $Fe(CN)_6^{3-/4-}$ redox system, which confirms the formation of a compact molecular layer (Figure 1.8c and 1.8d).

1.2.4 Thermal and Photochemical Reactions

Surface modification of alkene and alkyne derivatives on silicon surfaces has been extensively investigated and well established.[39-41] The process of coupling of unsaturated compounds (such as alkenes and alkynes) with hydrogen-terminated silicon surfaces is defined as hydrosilylation.[41] The hydrosilylation process can be accomplished through several approaches, such as UV irradiation, thermal reaction, radical initiated reactions and electrochemical grafting.[3,41,42] Among these derivatization methods, thermal reaction and UV irradiation were found applicable to graphitic carbon and diamond surfaces,[10,43] thus providing alternative methods for modification of carbon surfaces.

1.2.4.1 Thermal Reactions

Different kinds of alkenes, alkynes and their derivatives have been successfully bonded to PPF surfaces through heat treatment in an inert atmosphere[10]. The thermal reaction takes place between a hot PPF surface

(175–400℃) and a target reagent under a continued Ar purge. The resultant modification layers are quite stable and can survive sonication in tetrahydrofuran, repeated voltammetric cycling in propylene carbonate electrolyte, and treatment in mild aqueous acid and base.

Line profiles of tapping mode atomic force microscopy (AFM) images are shown in Figure 1.9A, with root-mean-square (rms) roughness of 0.34 nm for unmodified PPF and 0.60 nm for porphyrin-modified PPF surface, indicating a

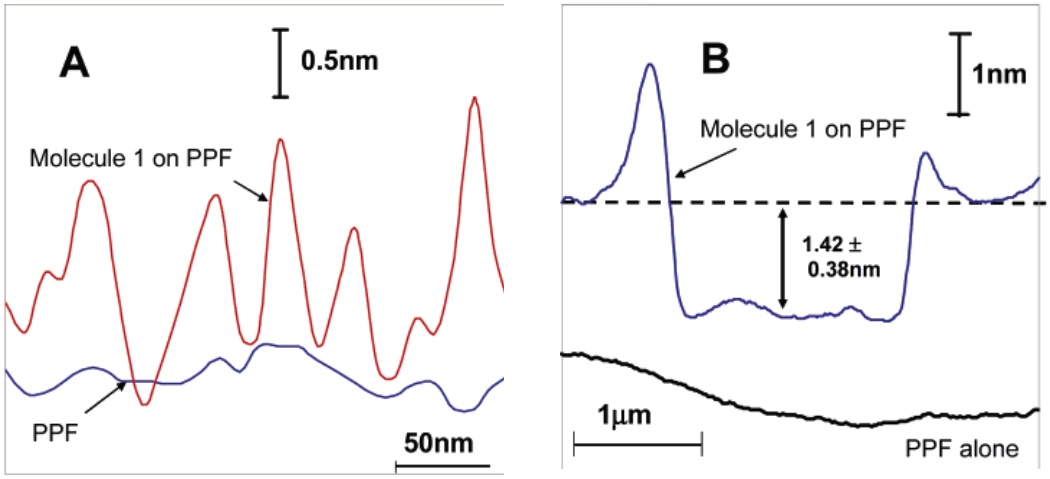

Figure 1.9 Experimentally determined noncontact AFM line profiles. (A) Comparison between the line profiles of PPF and PPF modified with molecule 1 (porphyrin) on a 250-nm scale. (B) Line profile through a scratch made in contact mode on PPF modified with porphyrin. The lower trace shows a profile of a scratch made on unmodified PPF, offset vertically for clarity (Figure adapted from ref.[10])

A thickness of 1.42 ± 0.38 nm for the porphyrin-modified film was determined through the line profile obtained from scratching a trench on the modified surface using contact mode (Figure 1.9B). Raman, Fourier-transform infrared (FTIR) and X-ray photoelectron spectroscopy (XPS) for the porphyrin-modified surface all showed characteristic peaks of porphyrin, providing evidence for the presence of porphyrin on the PPF surface. Furthermore, a tilt angle of 37°– 45° between the bonded porphyrin and the surface normal was determined through FTIR. As porphyrin and ferrocene are both electrochemically active species, cyclic voltammetry was carried out to examine their electrochemical behavior on the PPF surfaces. Cyclic voltammograms of the modified PPF surfaces exhibited representative voltammetric waves of porphyrin and ferrocene, as illustrated in Figure 1.10. A possible mechanism of thermal attachment of alkene and alkyne derivatives to PPF surfaces, which is based on Diels–Alder [4 + 2]- and [2 + 2]-cycloaddition reactions, is shown schematically in Figure 1.11.

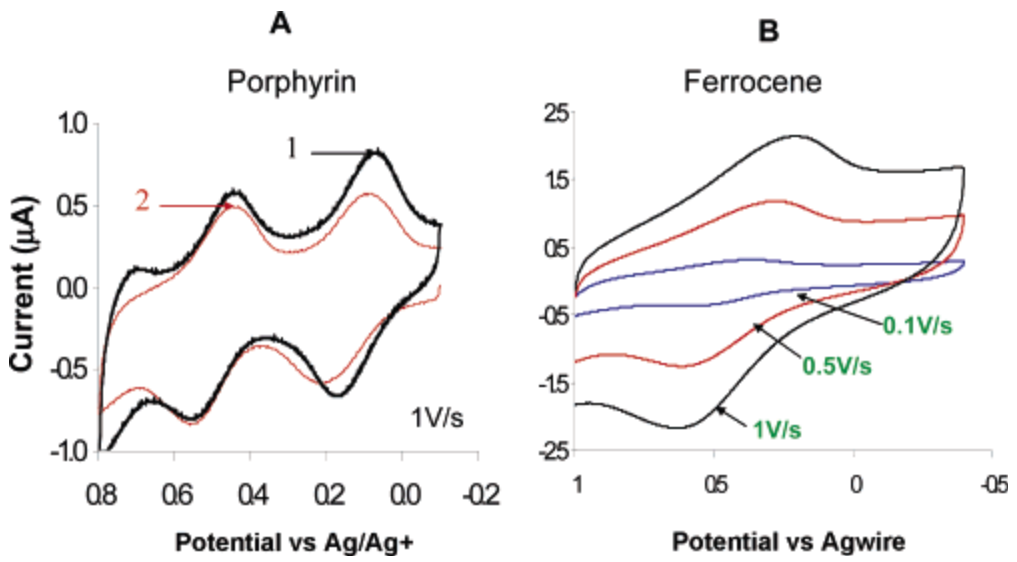

Figure 1.10 Cyclic voltammograms of PPF surfaces modified with: (A) porphyrin-alkyne 1 and porphyrin-alkene 2 (1 V s^{-1}); and (B) ferrocene-alkyne at different scan rates (Figure taken from ref.[10]).

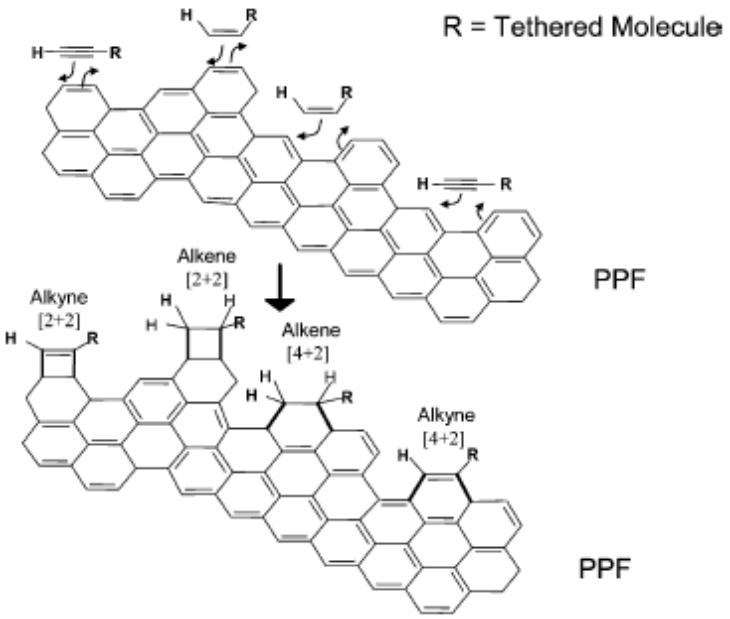

Figure 1.11 A proposed mechanism of alkene and alkyne modifications on PPF surfaces via [4 + 2]- and [2 + 2]-cycloaddition reactions (Figure adapted from ref.[10]).

1.2.4.2 Photochemical Reactions

Photochemical reactions in the presence of alkene and alkyne reagents originally developed for modifying Si surfaces[39,40] have been successfully applied to diamond,[44,45] glassy carbon and PPF surfaces.[46] Molecules with a terminal vinyl (C=C) group can be covalently bonded to H-terminated diamond surfaces through a photochemical process using 254 nm UV light. The photochemical functionalization scheme is depicted in Figure 1.12.

A possible mechanism of photochemical reactions on diamond surfaces was proposed by Nichols and colleagues.[43] Unlike the reaction on silicon surfaces, which is initiated by generation of surface radicals under UV illumination; the photochemical reaction on diamond surfaces is initiated by ejection of an electron from the diamond surface into the liquid phase. The subsequent reactions occurring on the surface undergo three possible pathways: (1) liquid-phase radical

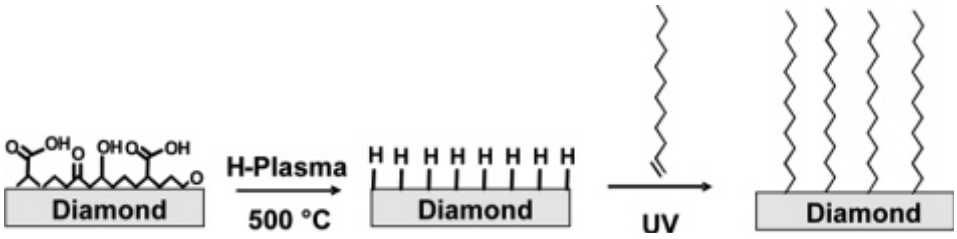

Figure 1.12 Reaction scheme for photochemical modification of H-terminated diamond surfaces with molecules bearing a terminal vinyl group (Adapted from ref.[44]).

surface, (2) the radical anions abstract H atoms from the surface, then creating surface radicals, which could form covalent bonds with C=C moieties of the liquid-phase molecules, and (3) positive holes are created on the surface, which perform as reactive surface sites for reaction with the alkene functionalities.

Diamond surface functionalization has potentially attractive applications in biological and chemical sensing.[42,45,47] After modifying an alkene-terminated molecule containing a reactive functional group on the diamond surface, further modifications such as DNA or protein attachments on top of the functional group could be achieved, an example of which is shown in Figure 1.13.

Photografting of alkenes and alkynes on polished glassy carbon and freshly prepared PPF surfaces has been reported by Downard and coworkers.[46] The photochemical reaction is carried out at the wavelength of 254 nm in air without pretreatment of the substrate. AFM images and line profiles of a PPF surface before and after photografting of 1-decene are illustrated in Figure 1.14, implying that the modified surface is not completely covered by the molecular layer. Other characterizations, including water contact angle measurements, depth profiling measurements through AFM and surface concentration calculation through cyclic voltammograms, support the conclusion that photografted molecular layers are loosely packed on glassy carbon or PPF surfaces.

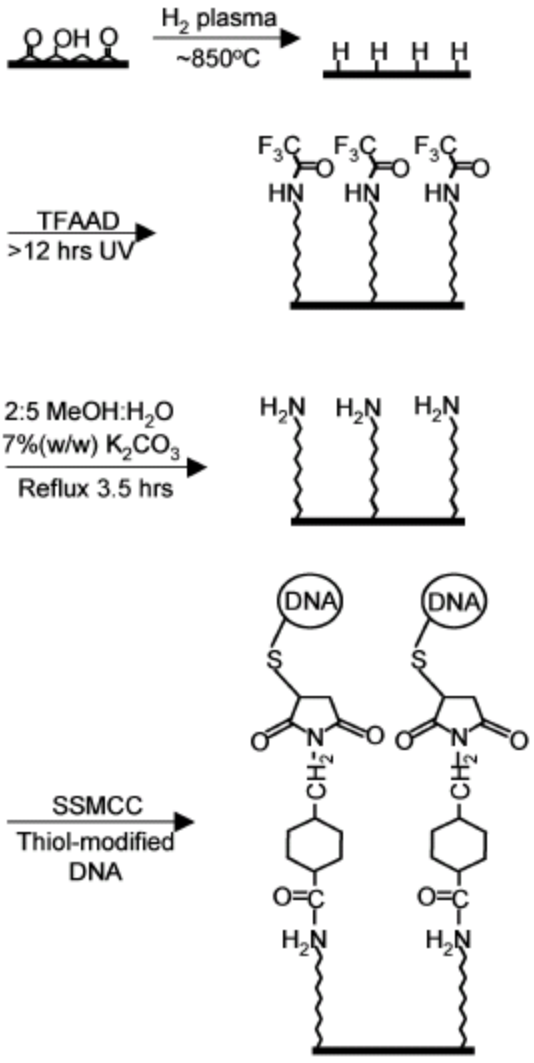

Figure 1.13 Reaction scheme for attachment of DNA to diamond surfaces. TFAAD is trifluoroacetamide-protected 10-aminodec-1-ene; SSMCC is sulfosuccinimidyl-4-(*N*- mal eimidomethyl) cyclohexane-1-carboxylate (Adapted from ref.[47])

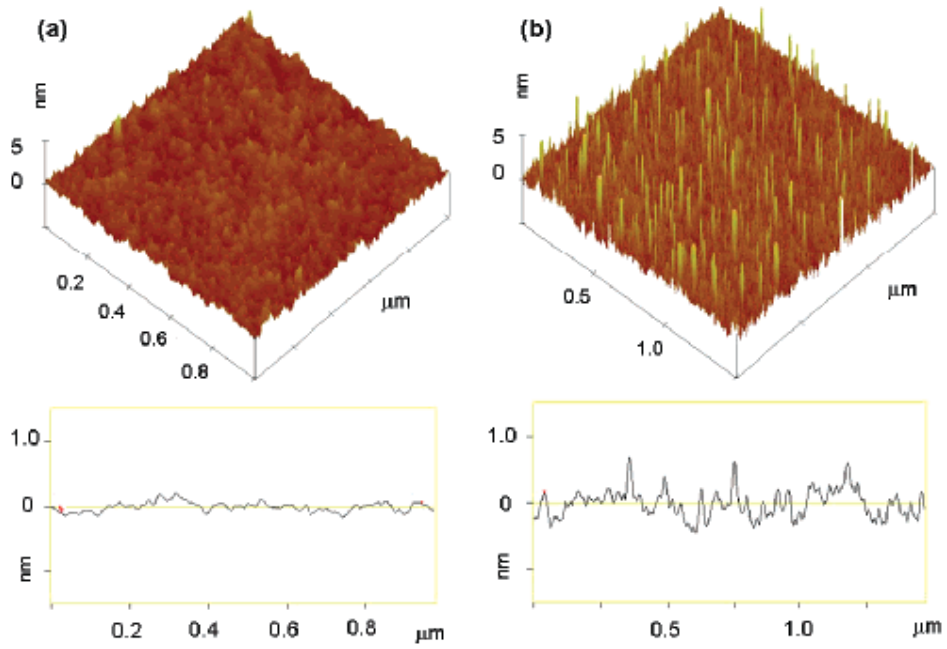

Figure 1.14 AFM images and line profiles of (a) bare PPF before modification and (b) PPF surface after modification with 1-decene (Figure adapted from ref.[46]).

1.3 Layer-by-Layer Assembly and Thiol-Ene Reaction

In the past decades, several techniques, such as Langmuir-Blodgett method,[48] self-assembly approach,[49] atomic layer deposition[50] and molecular layer deposition (MLD)[51] have been exploited for manufacturing polymeric films on solid surfaces. Of these techniques, the MLD method is an effective tool for fabricating polymer thin films with high quality and large-scale uniformity.

This MLD method, which is achieved through stacking molecules one by one in order of preference on substrates, is shown schematically in Figure 1.15. The

MLD growth is based on sequential and self-limiting surface reactions, which consequently produce continuous, conformal and pinhole-free polymer films. Various kinds of organic and hybrid organic-inorganic polymer films, such as 1,4-phenylene diamine/pyromellitic dianhydride,[52] adipoyl chloride/ 1,6-hexanediamine[53] and trimethylaluminum/ethylene glycol,[54] have been manufactured through the MLD approach. In principle, there are two ways to accomplish the molecular layer deposition: vapor-phase deposition polymerization and solution-phase layer-by-layer growth. Herein, the method of solution-phase layer-by-layer growth will be elaborated in the following section.

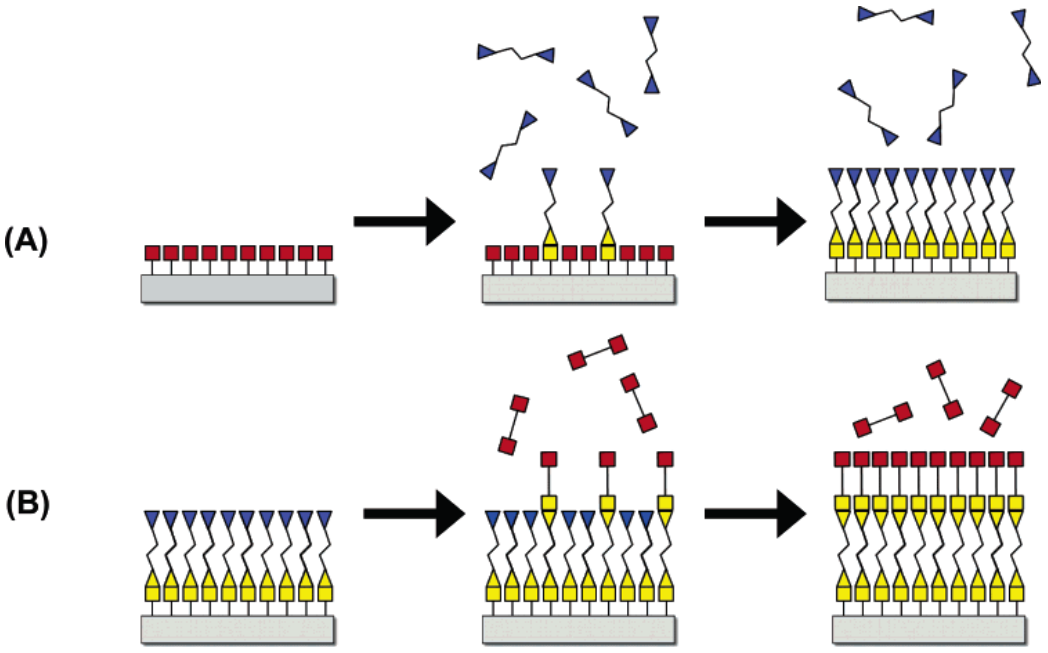

Figure 1.15 Schematic of the molecular layer deposition (MLD) based on sequential and self-limiting surface reactions (Figure adapted from ref.[53]).

1.3.1 Layer-by-Layer Assembly

Layer-by-layer (LBL) assembly is a useful and promising technique for fabrication of functional polymeric films on various substrates. The layer-by-layer growth is implemented through alternating reactions of bifunctional monomers, which result in high quality polymer multilayers.[51,55] To be specific, "A–M–A" and "B–N–B" can be regarded as two bifunctional monomers, in which "A" and "B" stand for chemical functional groups and "M" and "N" represent organic fragments. For the first step, one functional group in the bifunctional molecule "A–M–A" will react with a substrate, leaving another functional group standing opposite the surface. This functional group then undergoes a subsequent chemical reaction with one functional group of another bifunctional molecule "B–N–B", thus forming two molecular layers on the substrate. By repeating this process, the polymeric multilayer structure can be fabricated. An example of the LBL assembly is shown in Figure 1.16.

A wide range of chemical interactions have been developed for construction of LBL multilayers. The pioneering work of the LBL assembly was reported by Iler in 1966,[56] where electrostatic interactions between positively and negatively charged species were employed. Subsequently, additional intermolecular reactions, such as hydrogen bonding,[57,58] covalent bonding[59,60] and coordination chemistry,[61,62] were exploited for fabrication of LBL multilayer films. These

versatile LBL deposition methods provide a way for producing high quality films and tailoring molecular structures with precise control of film thickness, large-scale uniformity and excellent conformality.

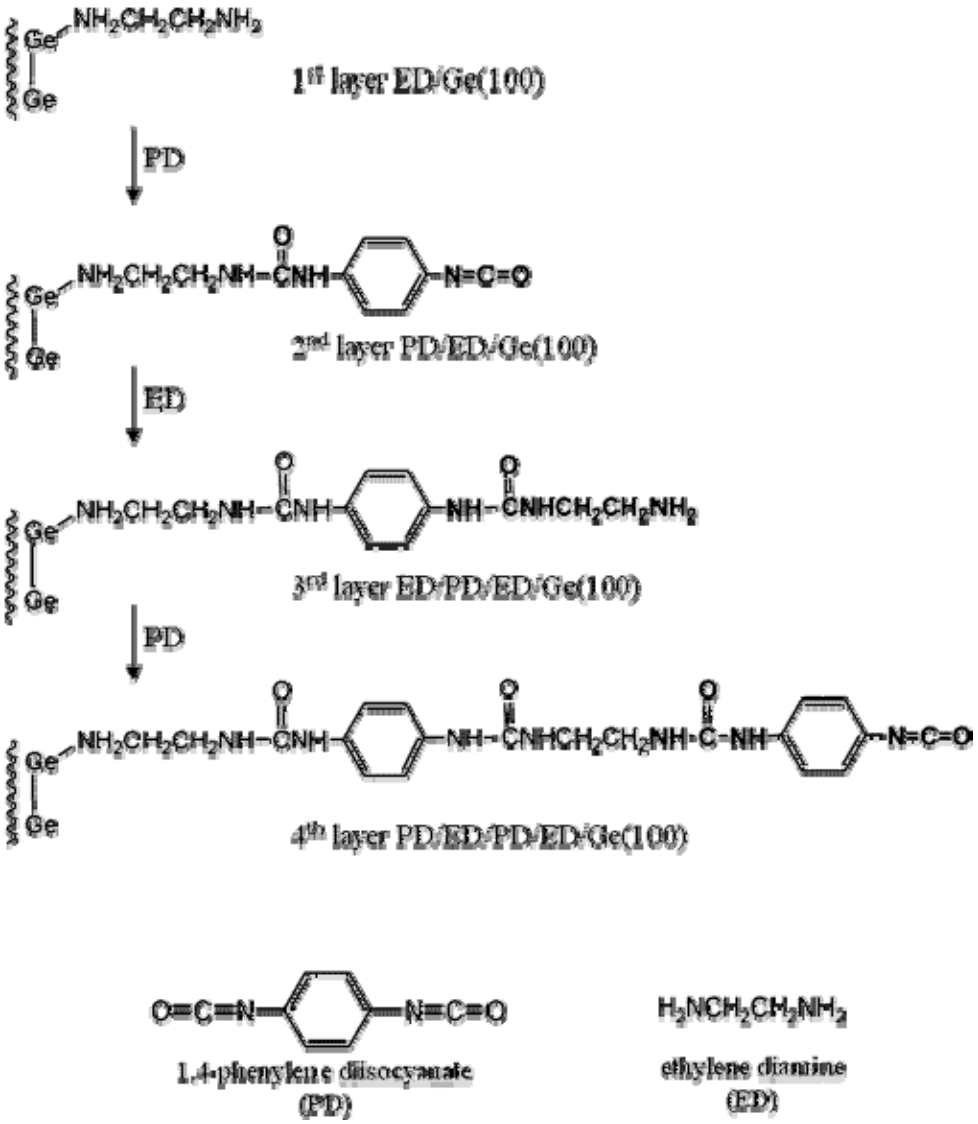

Figure 1.16 Schematic illustration of the reaction route for layer-by-layer growth of polyurea films on Ge(100) surface (Figure adapted from ref.[63]).

1.3.2 Thiol-Ene Reaction

Among versatile methods of manufacturing LBL multilayer films, thiol-ene polymerization is an effective method which can be accomplished in a simple and reliable manner. The study of thiol-ene reaction, including kinetics, mechanism and applications, has been extensively investigated during the past century.[64-66] Thiol-ene polymerization undergoes a free-radical step-growth mechanism, which

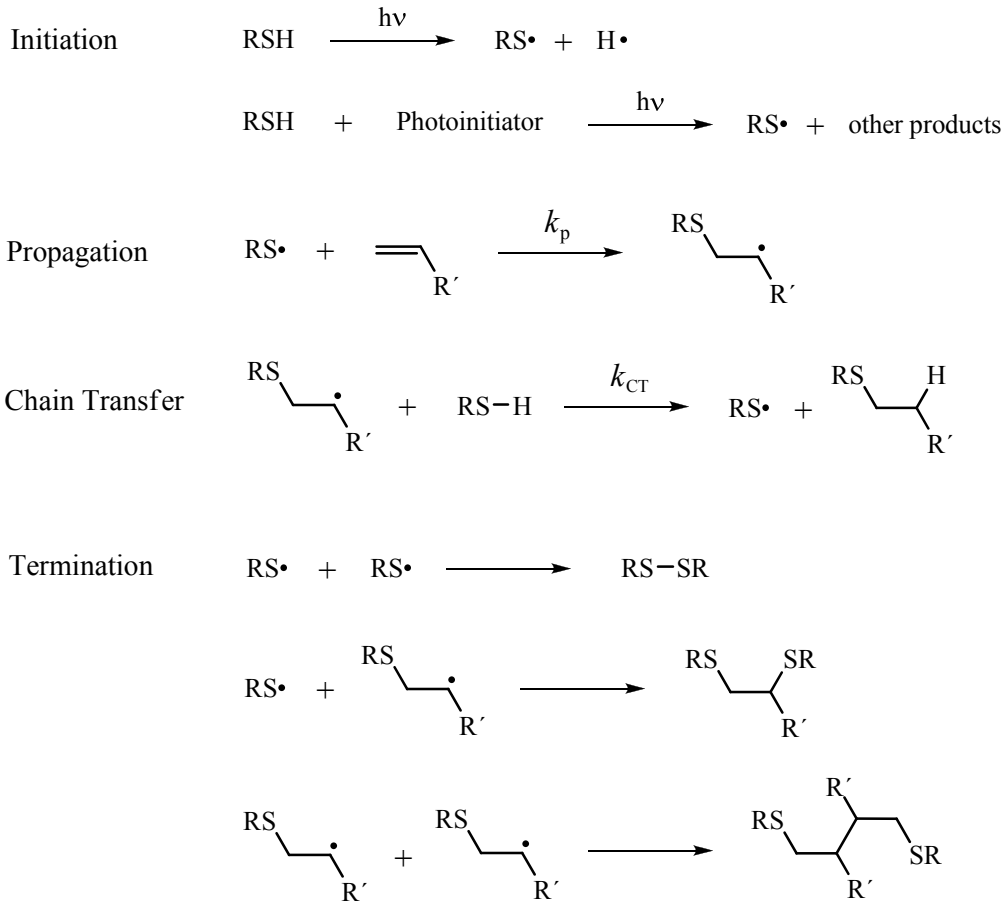

Scheme 1.5 Mechanism of thiol-ene polymerization process (Reproduced from ref.[67]).

is depicted in Scheme 1.5. The process of thiol-ene polymerization is summarized here based on several literatures.[67-70] Under irradiation of ultra-violet (UV) light, a thiol group cleaves into a thiyl radical and a hydrogen radical, which readily initiate a thiol-ene polymerization. After initiation, two steps are followed to accomplish the polymerization process: (1) the thiyl radical propagates across a carbon-carbon double bond, generating a carbon-sulfur bond and a carbon radical; and (2) this carbon radical abstracts a hydrogen atom from another thiol group, which regenerates a thiyl radical to restart the process. These propagation and chain transfer steps take place in an alternating way, which lead to the addition of thiol moieties to ene functionalities. Radical termination occurs via radical-radical recombination, where carbon-carbon, sulfur-sulfur, or carbon-sulfur radicals combine to terminate the reaction.

The rate-determining step of thiol-ene reaction was found to be chain transfer of a carbon-centered radical to a thiol functional group, rather than propagation of a thiyl radical through an unsaturated ene functionality.[68,71] The overall reaction rate is highly dependent on the electron density of the carbon-carbon double bond. An electron-rich ene functionality with electron-donating substituents attached on it possesses a faster reaction rate than an electron-poor ene moiety linked with electron-withdrawing groups.[67,69,72] Besides, the reaction rate of thiol-ene

polymerization is also determined by the structure of thiol-terminated molecules.[67,69]

There are several distinctive advantages of thiol-ene photopolymerization as compared to traditional free-radical polymerizations. A significant advantage of thiol-ene reaction is the ability of initiating a polymerization process without an added photoinitiator.[66,73] In this case, thick coatings can be achieved since UV light is able to penetrate thicker films without light attenuation resulting from absorption by the photoinitiator. In addition, polymers age much more slowly during long-term exposure to UV light due to the absence of degradation effects caused by the photoinitiator. Another beneficial advantage of thiol-ene reaction is that the polymerization process is not significantly inhibited by the presence of oxygen,[67,74] which makes this reaction more applicable. Other advantages of thiol-ene systems include a self-initiated rapid reaction,[73,75] formation of uniform crosslinked networks,[65,76] and incorporation of various thiol-ene comonomer pairs.[67,77] All of these advantages make thiol-ene systems chemically versatile for surface modification with precise control of film properties. Moreover, these advantages allow widespread applications of thiol-ene reactions in fabrication of surface-bound polymer films.[78-81]

1.4 Molecular Electronic Junctions

"Molecular junction" is the term describing an electron transport system which consists of two metallic or semiconducting solids as the contacts and a single molecule or array of molecules oriented in parallel performing as active electronic components in between two contacts. The study of donor-bridge-acceptor (DBA) molecules[82-84] (Figure 1.17a), which focuses on how the structure of "bridge" molecules affects electron transport rates, provides a fundamental idea for the development of molecular junctions. A molecular junction (Figure 1.17b) can be conceptually regarded as replacing the donor and acceptor moieties of a DBA molecule with two conducting solids. Theoretical and experimental studies of molecular electronic junctions have been well developed and actively investigated since the first report of a molecular rectifier proposed by Aviram and Ratner in 1974.[85]

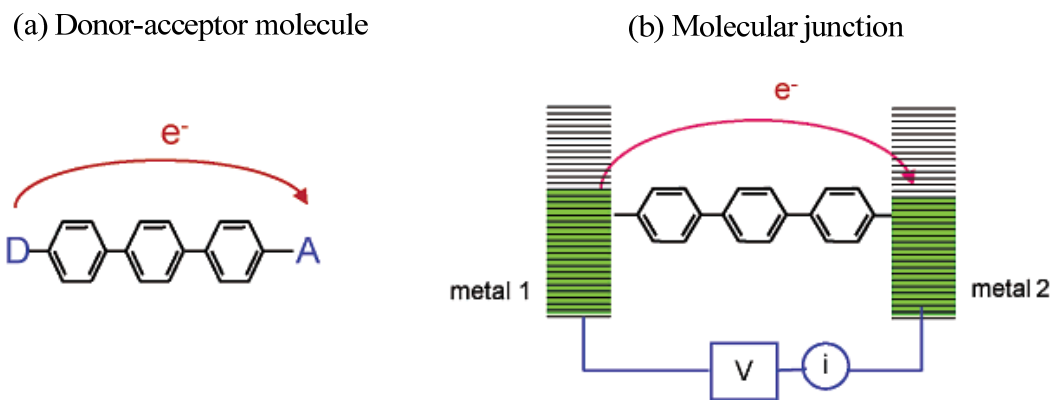

Figure 1.17 Electron transfer in donor-bridge-acceptor molecules (a) and molecular junctions (b) (Figure adapted from ref.[86]).

In a molecular junction, there are basically three components: a bottom contact, a top contact and a molecular layer in electronic contact with the two contacts. The materials commonly used as "contacts" include metallic conductors, with properties of high electrical conductivity and uniform density of electronic states, and semiconductors, having conducting bands, nearly full valence bands and relatively narrow band gaps, exhibiting an electrical characteristic between that of conductors and insulators. The organic molecular layer in between two contacts, with the critical dimension in the range of one to a few nanometers,[86,87] plays an important role in electron transport through the molecular junction. There are several approaches to attach the molecular layer to the substrate, including Au/thiol self-assembled monolayer (SAM),[88-90] Langmuir-Blodgett (LB) structures,[91,92] Si–C and Si–O–C bonds,[41,93,94] and carbon-carbon bonds.[44,45,95] The molecule/substrate bonds are relatively weak for SAM and LB structures, while much stronger bonds are formed for the case of Si–C bonds, Si–O–C bonds and carbon-carbon bonds. Different types of bonding, together with their corresponding bond energies are shown schematically in Figure 1.18.

The investigation of electron transfer (ET) mechanisms in molecular junctions has attracted intense research effort, which concentrates on how an electron is transmitted from one contact to another across a gap containing one or more oriented molecules. The ET mechanism is influenced by a number of factors,

such as molecular structure, substrate/molecule bonding, spacing distance and temperature. Several of the proposed mechanisms will be discussed in more detail in the following sections.

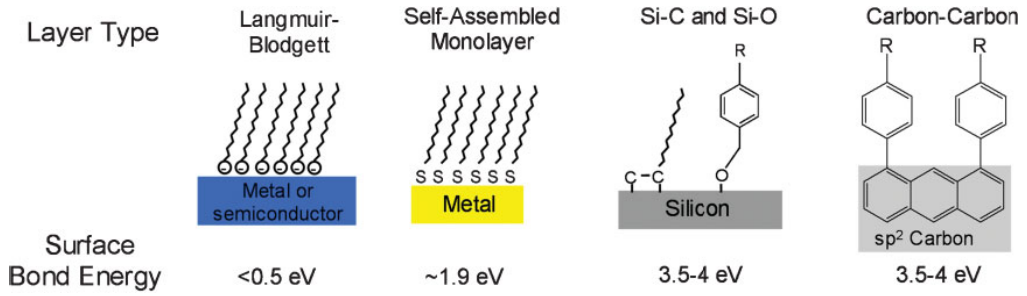

Figure 1.18 Different kinds of surface bonds and corresponding surface bond energies (Figure adapted from ref.[96]).

Coherent tunneling

The ET mechanism for coherent tunneling is applicable to molecular junctions with short distances (normally less than 25Å) between two conductors with or without molecular layers. The ET rate of coherent tunneling is exponentially dependent on the barrier thickness (i.e. distance between contacts), as denoted by Simmons relation[97,98] (Equation 1.1), where J = current density, q = electron charge, V = applied voltage, h = Plank's constant, m = electron mass, Φ = barrier height, and d = barrier thickness.

$$J = \frac{q^2 V}{h^2 d}(2m\Phi)^{1/2} \exp\left[\frac{-4\pi d}{h}(2m\Phi)^{1/2}\right] \qquad \text{(Equation 1.1)}$$

A simplified form of Simmons equation is given below[86] (Equation 1.2), where B is a constant and β (units of $Å^{-1}$ or nm^{-1}) is a common parameter describing the distance dependence, which is proportional to the square root of the barrier height.

$$J = Be^{-\beta d} \qquad \text{(Equation 1.2)}$$

When there is a vacuum gap between two conductors (i.e. no molecular layer), an electron can transmit from one conductor to another while the gap is small enough to allow overlap of electron wave functions of the conductors[97,98] (Figure 1.19A). When there is a molecular layer in the tunneling gap (Figure 1.19B), the ET rate can be increased greatly due to the effects of "superexchange".[99-102] In this instance, the orbitals and electrons of the molecule are involved in the electron transport process through interactions with the tunneling electron; as a consequence, barrier height and β are effectually decreased and the tunneling rate is enhanced remarkably.

Coherent tunneling is an electron transfer process without dephasing of the tunneling electron and is independent of temperature. However, when a lower tunneling barrier is created through molecular vibrations or internal rotations, the enhanced tunneling process would be temperature dependent.[103]

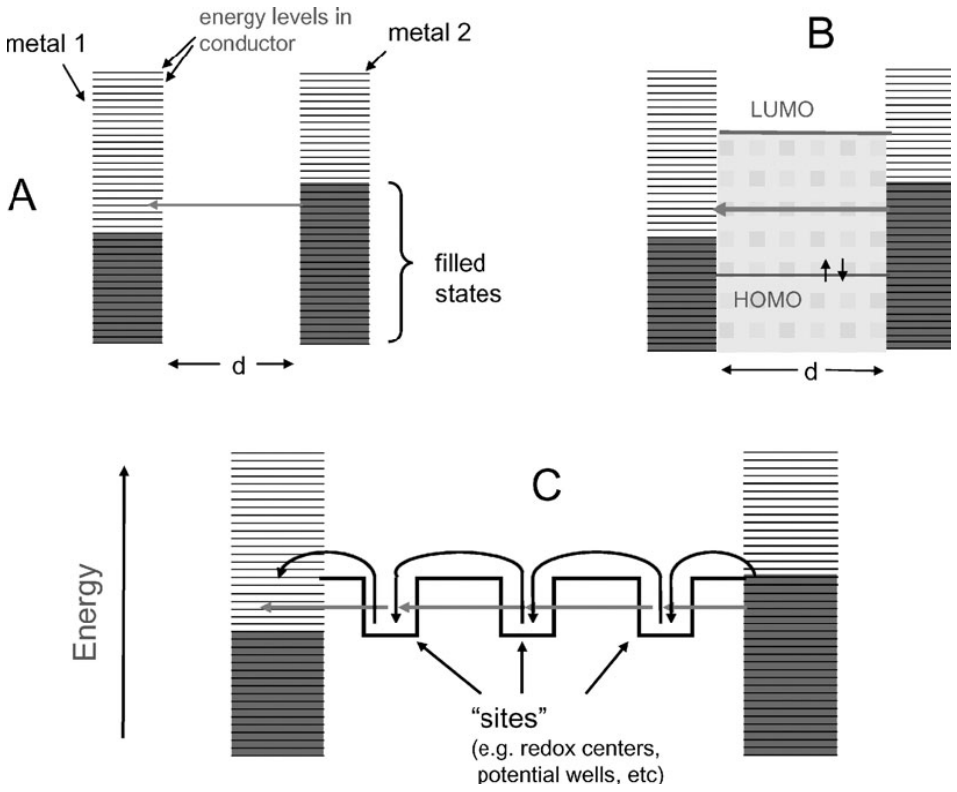

Figure 1.19 A. Energy levels for a vacuum gap between two conductors, with the shaded regions in the conductors representing filled electronic states, and the arrow representing coherent electron tunneling. **B.** Tunneling through a molecular layer between two conductors spaced apart by a distance d. **C.** ‘‘Incoherent’’ or ‘‘diffusive’’ tunneling (straight arrows) and activated redox exchange (curved arrows) among ‘‘sites’’ or redox centers in a relatively thick molecular layer. (Figure taken from ref.[104])

Incoherent, Diffusive Tunneling

When a molecular layer is too thick for an electron to transmit from one conductor to another via coherent tunneling, another mechanism, “incoherent” or “diffusive” tunneling, is involved. In the early 1990s, some interesting electron

transport phenomena in a DNA helix (about 40 Å thick) were observed,[105-107] which brought about the proposal of incoherent tunneling. For incoherent tunneling, an electron tunnels through the gap between the conductors following a series of steps, which refers to transmitting through a sequence of potential wells[108] (Figure 1.19C). The tunneling electron will "reside" in the potential wells for a relatively long time compared to coherent tunneling, which causes the disturbance of the electron phase. This process is composed of several consecutive steps and the electron tunneling may follow a random path between a series of sites.

Hopping Mechanism

Similar to incoherent tunneling, "hopping" mechanism proposes that the electron transfers between a series of "sites" (Figure 1.19C). Unlike tunneling, hopping involves thermal activation and nuclear motion, and often involves "redox exchange" during electron tunneling.[109-112] Instead of tunneling through the barrier thickness for incoherent tunneling, hopping mechanism is correlated with electron motion over the barrier. Besides, hopping is an extreme opposite case relative to coherent tunneling. The electron transport through hopping process is based on Marcus theory,[113] which describes the rates of electron transfer moving or hopping from one chemical species to another. When the

electron is transmitted to one of the "sites", thermal motion of nuclei and nuclear reorganization of the molecular structure occur, which allows the electron to pass through a sequence of discrete sites. As hopping refers to transfers between comparatively stable sites, it does not depend on the barrier distance between two conductors and since hopping is thermally activated, it is strongly temperature dependent. In brief, hopping is a relatively slower and long-range electron transport process.

1.5 Research Objectives

The original idea of this research was stimulated by the previously demonstrated layer-by-layer assembly of multilayers on silicon surfaces through the thiol-ene reaction. The main objective of the research described herein is to incorporate molecular multilayers, which contain molecules with intriguing functional groups, in molecular electronic junctions via the method of thiol-ene reaction. The greatest challenge is to find an appropriate "primer" molecule embodying two functional groups at its ends, one of which can be strongly bonded to PPF surfaces and the other of which is able to participate in thiol-ene reaction with another functional group of the second molecular layer. Several approaches, including oxidation of amines, thermal reactions and photochemical reactions have been attempted. However, none of them were found to be an excellent

approach for attaching the "primer" molecule, in that the resulting molecular layer achieved through above three methods was either loosely packed, or the available functional groups to take part in thiol-ene reaction were limited. Finally, reduction of *in situ* generated styrene diazonium salts was chosen as the method for anchoring the first molecular layer on PPF surfaces, for the reason that the resultant film was compactly packed and the alkene functionalities exposed on the surfaces can participate in subsequent thiol-ene reactions.

Chapter 2 describes the surface modification of PPF surfaces through the method of reduction of *in situ* generated styrene diazonium salts, as well as surface characterization of the resulting styrene molecular layers. In Chapter 3, a bonding of a second molecular layer of ferrocene-thiol through the method of thiol-ene reaction is decribed. As ferrocene is an electroactive species, quantitative surface coverage of ferrocene modified PPF surfaces was determined from voltammetry of surface attached ferrocene. Chapter 4 describes the electronic properties of two kinds of molecular junctions (PPF/Styrene/Cu/Au and PPF/Styrene/Fc/Cu/Au), which are fabricated by depositing metal top contacts through e-beam evaporation on the molecular layers bonded to PPF. In addition, possible electron transfer mechanisms for both of the molecular junctions are described.

Chapter 2. First Layer: Styrene Modification of Pyrolyzed Photoresist Films through Reduction of *in situ* Generated Diazonium Salts

Reduction of *in situ* generated diazonium salts is an innovative approach for modification of metal and carbon surfaces.[20,114] This *in situ* procedure provides a simple and straightforward way for surface modification. Traditionally, surface derivatization is accomplished through reduction of isolated diazonium salts, which are synthesized before surface modification by isolating the pure products from reaction solutions. While for the *in situ* procedure, modification is carried out directly in the reaction solution without isolation and purification steps. In this case, surface modification is simplified by combining two steps, synthesis of diazonium salts and reduction of the corresponding diazonium cations, into one step. In the current work, styrene molecular layers are modified on PPF surfaces through the method of reduction of *in situ* generated diazonium cations for the following two reasons. On the one hand, the particular molecule, styrene is selected since it can form a covalent bond with the PPF surface while leaving the double bond available for attachment of the second layer. On the other hand, the *in situ* procedure can effectively prevent polymerization of styrene diazonium cations. Furthermore, effectiveness of the method of reduction of *in situ* generated

diazonium salts, compared to the well-established method, reduction of isolated diazonium cations, is investigated.

2.1 Experimental

2.1.1 Reagents

All the reagents were used as received, including hydrochloric acid (ACS Grade, 12M), acetone (HPLC Grade), 2-propanol (HPLC Grade), methanol (HPLC Grade) and ethyl ether (anhydrous ACS) from Fisher Scientific, sodium nitrite ($NaNO_2$, Reagent A.C.S.) from ACP Chemicals Inc., catechol 99+% (1,2-dihydroxybenzene) from Acros Organics, 4-aminostyrene (97%, stabilized) from Alfa Aesar, 3-fluoro-2-methylaniline (99%) and tetrabutylammonium bromide (ReagentPlus, 99%) from Sigma-Aldrich and acetonitrile (anhydrous, HPLC Grade) from Caledon Laboratories Ltd. Water was obtained from a Millipore system (18 MΩ·cm).

Trifluoromethylphenyl (TFMP) diazonium salts and tetrabutylammonium tetrafluoroborate ($TBABF_4$) were synthesized and isolated as fluoroborate salts. To prepare TFMP diazonium salts, an amount of 0.01 mol of the precursor, 4-(trifluoromethyl) aniline (99%, Aldrich), was dissolved with a minimum amount of 48 wt. % HBF_4 (Sigma-Aldrich). Separately 0.03 mol of $NaNO_2$ was dissolved in a minimum amount of ultrapure water. Both of the solutions were

cooled to 0℃ in an ice bath and the cold $NaNO_2$ solution was added dropwise to the precursor solution while keeping the temperature under 4℃. After leaving the reaction for 30 min while stirring, the precipitate was vacuum filtered and washed with cold ethyl ether. The precipitate was then dissolved in a minimum amount of cold acetonitrile and undissolved impurities were filtered out by gravity filtration. Recrystallization procedure was followed by adding cold ethyl ether into the filtered solution and the product, TFMP diazonium tetrafluoroborate, was obtained through vacuum filtration.

For the preparation of $TBABF_4$, 100g tetrabutylammonium bromide was mixed with 43 mL of 48% HBF_4; then 26 mL methanol and 26 mL Millipore water were added to the mixture. After all solids dissolved, the mixture was added dropwise to 400 ml ultrapure water under stirring and after completion of the addition, the solution was cooled in an ice bath for 0.5h. By vacuum filtering the solution, the product $TBABF_4$ was obtained. In order to synthesize the pure product, recrystallization steps were followed by dissolving the product with the minimum amount of methanol and again adding the solution dropwise to Millipore water. The purer product was then obtained by vacuum filtration and by repeating the recrystallization steps, ultra pure $TBABF_4$ could be synthesized.

2.1.2 Preparation of Pyrolyzed Photoresist Films (PPFs)

Pyrolyzed photoresist films were prepared according to a well-established procedure.[7,11] A silicon wafer (1.3cm × 1.9cm) covered with ~200 nm thermally grown SiO_2 layer was sonicated in acetone, 2-propanol and ultrapure water sequentially for 10 minutes each and then dried with nitrogen gas. The cleaned silicon wafer was spin-coated with a commercially available positive photoresist AZ4330-RS (AZ Electronic Materials) at 6000 rpm for 30 seconds with two coatings on a spin coater (Model P6700, Specialty Coating Systems Inc.). The spin-coated samples were soft-baked at 90℃ for 20 min and then transferred into to a tube furnace (Lindberg/Blue) equipped with a quartz tube. Under continuous flowing of forming gas (95% N_2 + 5% H_2) at 100 mL/min, the samples were heated at the rate of 10°/min to 1000℃, held at 1000℃ for 1h to accomplish pyrolysis and slowly cooled to room temperature. The prepared PPF samples were then stored in a Petri dish covered with aluminum foil.

2.1.3 Preparation of Diazonium Salt Solutions

The solution for *in situ* generation of styrene diazonium cations was prepared according to a reported procedure.[115] Two stock solutions (0.1M $NaNO_2$ and 0.5M HCl) were prepared beforehand by dissolving 0.69g $NaNO_2$ in 100 mL water and adding 4.2 mL concentrated HCl in 100 mL water. Under stirring, an amount of

4.8 μL of neat 4-aminostyrene (final concentration: 2mM) was added to 20 mL of 0.5M HCl until mixed uniformly and then 400 μL of 0.1M $NaNO_2$ (final concentration: 2mM) was added to the solution. The solution was allowed to react for 70 min under continuous stirring prior to electrochemical modification. The preparation for the solution of *in situ* generation of 3-fluoro-2-methylphenyl diazonium salts followed the same procedure as that of styrene diazonium salts.

An amount of 0.0078g of as-prepared trifluoromethylphenyl diazonium salts was added to the electrolyte solution containing 0.2M tetrabutylammonium tetrafluoroborate ($TBABF_4$, the supporting electrolyte) in acetonitrile (ACN) solution. This solution was used immediately after preparation.

2.1.4 Electrode Modification

Electrochemical modification of PPF electrodes was implemented with a BASi Epsilon-EC potentiostat (Bioanalytical Systems Inc.). A Ag/AgCl (saturated NaCl) reference electrode was prepared by electrochemically coating a Ag wire with AgCl and immersing this wire into a saturated NaCl solution. The calibration of this reference electrode was carried out in the solution of 1 mM ferrocyanide [$Fe(CN)_6^{4-}$] in 0.1M KCl and an $E_{1/2}$ was observed at 230 mV versus Ag/AgCl/sat'd NaCl. Another reference electrode Ag/Ag^+ (0.01 M $AgNO_3$ in 0.1M $TBABF_4$ + ACN solution) was calibrated in a 1 mM of ferrocene (Fc) in

ACN solution with $E_{1/2}$ of ferrocene at 89 mV versus Ag/Ag^+, yielding the Ag/Ag^+ potential to be +0.22V versus aqueous saturated calomel electrode (SCE), which is based on an $E_{1/2}$ of Fc at +0.31V versus aqueous SCE.[116] These two reference electrodes were used in different derivatization solutions, with Ag/Ag/sat'd NaCl applied in the aqueous solution containing HCl and Ag/Ag^+ electrode performed in the nonaqueous solution containing ACN. A platinum wire was used as the counter electrode and a PPF sample on Si/SiO_x was utilized as the working electrode. The PPF sample was mounted vertically on a metal clamp, which was connected with an alligator clip to the potentiostat. Before modification, the solution containing desired diazonium salt was deaerated with high-purity Argon for 10-15 min, and the PPF electrode was rinsed with 2-propanol and acetonitrile respectively and blown dry with nitrogen. The electrode modification was accomplished either by scanning cyclic voltammograms (CVs) with different cycles or by applying controlled potential electrolysis (CPE) at the reduction potential of the corresponding diazonium salt for various times. Figure 2.1(a) shows a typical cyclic voltammogram of reduction of styrene diazonium cations with four consecutive scans. The voltammogram of the first cyclic scan shows a chemically irreversible broad reduction peak at the potential of -500 mV. With successive cyclic scans, the voltammetric reduction peaks keep decreasing, which indicates that a passivated layer was formed on the

PPF surface after one voltammetric scan and this molecular layer prevented further reactions occurring on the surface. Figure 2.1(b) illustrates a current vs. time CPE curve of the reduction of styrene diazonium ions with the potential held at -500 mV for 4 minutes. After modification, the PPF electrode was cleaned with acetonitrile and ready for characterization.

2.1.5 UV-Vis Monitoring of *in situ* Generated Styrene Diazonium Salts

A solution containing 20 mM of 4-aminostyrene and 20 mM of $NaNO_2$ in 0.5M HCl was prepared. A certain amount of this as-prepared solution was transferred to a cuvette with the path length of 1 cm and the synthesis of styrene diazonium salts was monitored by UV-Vis spectroscopy. UV-Vis spectra were recorded from the beginning of the reaction for a total of 300 min. To be specific, the spectra were taken every 2 min for the first 30 minutes (0~30 min), every 5 min (30~60 min), every 10 min (60~120 min) and every 30 min (120~300 min). The spectrum of the solution containing 20 mM of 4-aminostyrene alone in 0.5M HCl was recorded as well.

2.1.6 Catechol and Ferrocyanide Tests

An amount of 0.011g of catechol solid was dissolved in 100 mL 0.1 M HCl to make a catechol solution with a concentration of 1 mM. Cyclic voltammograms of

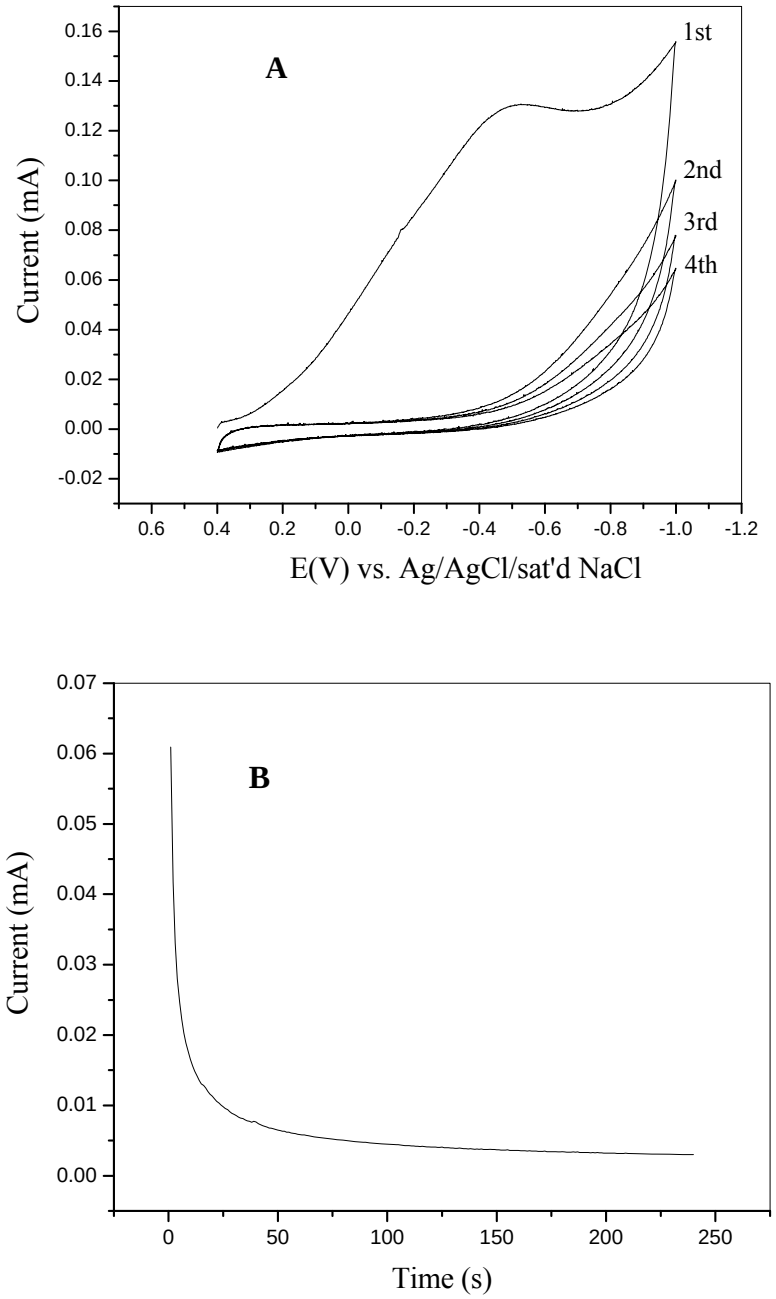

Figure 2.1 Reduction of *in situ* generated styrene diazonium salts. (A) Cyclic voltammogram with four consecutive scans from 400 mV to -1000 mV (scan rate = 200 mV/s); (B) controlled potential electrolysis (CPE) at -500 mV for 4 min.

catechol solution were performed on a BASi Epsilon-EC potentiostat with an O-ring cell apparatus, the photograph of which is shown in Figure 2.2. The cyclic voltammograms were recorded for both unmodified PPF and styrene-modified PPF surfaces. A PPF sample was placed horizontally on a Teflon base plate and then, a Teflon cell, having a hole in the bottom, was secured by five screws on top of the base plate. A Viton O-ring was positioned under the hole to seal the catechol solution above the sample. Electric contact to the PPF surface was made

Figure 2.2 Photograph of the O-ring apparatus. A PPF sample is mounted horizontally between a Teflon base plate and a Teflon cell, which has a hole in the bottom and is secured on top of the base plate by five screws. A Viton O-ring placed under the hole is used to seal the solution above the PPF sample. Electric contact to the PPF surface is made using a silver stripe placed on the surface but not exposed to the solution.

using a silver stripe placed on the surface not exposed to the solution. The Teflon cell was filled with the catechol solution, which was purged with high-purity Ar for 5 min before electrochemical measurements. Ag/AgCl/sat'd NaCl was utilized as the reference electrode and Pt wire was used as the counter electrode. The geometric area of the working electrode (PPF) was defined by the area of the Viton O-ring, which is 0.28 cm^2.

For ferrocyanide test, a solution containing 1 mM of ferrocyanide [$Fe(CN)_6^{4-}$] in 1M KCl was prepared and the procedure for ferrocyanide test on unmodified and modified PPF surfaces was the same as that for catechol test.

2.1.7 Characterization

UV-Vis spectra were collected using a UV-Vis spectrophotometer (Agilent 8453) and the path length of the cuvette was 1 cm. Mass spectra were obtained on a mass spectrometer (Agilent 1959D) connected with a liquid chromatograph (Agilent Series 1100). AFM measurements were performed on an atomic force microscope (Dimension 3100, Digital Instruments) using commercially available Si cantilever tips (NSC15/AlBS, MikroMasch) for both contact mode and tapping mode. And XPS analysis was performed on an AXIS 165 spectrometer (Kratos Analytical) equipped with a monochromatic Al Kα source (hν = 1486.6 eV) at a

power of 210 W. Analysis for all the samples was carried out in the analytical chamber with a base pressure lower than 2×10^{-8} Pa.

2.2 Results and Discussion

2.2.1 UV-Vis Monitoring of Styrene Diazonium Salt Synthesis

When modifying electrodes through reduction of isolated diazonium salts, the corresponding diazonium cation is synthesized in advance and then dissolved in electrolyte/solvent solution for derivatization with known concentration. Herein, the method of reduction of *in situ* generated diazonium ions for surface modification was employed. Since derivatization was carried out directly in the reaction solution, the concentration of diazonium cations was left unknown. Therefore, UV-Vis spectroscopy was applied for the purpose of monitoring the evolution of the amount of *in situ* generated styrene diazonium ions in the reaction solution with time. Figure 2.3 illustrates the UV-Vis spectra of *in situ* generated styrene diazonium salts from the beginning of the reaction until the reaction progressed for 300 min. The initial spectrum shows a characteristic absorption peak at 247 nm, which is attributed to the absorption of the precursor, 4-aminostyrene. This assignment is confirmed by the measurement of a spectrum for the solution containing 4-aminostyene alone in 0.5 M HCl, which is shown in Figure 2.3. This absorption peak keeps decreasing with the evolution of the

reaction time and meanwhile, two new absorption peaks at 278 nm and 320 nm are observed, which are ascribed to the absorption of generated styrene diazonium ions. These two absorption peaks cannot be confirmed by the spectrum of a solution containing only styrene diazonium ions in 0.5 M HCl, in that styrene diazonium salts are difficult to be separated from impurities and easy to

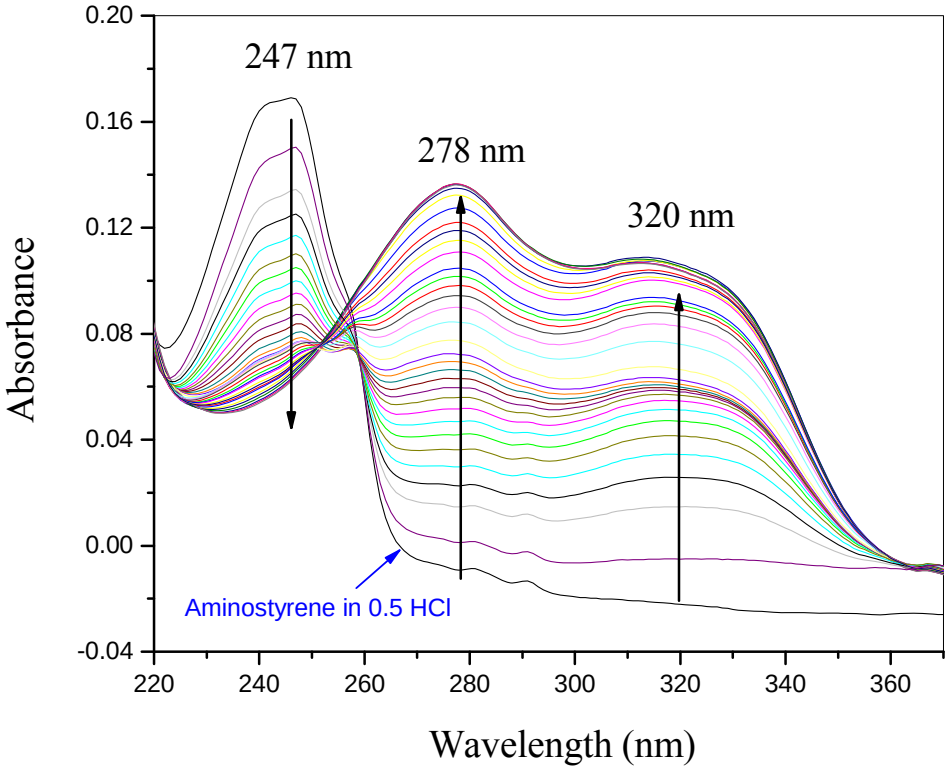

Figure 2.3 UV-Vis spectra of *in situ* generated styrene diazonium salts from the beginning of the reaction until the reaction lasting for 300 min. The spectrum was taken every 2 min for the initial 30 min (0~30 min), every 5 min (30~60 min), every 10 min (60~120 min) and every 30 min (120~300 min). The spectrum of aminostyrene in 0.5 M HCl before adding $NaNO_2$ is also shown (pointed by the blue arrow).

polymerize after being prepared. Instead, these two absorption peaks are compared with a previously reported result.[20] In that report, the wavelengths for UV absorption of 4-nitrophenyl diazonium ions were found to be 260 nm and 310 nm, which are quite close to the two values in the current work. The difference in the absorption wavelengths for these two species is probably caused by the different functional group attached to the phenyl ring, one of which is nitro group and the other of which is olefin group.

Figure 2.4(a) shows an absorbance vs. time plot of the evolution of the generation of styrene diazonium salts for reaction lasting from 0 min to 300 min at the wavelengths of 278 nm and 320 nm. The absorbance of the diazonium salt at these two wavelengths continuously increases until 70 min and stays constant until 300 min. This observation indicates that the synthesis of styrene diazonium ions stopped after reaction proceeded for 70 min. Therefore, the reaction solution was left to react for 70 min before surface modification so that the solution contained the maximum amount of styrene diazonium cations. The precursor, 4-aminostyrene had been completely converted to the product, styrene diazonium salt after 70 min, which is demonstrated by comparing the initial spectrum with the spectrum recorded after the reaction ran for 70 min [Figure 2.4(b)]. There is no observable characteristic absorption peak for the precursor but only peaks for styrene diazonium ion in the spectrum taken after 70 min. The UV-Vis spectra of

styrene diazonium ions were also recorded daily after being synthesized [Figure 2.4(c)]. The absorbance vs. time plot within 10 days indicates that the styrene diazonium ions degraded slowly.

2.2.2 Mass Spectroscopy Characterization

The mass spectra were recorded at the beginning of the reaction and after the reaction progressed for 70 min (Figure 2.5). The initial spectrum presents a maximum m/z peak at 120.4, which corresponds to the precursor, 4-aminostyrene (with a hydrogen ion attached). After reaction lasting for 70 min, a maximum m/z peak is observed at the position of 131.4, which is attributed to the product, styrene diazonium ion. The disappearance of the peak at 120.4 and the maximum peak at 131.4 indicate that 4-aminostyrene has been completely transformed to styrene diazonium salt after reaction lasting for 70 min, consistent with the UV-Vis results.

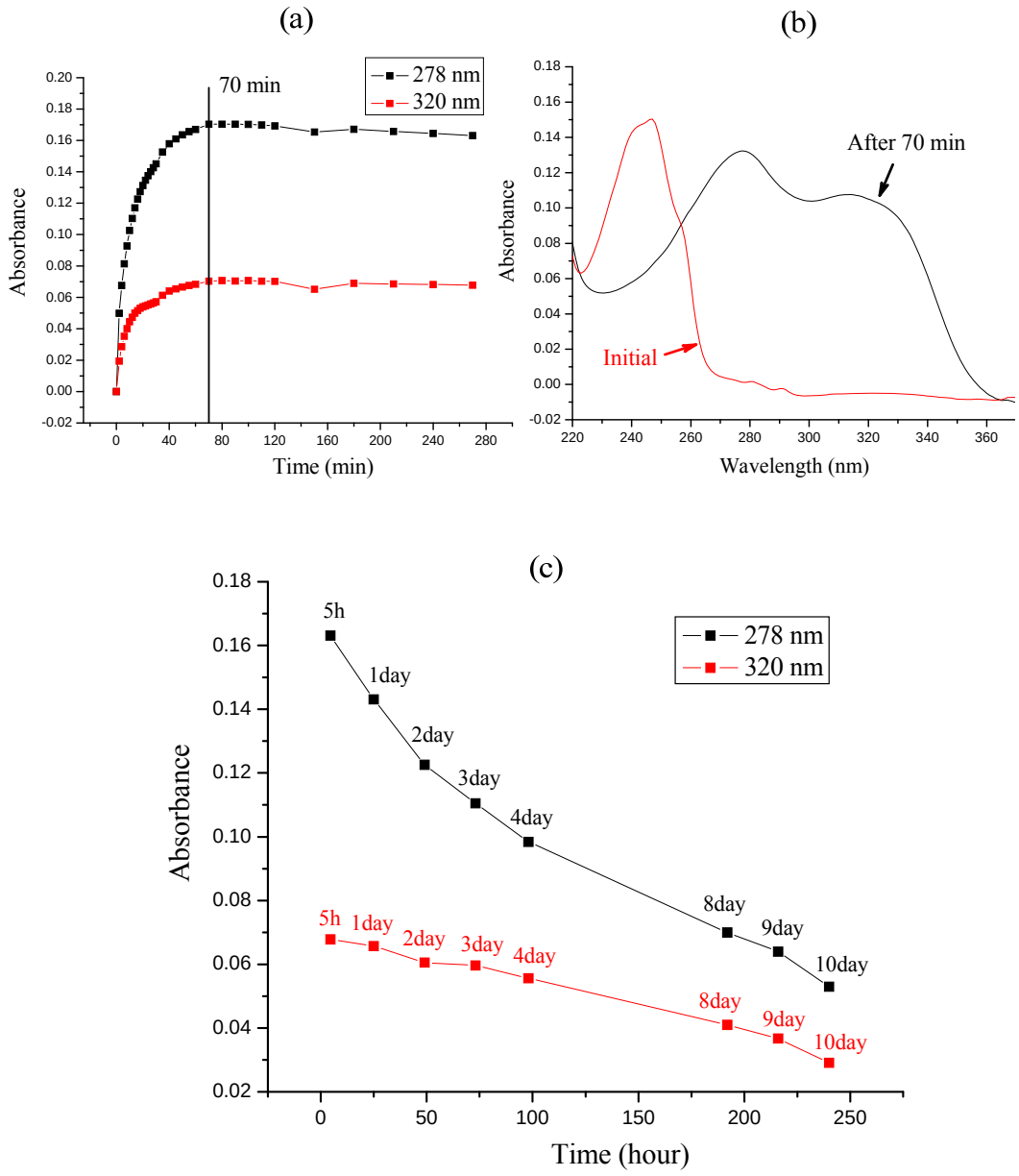

Figure 2.4 Absorbance vs. time plots at the wavelengths of 278 nm and 320 nm for the reaction time from 0 min to 300 min (a) and from the first day to 10 days (c). UV-Vis spectra taken at the beginning of the reaction and after reaction lasting for 70 min (b).

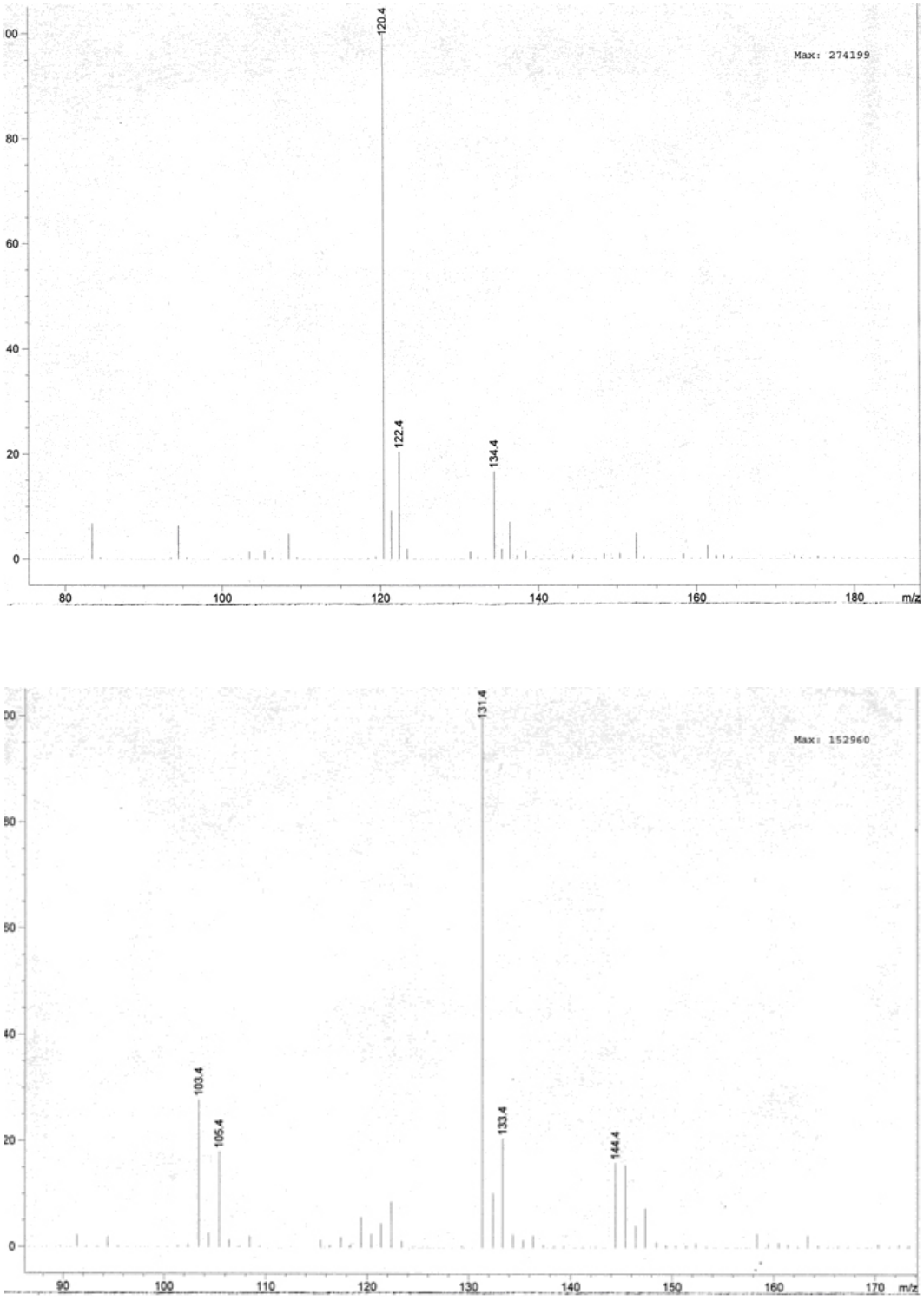

Figure 2.5 Mass Spectra recorded at the starting point of the reaction (top panel) and after reaction lasting for 70 min (bottom panel).

2.2.3 Film Thickness and Roughness Determined by AFM

The AFM "scratching" technique reported by Anariba et al.[26] is utilized here to determine the film thicknesses of the modified PPF surfaces by effectively removing the molecular layer without scratching the PPF surface. In the first place, an area of a modified PPF surface is selected and then contact mode AFM is applied to intentionally scratch a molecular layer deposited on the PPF surface within the selected area. Afterwards, tapping mode AFM is performed to scan an image with the same size as that of the original area. The resulting image contains both scratched and unscratched areas and by comparing the height difference between these two regions, the thickness of the molecular layer is determined.

The set-point voltage that is high enough to remove the molecular layer but not damage the PPF surface has been well investigated by Anariba and coworkers.[26] Herein, a set-point voltage of 0.25V was applied to all contact mode scratching experiments on modified PPF surfaces as it was found to be an effective force to disturb the molecular layer without affecting the PPF surface. Figure 2.6 illustrates two trapping mode AFM images: (a) bare PPF and (b) after scratching the unmodified PPF surface with the force of 0.25V and line profiles of these two AFM images. Since the AFM image of PPF after "scratching" shows some debris but no discernable damage and the corresponding line profile shows

no height difference between scratched and unscratched areas, it is demonstrated that the force of 0.25V is not aggressive enough to damage the PPF surface.

The film thickness of a modified PPF surface is obtained from the line profile across the trench of a "scratched" tapping mode image and a statistical process was applied to determine the film thickness. Figure 2.7 shows a tapping mode image after "scratching" the molecular layer (1μm × 1μm trench in a 5μm × 5μm image), the line profile across the trench of this image and schematic of the statistical approach for determining the molecular thickness. This image involves the styrene molecular layer modified on the PPF surface through controlled potential electrolysis (CPE) at -500 mV for 4 min. A rectangular box was applied on the tapping mode image across the "scratched" trench. Two points (one inside and one outside the trench) were defined along the rectangular box and by calculating the height difference between these two points, the thickness of the molecular layer is acquired. The height for each spot is the average value along the y-axis of the rectangle across the spot, namely a straight line across the spot as illustrated in Figure 2.7 (c).

Since each individual height is the average height calculated through Nanoscope software, the molecular thickness obtained is also an averaged value. Other point pairs were selected in the same fashion and several molecular thicknesses were obtained through calculating the height difference between each

point pair. By averaging all the calculated height differences, a statistical molecular thickness was obtained.

An example of the statistical method for calculating the film thickness is shown in Table 2.1. For each individual sample, six point pairs are selected and film thicknesses is acquired by calculating the height difference of each point pair. For determination of the film thickness of a modified PPF surface, two

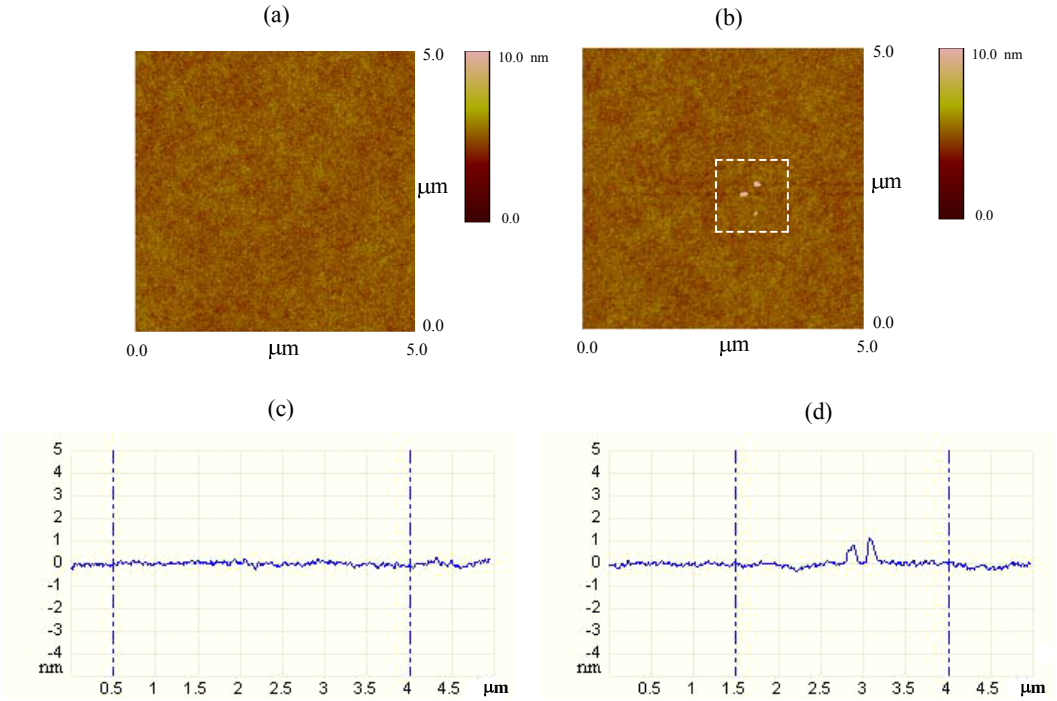

Figure 2.6 Tapping mode AFM images of (a) bare PPF and (b) PPF surface after "scratching" with the set-point voltage of 0.25V, showing some debris (inside the dashed square) but no recognizable damage. Line profiles of the corresponding AFM images: (c) bare PPF and (d) PPF surface after "scratching", which only shows two small bumps but no height difference between scratched and unscratched regions.

independent samples were employed and therefore, the film thickness calculated is the average value of 12 point pairs. Table 2.2 lists the thicknesses of styrene molecular layers modified under different derivatization methods, where each thickness is calculated over 12 point pairs as shown in Table 2.1. The surface roughness of each styrene layer is also listed in Table 2.2, which is obtained by

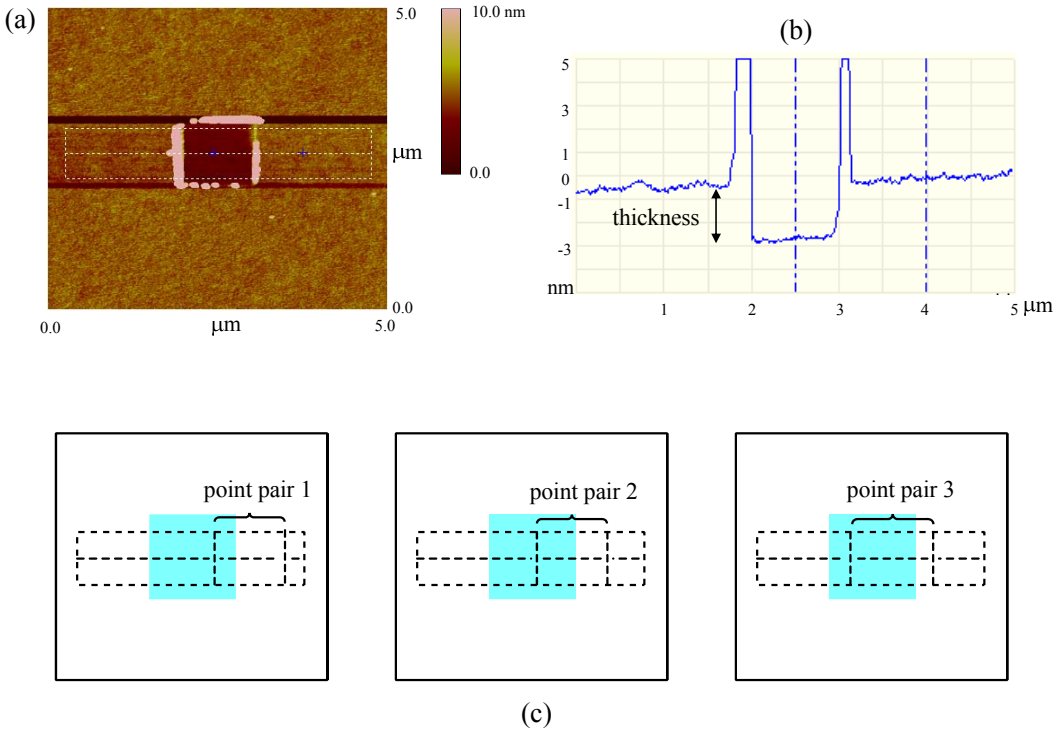

Figure 2.7 (a) A 5 µm × 5 µm tapping mode AFM image after "scratching" the molecular layer with a 1 µm × 1 µm scratched trench. The styrene molecular layer was modified on PPF surface through holding the potential at -500 mV for 4 min. (b) Line profile of this AFM image, showing that the film thickness is calculated by the height difference between scratched and unscratched regions. (c) Schematic of the statistical approach for determination of film thicknesses.

averaging the surface roughness of two independent samples for each modification condition. In addition, the evolution of film thickness of styrene modified PPF surfaces versus increased voltammetric scans and longer electrolysis is shown schematically in Figure 2.8.

Table 2.1 Statistical calculation of thickness of styrene layer deposited on PPF through CPE at -500 mV for 4 min.

	Sample 1	Sample 2
Point pair 1	2.611	2.633
Point pair 2	2.592	2.658
Point pair 3	2.588	2.591
Point pair 4	2.329	2.716
Point pair 5	2.649	2.792
Point pair 6	2.460	2.596
Mean	2.538	2.664
Std dev	0.121	0.078
Mean for 12 Point pairs	**2.601**	
Std dev for 12 Point pairs	**0.117**	

Table 2.2 Thickness and roughness of bare PPF and styrene molecular films deposited on PPF under different modification conditions determined by AFM.

	Derivatization methods	AFM thickness (nm)	Roughness (nm)
Bare PPF	none	none	0.267
Styrene_1 scan	CV from 0.4 to -0.6V at 200 mV/s, 1 scan	$1.548^{a} \pm 0.071^{b}$	0.279
Styrene_4 scans	CV from 0.4 to -0.6V at 200 mV/s, 4 scans	1.708 ± 0.106	0.318
Styrene_6 scans	CV from 0.4 to -0.6V at 200 mV/s, 6 scans	1.978 ± 0.106	0.320
Styrene_2 min	CPE at -500 mV for 2 min	2.382 ± 0.117	0.338
Styrene_4 min	CPE at -500 mV for 4 min	2.601 ± 0.117	0.361
Styrene_8 min	CPE at -500 mV for 8 min	2.793 ± 0.064	0.373
Styrene_10 min	CPE at -500 mV for 10 min	2.883 ± 0.124	0.407
Styrene_20 min	CPE at -500 mV for 20 min	2.927 ± 0.157	0.436
Styrene_30 min	CPE at -500 mV for 30 min	3.025 ± 0.165	0.473

[a] Mean value over 12 point pairs. [b] Standard deviation upon 12 point pairs. [c] Averaged value over two independent samples. The rms roughness was calculated by Nanoscope software within an area of 5μm × 5μm for each individual sample.

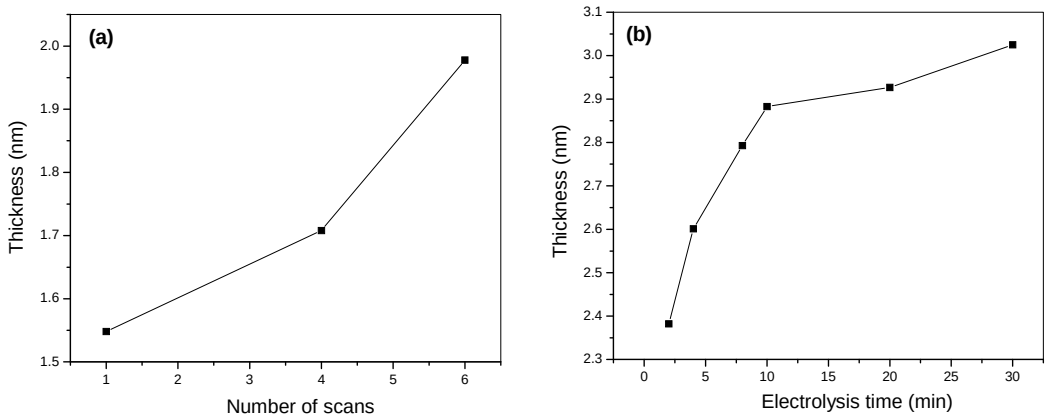

Figure 2.8 Evolution of film thickness of styrene layers with increased voltammetric scans (a) and longer electrolysis times (b).

The theoretical thickness of a monolayer of styrene was calculated by the software Gaussian 03. The thickness is defined as a single layer of styrene bonded vertically to the PPF surface, including the Van der Waals radius of the terminal atom H and the length of the C-C single bond between styrene and the PPF surface. The resulting calculated thickness of the styrene monolayer is 0.773 nm; thus, the theoretical thicknesses for two layers, three layers and four layers turn out to be 1.546 nm, 2.319 nm and 3.092 nm respectively. By comparing the theoretical thicknesses with the thicknesses listed in Table 2.2, the number of molecular layers of each modified PPF surface is estimated. Two molecular layers were readily formed on the PPF surface after one voltammetric scan (thickness: 1.548 nm) and the film thickness increased with more voltammetric scans but the thicknesses did not reach the number for three molecular layers, which was

possibly due to sporadic growth of the third layer on top of the second layer. While applying more voltammetric scans, the unmodified space of the third layer was covered with more styrene molecules and a full coverage was inclined to form on the third layer. A number of three molecular layers was achieved through holding the potential at -500 mV for 2 min (thickness: 2.382 nm). And in the same manner, the coverage of the fourth layer grew gradually with increased electrolysis time until the full coverage formed when holding the potential at -500 mV for 30min (thickness: 3.025nm). Furthermore, the surface roughness of modified PPF surfaces increased with more voltammetric scans and longer electrolysis time, but all of the modified surfaces were quite smooth with root-mean-square (rms) roughness less than 0.5 nm.

Based on the evolution of film thickness and roughness of the styrene molecular layer with increased number of scans and electrolysis times, the possible growth mechanism of the styrene molecular layer is proposed, which is illustrated schematically in Figure 2.9. After a styrene monolayer is formed on the PPF surface, styrene radicals in the solution are so aggressive that they are able to attack the phenyl ring or the olefin group of an anchored styrene molecule. As the C-C bond in the phenyl ring is more stable than the C=C double bond in the alkene group, a majority of styrene radicals are prone to attack the olefin group, leaving a small number of aryl radicals attaching to the phenyl ring. With

continuous growth, styrene multilayers are formed on the PPF surface in a disorderly and random manner.

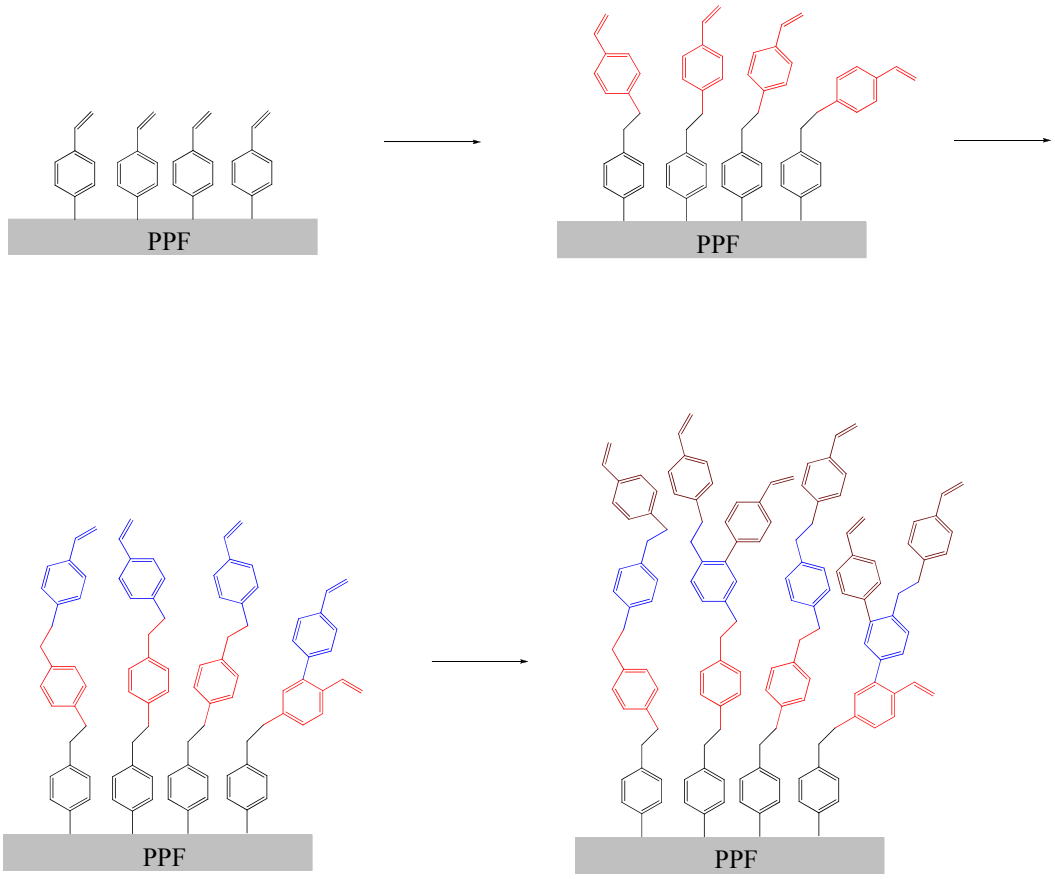

Figure 2.9 Proposed growth mechanism of styrene molecular layers.

2.2.4 Surface Coverage

2.2.4.1 Catechol Test

Catechol test is applied herein for the purpose of estimating the surface coverage of styrene modified PPF surfaces. When catechol is adsorbed on a carbon surface, oxidation of catechol can take place through electron transfer from catechol to the surface.[117] However, when the carbon surface is covered with a molecular layer, electron transfer will be completely inhibited in that the adsorption of catechol to the carbon surface is prevented by the molecular layer. Through cyclic voltammetry, oxidation and reduction peaks of catechol on carbon surfaces are observable and electron transfer rate is indicated by ΔE_p (difference between anodic peak potential and cathodic peak potential) and the magnitude of the current for both anodic and cathodic peaks. Increased ΔE_p and decreased magnitude of current indicate that the catechol electron transfer rate on carbon surfaces is slower, thus resulting in the formation of a more compact molecular layer on the surface.[118] Once the PPF surface is sufficiently covered to prevent catechol adsorption, the electron transfer rate becomes negligible.[118]

Figure 2.10 illustrates cyclic voltammograms of 1 mM catechol in 0.1 M HCl on bare PPF and styrene modified PPF surfaces. The ΔE_p value for the styrene modified PPF surface with one voltammetric scan increases compared to that for bare PPF and keeps increasing with more cyclic scans and longer electrolysis time

for styrene modification, until anodic and cathodic peaks completely disappear for a PPF surface modified by CPE at -500 mV for 30 min. At the same time, peak current for both anodic and cathodic peaks diminishes with increased voltammetric scans and longer electrolysis time. The increasing ΔE_p and decreasing magnitude of current provide evidence that the coverage of styrene molecular layers on PPF surfaces increases with more cyclic scans and longer duration of electrolysis until saturation coverage is achieved with electrolysis time of 30 min. It is difficult to state surface coverage quantitatively due to the complexity of the catechol oxidation reaction, but the absence of voltammetric peaks implies styrene coverage of at least 99%.[118]

2.2.4.2 Ferrocyanide Test

The film density of styrene modified PPF surfaces was also evaluated by cyclic voltammetry of the $Fe(CN)_6^{3-/4-}$ redox probe system. A densely packed and well-insulating layer is indicated by a higher value of ΔE_p and a lower peak current. Figure 2.11 shows cyclic voltammograms of 1 mM $Fe(CN)_6^{4-}$ in 1 M KCl on both bare PPF and styrene modified surfaces. There are no observable oxidation and reduction peaks for PPF surfaces modified with styrene through CPE for different times and the curves appear to be completely flat for surfaces modified with 10 min, 20 min and 30 min. The disappearance of anodic and

cathodic peaks and the lower peak current indicate that compactly packed styrene layers, which prevent electron transfer for $Fe(CN)_6^{4-}$, were formed on PPF surfaces.

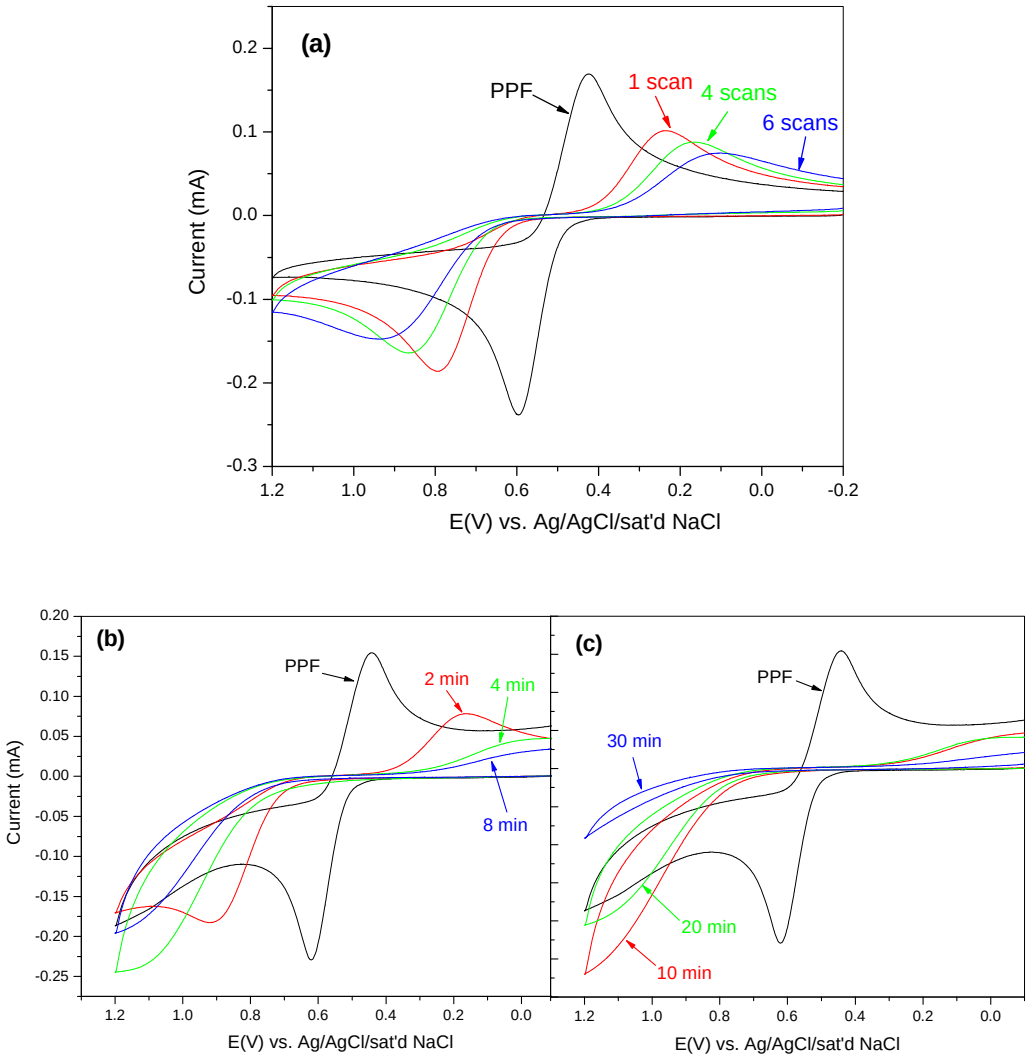

Figure 2.10 Voltammograms of 1 mM catechol in 0.1 M HCl on bare PPF and styrene modified PPF surfaces prepared through cyclic voltammetry with different scans (a) and CPE at -500 mV for different duration time [(b) and (c)]. Scan rate: 200 mV/s.

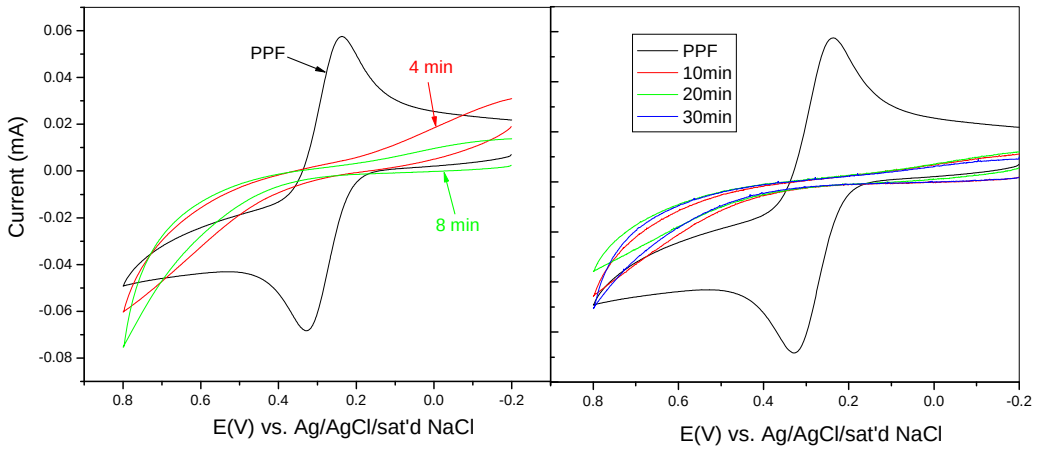

Figure 2.11 Cyclic voltammograms of 1 mM $Fe(CN)_6^{4-}$ in 1 M KCl on bare PPF and styrene modified PPF surfaces through CPE for different electrolysis time. Scan rate: 100 mV/s.

2.2.5 X-ray Photoelectron Spectroscopy (XPS)

Since styrene contains only carbon and hydrogen, XPS cannot establish styrene coverage on a carbon electrode surface. Therefore, another molecule, 3-fluoro-2-methylaniline, which contains a XPS marker fluorine and has a similar structure as that of 4-aminostyrene was selected as the precursor. The modification procedure for reduction of *in situ* generated 3-fluoro-2-methylphenyl (FMP) diazonium salts strictly followed that for styrene diazonium cations and the resulting molecular layers were characterized by XPS. Table 2.3 lists the surface composition of FMP layers (Figure 2.12a) deposited on PPF surfaces through CPE with different electrolysis times. For modification with increased electrolysis time, the atomic concentration of fluorine and the ratio of fluorine to carbon (F/C)

increase gradually, indicating the formation of more densely packed molecular layers.

(a) FMP molecular layer (b) TFMP molecular layer

Figure 2.12 Schematic illustration of (a) 3-fluoro-2-methylphenyl (FMP) molecular layer and (b) trifluoromethylphenyl (TFMP) molecular layer.

Table 2.3 Surface composition of modified PPF surfaces determined by XPS

	Atomic concentration				
	O%	N%	F%	C%	F/C ratio
FMP_4 min	6.78	0.88	4.73	87.61	0.054
FMP_8 min	5.70	1.25	5.07	87.98	0.058
FMP_10 min	5.58	1.29	5.11	88.02	0.058
FMP_20 min	4.81	1.37	5.39	88.43	0.061
FMP_30 min	5.12	1.30	5.60	87.98	0.064
TFMP_4 min	3.15	0.79	14.27 (/3= 4.76)	81.79	0.058[a]
TFMP_8 min	3.44	0.38	15.88 (/3= 5.29)	80.29	0.066
TFMP_30 min	3.40	0.59	19.02 (/3= 6.34)	76.99	0.082

[a] Dividing F% by three and then divided by C%.

In order to compare the effectiveness of reduction of *in situ* generated diazonium ions and reduction of isolated diazonium salts, trifluoromethylphenyl (TFMP) molecular layers were attached on PPF surfaces through reduction of TFMP diazonium salts, which were prepared beforehand and dissolved in 0.2 M $TBABF_4$ + ACN solution immediately before derivatization. The surface composition of TFMP layers (Figure 2.12b) modified with different electrolysis time is listed in Table 2.3 and since there are three F atoms in a single TFMP molecule and only one F atom in a single FMP molecule, the atomic concentration of the F atom for TFMP layers is divided by three so as to be comparable to the F concentration for FMP layers. By comparing the concentration of fluorine and F/C ratio for both FMP and TFMP layers (Table 2.3), it is apparent that the amounts of fluorine for these two kinds of molecular layers are approximately equal, although with slightly less fluorine for the FMP molecular layers. The comparable surface composition of the characteristic element F for both FMP and TFMP molecular layers provide the evidence that surface modification achieved through reduction of *in situ* generated diazonium salts is as efficient as that accomplished through reduction of isolated diazonium cations, a method which has been well established and comprehensively investigated.

For the purpose of estimating the percentage of a full coverage in terms of %F for both FMP and TFMP molecular layers, the F/C ratios were compared with

a reported value,[118] the F/O ratio of a TFMP molecular layer on polished glassy carbon (GC). In that report, the resulting TFMP layer completely inhibited the electron transfer between catechol and GC electrode, an indication of a full coverage. The F/C ratio of the TFMP layer on GC surface is 0.25. It is divided by 3 herein so as to be comparable with the F/C ratios obtained in the current work. It was found that 65% ~ 77% of a full coverage was achieved for the FMP modified PPF surfaces and the percentage for the TFMP modified PPF surfaces was 70% ~ 99%, which is close to a full coverage.

2.3 Conclusion

Styrene molecular layers were successfully attached to the PPF surfaces through the method of reduction of *in situ* generation of styrene diazonium salts. The synthesis of styrene diazonium cations was monitored by both UV-Vis spectroscopy and mass spectroscopy. It was found that the precursor, 4-aminostyrene, had been completely converted to the product, styrene diazonium cation after the reaction progressed for 70 min. The styrene layers were derivatized on the PPF surfaces through either cyclic voltammetry with different number of scans or controlled potential electrolysis of different duration, and the resulting film thickness and film roughness were measured by AFM. Both thickness and roughness of the styrene molecular layers increased gradually with

repeated voltammetric scans and longer electrolysis time. The surface coverage of the grown styrene layers was evaluated by catechol and ferrocyanide voltammetry, the result of which showed that more compactly packed films were formed with increased cyclic scans and electrolysis time. This result, combined with the evolution of film thickness and roughness measured by AFM, demonstrated that the initial styrene film formed rapidly and then the film was slowly thickened with gradual removal of pinholes.

The PPF surfaces were also modified with the FMP molecular layer, which has a similar structure to styrene but contains fluorine to enable XPS characterization. The amount of fluorine on the PPF surface was found to increase gradually with more cyclic scans and longer electrolysis time, indicating the formation of more compact films, a result that is in accordance with the results obtained from AFM measurements and catechol and ferrocyanide voltammetry. Furthermore, it was demonstrated that the method of reduction of *in situ* generated diazonium cations is as efficient as that of reduction of solutions prepared from isolated diazonium salt by comparing the amount of fluorine for both FMP and TFMP molecular layers.

Chapter 3. Second Layer: Ferrocene Attachment on Styrene Layers through Thiol-Ene Reaction

The thiol-ene reaction, which is accomplished through reaction between an alkene moiety and a thiol functionality, provides a simple and effective way for construction of polymeric multilayer films on solid substrates. The incorporation of organic molecules with novel functionalities and special properties on various surfaces could be achieved through thiol-ene reaction with precise interface control. Furthermore, the thiol-ene reaction allows for the growth of a thin and conformal film at the atomic level based on sequential and self-limiting reactions. In this study, the functional group ferrocene attached with a thiol moiety was selected as the modifier for thiol-ene reaction with the ene functionality of the first modified styrene layer. Since ferrocene is an electroactive species, quantitative surface coverage of ferrocene-modified surfaces could be obtained based on cyclic voltammograms of surface-bound ferrocene.

3.1 Experimental

3.1.1 General

Thiol-ene reactions were carried out in a nitrogen-filled Vacuum Atmospheres glovebox. The reagents, tetrahydrofuran (Optima Grade, Fisher) and

acetonitrile (Optima Grade, Fisher) used in the glovebox were further purified, dried and degassed on an Innovative Technologies solvent purification system. Acetonitrile (anhydrous, HPLC Grade) from Caledon Laboratories Ltd. and tetrahydrofuran (suitable LC, GC) from OmniSolv were used as received in the lab atmosphere. 6-(Ferrocenyl)hexanethiol was purchased from Aldrich and stored in the glovebox. Ultrapure deionized water was obtained from a Millipore system (18 MΩ·cm). Tetrabutylammonium tetrafluoroborate ($TBABF_4$) was synthesized according to the procedure described in Chapter 2.

3.1.2 Ferrocene-Thiol Attachment through Thiol-Ene Reaction

Different concentrations (0.1 mM, 0.5 mM, 1 mM, 2 mM, 5 mM and 10 mM) of 6-(Ferrocenyl)hexanethiol (Fc-thiol) were prepared inside the glovebox by adding different amounts of neat Fc-thiol in acetonitrile (ACN) solution and stored in the glovebox afterwards. A styrene-modified PPF substrate, which was prepared by reduction of *in situ* generated styrene diazonium salts as described in Chapter 2, was placed in a Teflon cell. The Teflon cell is 1.5 cm in width, 2.0 cm in length and 0.5 cm in depth. A thin layer (0.03 ~ 0.05 cm) of Fc-thiol solution was applied on the PPF substrate and a quartz slide was utilized to cover the Teflon cell so as to prevent evaporation of the Fc-thiol solution. Thiol-ene reaction between surface-bound styrene and Fc-thiol was accomplished through

irradiation of UV light at the wavelength of 254 nm for 30 min, as shown schematically in Figure 3.1(a). The path length of UV light in the Fc-thiol solution equals the thickness of the solution on the surface, which is 0.03 ~ 0.05 cm. The resulting sample (PPF/Styrene/Fc) was rinsed with tetrahydrofuran (THF) right after surface modification in the glovebox. Then it was taken out of the glovebox, sonicated in THF for 2 min, rinsed with THF and ACN sequentially and finally blown dry with nitrogen gas. A control sample was prepared as well by immersing the styrene-modified PPF substrate into Fc-thiol solution but with no UV irradiation for 30 min and the control sample was cleaned afterwards using the same procedure.

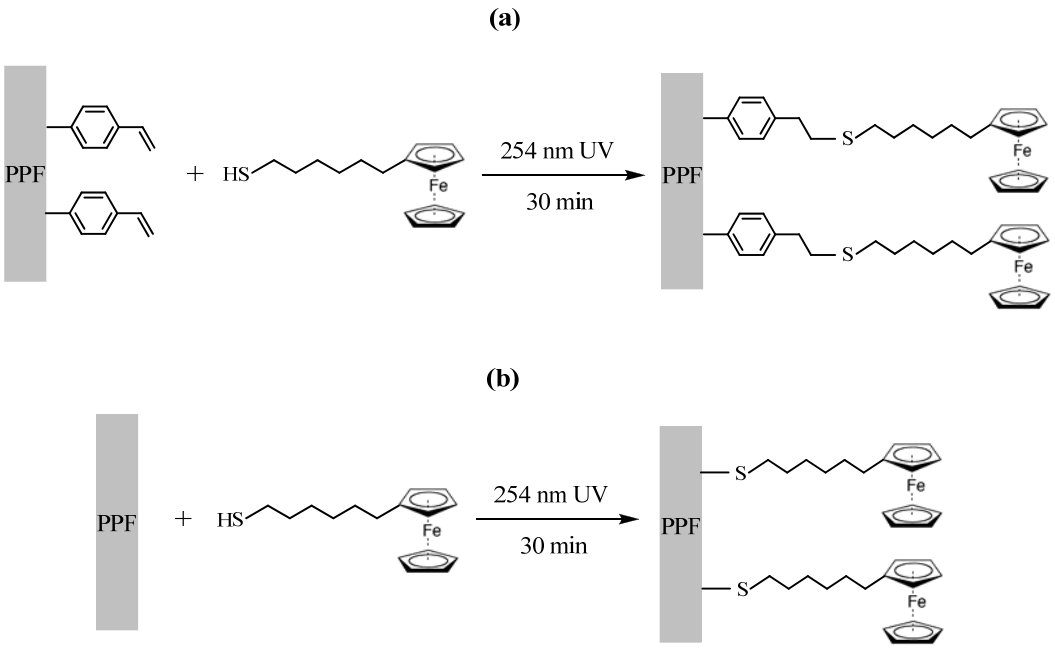

Figure 3.1 Thiol-ene reaction of Fc-thiol with (a) styrene modified PPF surface and (b) bare PPF. The resulting film is defined as PPF/Styrene/Fc and PPF/Fc, respectively.

Thiol-ene reaction between Fc-thiol and a bare PPF (i.e. an unmodified PPF) was implemented by soaking the bare PPF in Fc-thiol solution with radiation of 254 nm UV light for 30 min, the process of which is illustrated in Figure 3.1(b). The resultant film is defined as PPF/Fc. A control sample was also prepared using the same procedure but without UV irradiation. The cleaning procedure for both PPF/Fc and the corresponding control sample was the same as that for PPF/Styrene/Fc.

3.1.3 Electrochemical Measurements of Surface Coverage

Quantitative surface coverage of ferrocene (Fc) modified PPF surfaces can be calculated based upon cyclic voltammograms of surface-bound Fc in 0.1 M $TBABF_4$/ACN solution. An O-ring cell apparatus, as described in Chapter 2, was used to conduct the electrochemical measurements. The Teflon cell was filled with 0.1M $TBABF_4$ + ACN solution and the solution was purged with high-purity Argon for 5 min before measurements. Three electrodes were incorporated in the Teflon cell for electrochemical measurements on a BASi Epsilon-EC potentiostat (Bioanalytical Systems Inc.). The Fc-bound PPF surface performed as the working electrode, the area of which exposed in the solution was the same as that of the O-ring, 0.28 cm^2. Ag/Ag^+ (a Ag wire in 0.01 M $AgNO_3$ in 0.1M $TBABF_4$ + ACN solution) was used as the reference electrode, which was calibrated as

described in Chapter 2, and a Pt wire was utilized as the counter electrode. Cyclic voltammetry (CV) was conducted on all of the as-prepared samples, including both Fc-modified PPF surfaces and their corresponding control samples, for the purpose of determination of quantitative surface coverage based upon the amount of Fc anchored on the surfaces.

Catechol test was carried out on both Fc-modified PPF surfaces and bare PPF in order to determine surface coverage qualitatively, as described in Chapter 2.

3.2 Results and Discussion

3.2.1 Calculation of Surface Coverage

Surface coverage of Fc was determined by integration of either cathodic or anodic peak in a CV curve of surface-bound Fc and geometric area of PPF surface. The quantitative calculation of surface coverage is based upon Equation 3.1,[116] where Γ represents surface coverage in the unit of mol/cm^2, Q is the charge integration of either cathodic or anodic peak of a CV curve (unit: coulombs), n is the number of electrons involved in an electrode reaction, F is the Faraday constant (96485 C mol^{-1}) and A stands for the geometric area of the PPF surface (0.28 cm^2). As the redox couple involved here is ferrocene/ferrocenium (Fc/Fc$^+$), the number of electrons transferred during the reaction is n=1.

$$\Gamma = \frac{Q}{nFA} \qquad \text{(Equation 3.1)}$$

Figure 3.2 shows cyclic voltammograms of surface-bound Fc of a PPF/Styrene_4 min/Fc surface in 0.1M $TBABF_4$/ACN solution. The sample was prepared through reduction of *in situ* generated diazonium salts by holding the potential at -500 mV for 4 min for attachment of the styrene layer and through thiol-ene reaction by exposing 1 mM Fc-thiol on the styrene layer under 254 nm UV light for 30 min for attachment of the Fc layer. There are totally four CV curves involved in Figure 3.2, which were obtained using different voltammetric scan rates. Surface coverage of Fc for each voltammogram was calculated based on both anodic and cathodic peaks, where charge integration Q of these two peaks was calculated through Origin software. A baseline at the bottom of each peak was selected and the area between the peak and the baseline, i.e. the total charge Q, was integrated by the software. Afterwards, two numbers of surface coverage calculated from the anodic and the cathodic peak respectively were averaged. The same calculation was applied on all the other three voltammograms and surface coverage of PPF/Styrene_4 min/Fc was obtained by averaging the numbers of surface coverage calculated from four cyclic voltammograms. An example of the calculation process for PPF/Styrene_4 min/Fc is shown in Table 3.1. Cyclic voltammogram of the corresponding control sample was also scanned and there is no observable Fc peak present in the CV curve (Figure 3.2), indicating that the

cleaning procedure for as-prepared samples was effective enough to remove physically adsorbed Fc-thiol on the surface.

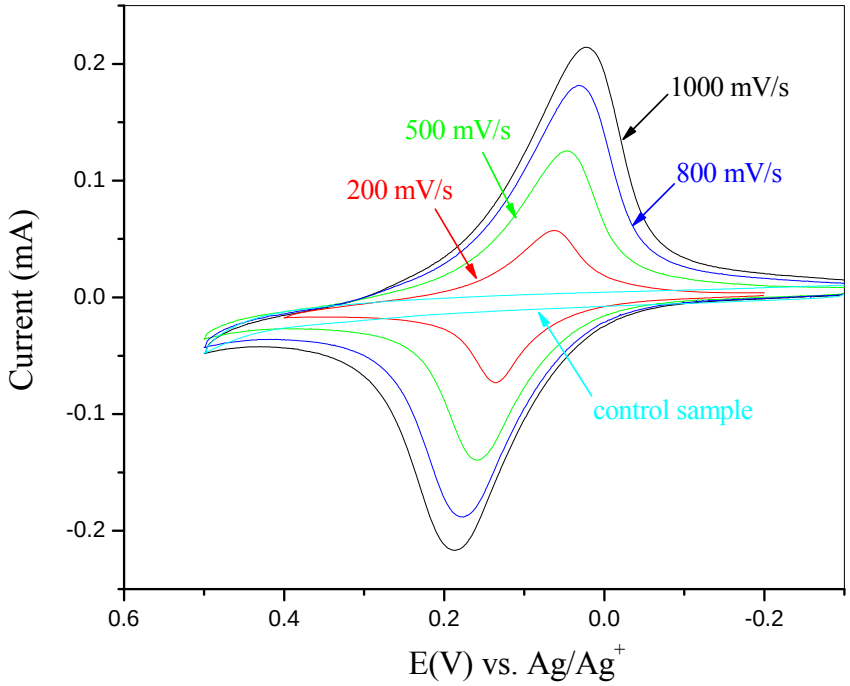

Figure 3.2 Cyclic voltammograms of surface-bound Fc in 0.1 M $TBABF_4$/ACN solution under different scan rates for a PPF/Styrene/Fc sample and its corresponding control sample.

To examine reproducibility of surface coverage, several PPF/Styrene_4 min/Fc samples were prepared in the same manner and surface coverage was measured and calculated for each sample. The calculated surface coverage for five different samples, each of which is the averaged value for four voltammograms, is listed in Table 3.2. Surface coverage of the other two kinds of samples is also

listed in Table 3.2, which are PPF/Styrene_8 min/Fc modified through CPE at -500 mV for 8 min for the styrene layer and exposing 1 mM Fc-thiol under 254 nm UV for 30 min and PPF/Fc modified through 1 mM Fc-thiol reacting directly with the PPF surface. Surface coverages for different samples but with the same modification procedure show significant variation, the reason for which will be discussed in the following section.

Table 3.1 Calculation of surface coverage of surface-bound Fc of a PPF/Styrene/Fc sample based on both anodic and cathodic peaks.

Scan rate	Surface coverage of Fc (Γ, mol/cm^2)		
	Anodic peak	Cathodic peak	Average
200 mV/s	3.61×10^{-10}	4.70×10^{-10}	4.16×10^{-10}
500 mV/s	4.14×10^{-10}	4.56×10^{-10}	4.35×10^{-10}
800 mV/s	4.11×10^{-10}	4.55×10^{-10}	4.33×10^{-10}
1000 mV/s	4.30×10^{-10}	4.58×10^{-10}	4.44×10^{-10}
		Total Average	**4.32×10^{-10}**

Table 3.2 Surface coverage of surface-bound Fc for different samples prepared under diverse modification conditions.

Modification conditions	Surface coverage of Fc (Γ, mol/cm^2)	Mean ± Std dev
PPF + Styrene_4min + 1mM Fc-thiol (PPF/Styrene_4 min/Fc)	4.32×10^{-10} 5.15×10^{-10} 5.28×10^{-10} 8.50×10^{-10} 9.04×10^{-10}	**$6.46 \times 10^{-10} \pm 2.15 \times 10^{-10}$**
PPF + Styene_8min + 1mM Fc-thiol (PPF/Styrene_8 min/Fc)	1.08×10^{-10} 1.24×10^{-10}	**$1.16 \times 10^{-10} \pm 1.13 \times 10^{-11}$**
PPF + 1mM Fc-thiol (PPF/Fc)	2.23×10^{-10} 3.08×10^{-10} 3.70×10^{-10} 5.02×10^{-10} 7.30×10^{-10}	**$4.27 \times 10^{-10} \pm 1.98 \times 10^{-10}$**

3.2.2 UV-Vis Absorption of Ferrocene-Thiol

Figure 3.3 shows UV-Vis spectrum of 1 mM Fc-thiol in ACN solution, which was collected on an Agilent 8453 UV-Vis spectrophotometer. There is a small bump observed at the wavelength of 254 nm, which indicates that Fc-thiol absorbs

UV light at 254 nm. According to Beer's law, molar absorptivity ε of 1 mM Fc-thiol could be calculated based on Equation 3.2, where A represents the

$$A = \varepsilon bc \qquad \text{(Equation 3.2)}$$

absorbance of a certain solution, b is the path length and c is the concentration of the absorber. Here, a cuvette with the path length of 1 mm was used and the absorbance of 1 mM Fc-thiol at the wavelength of 254 nm is found to be 0.24 in the spectrum. Therefore, the molar absorptivity of 1 mM Fc-thiol is calculated to be 2400 M^{-1} cm^{-1} at 254 nm.

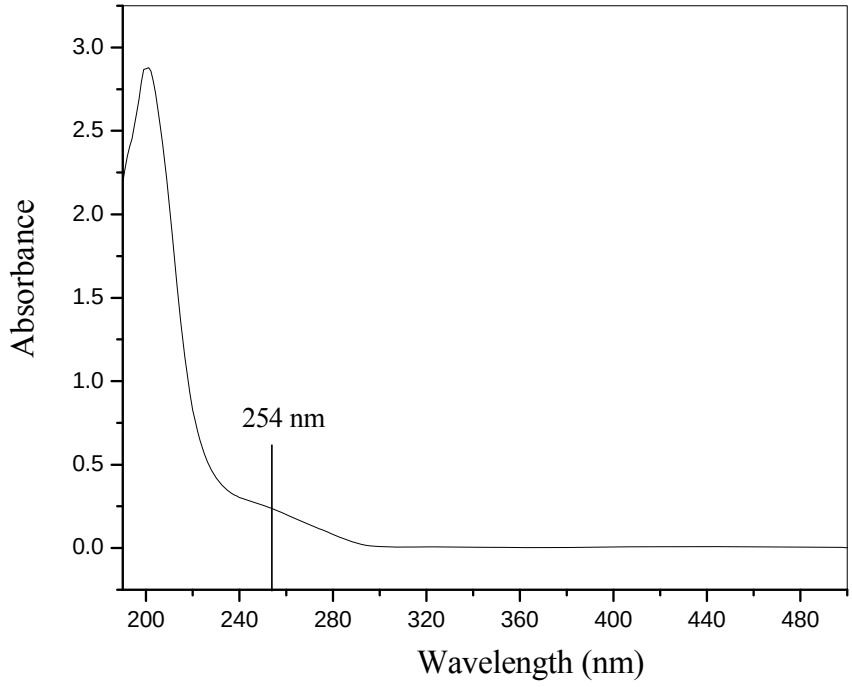

Figure 3.3 UV-Vis spectrum of 1 mM Fc-thiol in ACN solution.

The path length of 1 mM Fc-thiol on the PPF surface when doing surface modification can be estimated by the total volume applied on the surface and the area of the solution spreading out on the surface. Before thiol-ene reaction, a volume of about 30 – 50 μL of 1 mM Fc-thiol was applied on the PPF surface and the solution spread out to form a thin layer with the area of about 1.3 cm × 1.3 cm. The area of the drop was not controlled, and varied from sample to sample. The shape of the solution on the surface could be regarded as a cube and through dividing the total volume (30 ~ 50 μL) by the length (1.3 cm) and the width (1.3 cm), the thickness of the Fc-thiol solution, i.e. the path length of UV light through 1 mM Fc-thiol, is calculated to be 0.03 ~ 0.05 cm. After substitution into Equation 3.2, the corresponding absorbance of 1 mM Fc-thiol is estimated to be 0.072 ~ 0.12 at 254 nm. Then, the transmission of UV light through 1 mM Fc-thiol solution can be calculated based on Equation 3.3, giving the result of 76% ~ 83%, which means 1 mM Fc-thiol is not totally transparent to 254 nm UV light and

$$T = 10^{-A} \qquad \text{(Equation 3.3)}$$

thus, availability of the UV light for thiol-ene reaction is reduced to some extent by absorption of Fc-thiol. Also, because of the variability of the volume of 1 mM Fc-thiol solution applied on the surface and the area of the thin layer, UV light absorption of 1 mM Fc-thiol varied from sample to sample. Therefore, Fc-thiol

absorption of UV light is considered as one possible reason for the variation in Fc coverage for different samples apparent in Table 3.2.

To further investigate this effect, several Fc-thiol solutions with different concentrations were prepared and each was applied on styrene-modified PPF surface for thiol-ene reactions. Table 3.3 lists surface coverage of Fc for samples modified with six different concentrations of Fc-thiol for two batches at each concentration. Modification of the styrene layer for all the samples was accomplished through CPE at -500 mV for 4 min. For modification with 0.1 mM Fc-thiol, very small Fc peaks are observed in the CV curve, resulting in a surface coverage less than 2×10^{-11} mol/cm^2. Surface coverage of Fc dramatically increases when the concentration is increased from 0.1 mM to 0.5 mM and from 0.5 mM to 1 mM. However, when the concentration is higher than 1 mM, surface coverage of Fc starts to decrease. This is because Fc-thiol solution with higher concentrations is more opaque to the UV light; as a consequence, availability of the UV light for thiol-ene reaction diminishes with increased concentrations. Although surface coverage of the two replicate batches varies, the highest surface coverage of Fc was achieved through using 1 mM Fc-thiol for both batches. As a result, the concentration of 1 mM was used for conducting all the thiol-ene reactions either on styrene-modified PPF surfaces or bare PPF.

In order to compensate for the problem of UV absorption by Fc-thiol solution, longer UV exposure time, including 60 min and 90 min, was attempted on styrene-modified PPF surfaces using 1mM Fc-thiol. However, the resultant surface coverage turned out to be comparable with the surface coverage obtained by using 30 min exposure time. Therefore, we took 30 min as the UV exposure time for all the thiol-ene reactions.

Table 3.3 Surface coverage of Fc for PPF/Styrene/Fc samples prepared through holding the potential at -500 mV for 4 min for the styrene layer and with different concentrations of Fc-thiol applied on the styrene-modified surface for thiol-ene reaction.

Concentration of Fc-thiol	Surface coverage of Fc (Γ, mol/cm^2)	
	Batch 1	Batch 2
0.1 mM	less than 2×10^{-11}	less than 2×10^{-11}
0.5 mM	4.32×10^{-10}	1.46×10^{-10}
1 mM	**9.04×10^{-10}**	**5.20×10^{-10}**
2 mM	3.97×10^{-10}	2.92×10^{-10}
5 mM	3.76×10^{-10}	1.63×10^{-10}
10 mM	1.42×10^{-10}	1.41×10^{-10}

3.2.3 Catechol Test Comparison between PPF/Styrene/Fc and PPF/Fc

From Table 3.2, it is apparent that the averaged values of surface coverage over five independent samples for PPF/Styrene_4 min/Fc and PPF/Fc surfaces are close to each other, with a lower surface coverage observed for PPF/Fc. As both samples, with or without the styrene layer, has similar surface coverage of Fc, catechol test was carried out in order to investigate the necessity of the styrene layer. Figure 3.4 illustrates cyclic voltammograms of 1 mM catechol in 0.1 M HCl on PPF/Styrene_4 min/Fc, PPF/Fc and a bare PPF. As described in Chapter 2, a higher surface coverage is indicated by a larger ΔE_p (potential difference between anodic peak and cathodic peak) and a lower current height for each peak. By comparing cyclic voltammograms of PPF/Fc and PPF/Styrene_4 min/Fc with that of bare PPF, it is found that ΔE_p for both surfaces has been increased; however, the coverage is significantly higher for the PPF/Styrene_4 min/Fc surface, as there are no observable anodic and cathodic peaks in the voltammogram. From catechol tests, it could be concluded that the styrene layer is indeed necessary for surface modification of PPF surfaces; otherwise, the resulting film is loosely packed, with many pinholes.

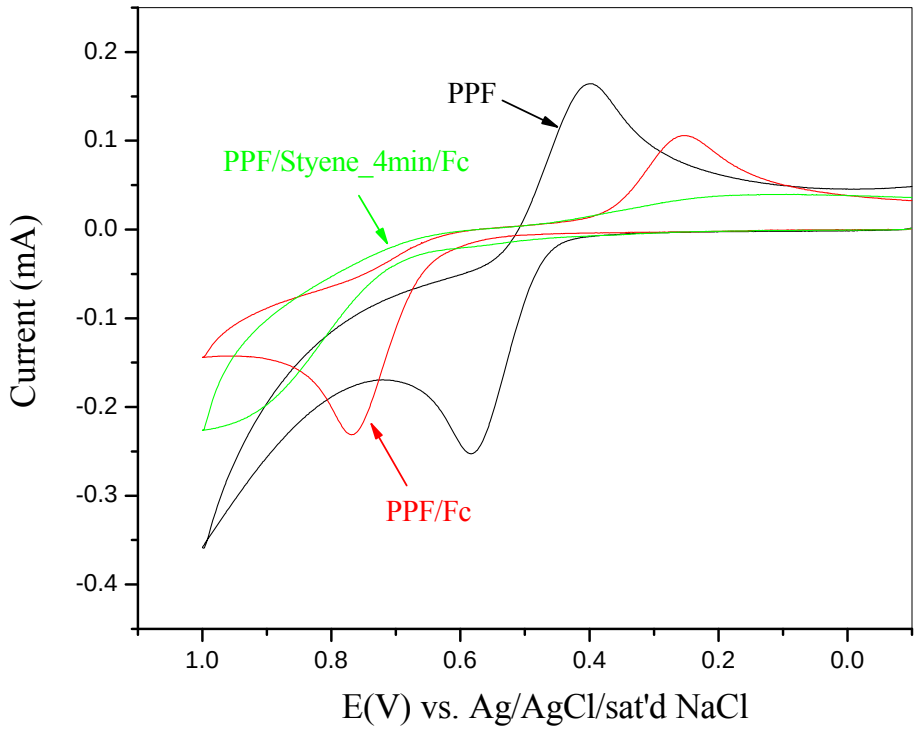

Figure 3.4 Cyclic voltammograms of 1 mM catechol in 0.1 M HCl on PPF/Styrene_4 min/Fc, PPF/Fc and a bare PPF. Scan rate = 200 mV/s.

3.2.4 Theoretical Calculation of Surface Coverage of Ferrocene

In order to evaluate the extent of ferrocene modification on the PPF/Styrene surface through thiol-ene reaction, theoretical surface coverage of Fc was calculated for comparison to the observed surface coverage. Since thiol functional group is attached on the side of a five-carbon ring of ferrocene, the orientation of ferrocene after surface modification is likely to be parallel to the PPF surface. Figure 3.5(a) shows a possible array of surface-bound Fc-thiol schematically,

which assumes that the alkane axis is perpendicular to the surface and the ferrocene axis is parallel to the surface. As the bond distance between Fe and one of the five-carbon rings (abbreviated as Cp) is 1.66 Å,[119,120] the length between two Cp rings is 3.32Å. The top view of the assumed arrangement of Fc-thiol on the surface is illustrated in Figure 3.5(b). Each circle represents a surface-bound Fc and the diameter of each circle equals the length of Fc, 3.32 Å. As shown, there are nine molecules of Fc-thiol closely packed within a square. The length of each side of this square equals (3.32 × 3) Å, since there are three molecules aligned in either sides. Thus, the area of this square is calculated to be $(3.32 \times 3)^2$ $Å^2$, namely 9.92×10^{-15} cm^2. Number of moles of Fc-thiol within the square can

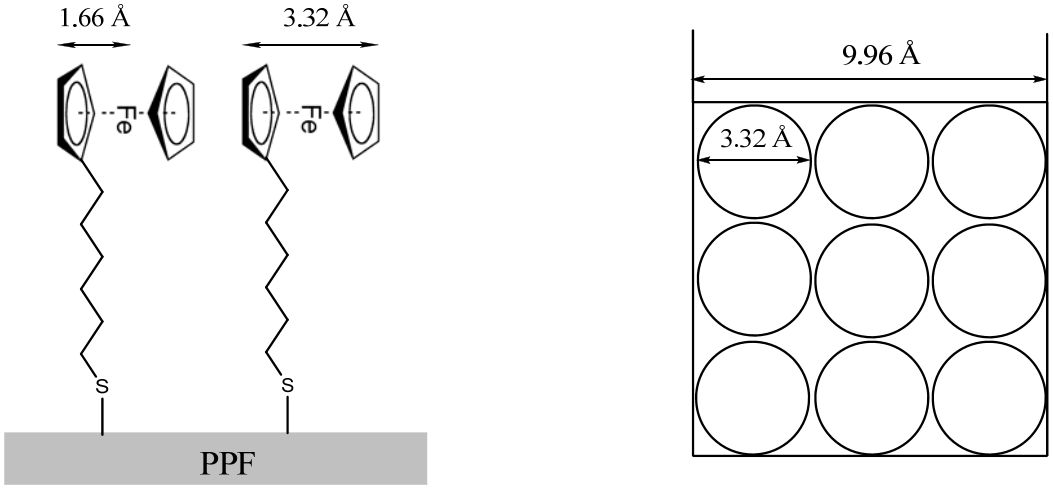

(a) Side view (b) Top view

Figure 3.5 Array of Fc-thiol on PPF surface: (a) side view and (b) top view. Figure (b) also illustrates the model for calculation of theoretical surface coverage of Fc.

be calculated through Equation 3.4, where N_A represents the Avogadro constant, 6.022×10^{23} mol^{-1}. The number of moles is calculated to be 1.49×10^{-23} through

$$\text{Number of moles} = \frac{\text{number of molecule}}{N_A} = \frac{9}{6.022 \times 10^{23}\ mol^{-1}} = 1.49 \times 10^{-23}\ mol$$

(Equation 3.4)

dividing nine by the Avogadro constant. Then, the theoretical surface coverage is calculated through dividing the number of moles by the surface area, which turns out to be 1.51×10^{-9} mol/cm^2 as shown in Equation 3.5.

$$\text{Theoretical surface coverage} = \frac{\text{number of moles}}{\text{surface area}} = \frac{1.49 \times 10^{-23}\ mol}{9.92 \times 10^{-15}\ cm^2} = 1.51 \times 10^{-9}\ mol/cm^2$$

(Equation 3.5)

The arrangement of Fc-thiol on the surface assumed in the current work is only one of the possibilities for calculating the theoretical surface coverage, as Fc axis is not necessarily parallel to the surface and the alkane axis may not be perpendicular to the surface. Nevertheless, this arrangement at least provides a way for estimating the possible maximum surface coverage for a Fc-modified surface.

The observed surface coverage of Fc is about half of that of the theoretical value for PPF/Styrene_4 min/Fc and less than half for PPF/Fc. The reason for the partial surface coverage could be attributed to three factors. First of all, not all the

styrene molecules were available to react with Fc-thiol. For styrene molecules standing perpendicular to the surface, they were readily to react with Fc-thiol; but for those askew arrayed on the surface, they had less possibility to react with Fc-thiol. Secondly, the Fc-thiol layer cannot compactly packed on top of the styrene layer as shown in Figure 3.5, in that the styrene layer grows on the PPF surface disorderly and randomly and the attachment of Fc-thiol highly depends on the orientation of the styrene molecules. Thirdly, Fc might rotate in its plane and in such a case, once a molecule of Fc-thiol had been attached on the surface, it could inhibit the attachment of another molecule next to it by occupying the space where another molecule should be attached.

3.3 Conclusion

In this work, ferrocene-thiol has been successfully modified on both styrene-modified PPF surfaces and bare PPF through thiol-ene reaction induced by UV light. Since ferrocene is an electroactive species, quantitative surface coverage of Fc bonded on the surfaces was calculated based on the total charge of either the anodic or cathodic peaks in the cyclic voltammogram of surface-bound Fc. As ferrocene absorbs UV light at the wavelength of 254 nm and thiol-ene reaction was carried out at the same wavelength, UV light available for thiol-ene reactions was attenuated by absorption of Fc-thiol. And since the thickness (i.e.

the path length) of Fc-thiol solution applied on the surfaces differs from sample to sample, the UV absorption of ferrocene varies from sample to sample. As a consequence, the observed surface coverage of Fc-modified PPF surfaces varies from sample to sample. In addition, it was found out that maximum surface coverage could be achieved through utilizing 1 mM Fc-thiol for thiol-ene reaction. Longer UV exposure time, including 60 min and 90 min, was used for thiol-ene reactions in order to compensate for the problem of UV absorption by Fc-thiol; however, longer exposure time did not increase the surface coverage as compared with 30 min exposure time.

The quantitative surface coverage based on the amount of surface-bound Fc for PPF/Styrene_4 min/Fc and PPF/Fc surfaces are close to each other. However, the catechol test revealed that PPF/Fc surface has a higher catechol activity than PPF/Styrene_4 min/Fc, indicating that there are more pinholes existing on the PPF/Fc surface, which leads to a lower surface coverage. Therefore, styrene layer is a requisite for high surface coverage, more closely packed and pinhole-free surfaces. Theoretical surface coverage of Fc was calculated in order to estimate the possible maximum surface coverage and to evaluate the extent of surface-bound Fc for both PPF/Styrene_4 min/Fc and PPF/Fc surfaces. It was found that PPF/Styrene_4 min/Fc and PPF/Fc surfaces were only partially covered with Fc instead of a full coverage.

Chapter 4. Molecular Electronic Junctions

In the realm of molecular electronics, molecular monolayers or multilayers, which are incorporated between two conducting materials, have significant effects on the electronic behaviors of molecular junctions. Molecular layers serve as the electron transfer mediators and electronic behaviors of molecular junctions can vary over a wide range when different molecular structures and conformations are involved. Modifications of molecular structure in molecular junctions should presumably have a large effect on junction conductance, thus permitting design of devices with a wide range of electronic behaviors. By incorporating molecules with specific functional groups, such as π-conjugated compounds,[86,121] redox species[122,123] and conducting polymers,[124,125] molecular junctions with diverse electronic characteristics have been demonstrated. In addition, a major research subject in the field of molecular electronics is to investigate electron transfer mechanisms of various molecular junctions.

In the current study, two kinds of molecular junctions, one with and one without a redox species in the molecular layer, were fabricated and their electronic behaviors were investigated. Ferrocene was chosen as the redox species because its energy level is close to the Fermi level of metals and therefore, distinctive electronic properties of ferrocene junctions are expected. Moreover,

the electron transfer mechanisms for these two kinds of molecular junctions were investigated using energy level diagrams.

4.1 Experimental

4.1.1 Preparation of PPF Stripes

The procedure for preparation of PPF stripes was mostly the same as that for preparation of PPFs depicted in Chapter 2, but with an added photolithography step. After cleaning, spin-coating and soft-baking, PPF samples were left in the air for couple of minutes to cool to room temperature. The samples were then covered with a photomask composed of four stripes each with a width of 0.5 mm and exposed to a 500 W Mercury lamp (Oriel Corporation) for 120s. Afterwards, the samples were soaked in a solution containing a photoresist developer AZ400K (AZ Electronic Materials) in ultrapure water with the ratio of 1:3 (v/v). Photoresist which had been exposed to UV light was removed by the photoresist developer and that covered with four opaque stripes remained. After copious rinsing with ultrapure water, a pattern consisting of four stripes each with the width of 0.5 mm was obtained. The patterned photoresist samples were transferred into a tube furnace fitted with a quartz tube. With a continuous flow of forming gas (95% N_2 + 5% H_2), PPF stripes were pyrolyzed at 1000℃ for 1 h and

allowed to cool to room temperature. The final result was four parallel pyrolyzed photoresist films (PPFs) each of which was 0.5 mm × 25 mm, and ~ 2 μm thick.

4.1.2 Surface Modification

The patterned PPF samples were modified with styrene through reduction of *in situ* generated diazonium salts and with ferrocene-thiol on bare PPF or on top of the styrene layer through thiol-ene reaction. The procedures for all the surface modification were exactly the same as that described in Chapters 2 and 3.

4.1.3 Electron Beam Evaporation

After being modified with molecular layers, PPF samples were transferred into an electron-beam (e-beam) evaporator (Lesker PVD75) for the purpose of depositing metals on top of the molecular layers. The samples were firstly mounted on a sample holder, then covered with a shadow mask consisting of two 0.2 mm wide lines aligned perpendicular to the PPF stripes and finally placed in the vacuum chamber with the molecule-modified surfaces facing the metal target. After the vacuum chamber was pumped down to ~ 2×10^{-6} torr, a tungsten filament inside the electron beam gun was heated and when the filament was hot enough, it begun to emit electrons. These continuously generated electrons then formed an electron beam, which was directed magnetically to a metal target to

cause evaporation of the metal. With continuous evaporation, a thin layer of metal could be deposited on top of the molecule-modified PPF surfaces. Herein, Cu was firstly deposited on the PPF surfaces with a thickness of 30 nm and then a layer of 15 nm Au was deposited on top of the Cu layer. The deposition rate for both Cu and Au layers was maintained at 1Å/s. After metal deposition, "crossbar" molecular junctions consisting of bottom electrodes (PPFs), molecular layers and top contacts [Cu (30 nm)/Au (15 nm)] were acquired, as shown schematically in Figure 4.1.

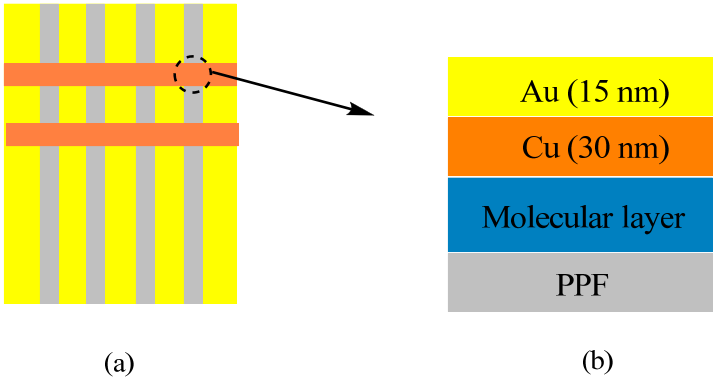

Figure 4.1 Schematic illustration of eight "crossbar" molecular junctions on a PPF sample: (a) top view and (b) side view of one junction.

4.1.4 Characterization of Electronic Behavior of Molecular Junctions

Electronic properties of molecular junctions were characterized using a "4-wire" configuration apparatus, in which ohmic losses for both PPF and Au leads were corrected. As illustrated in Figure 4.2, four probes were applied on PPF and Au leads, with +drive and +sense probes on the PPF lead and -drive and -sense probes on the Au lead. The current/voltage response of molecular junctions was measured based on the bias between V^{+}_{drive} and V^{-}_{drive}. V^{+}_{sense} and V^{-}_{sense} were

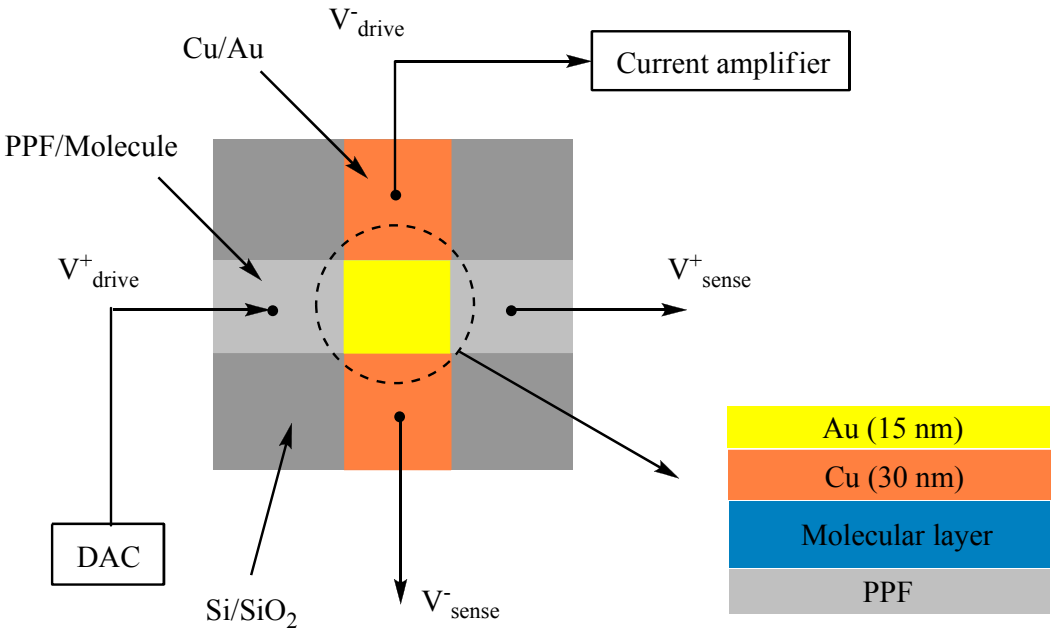

Figure 4.2 Schematic of measurements of electronic properties of PPF/Molecule/Cu/Au junctions with a "4-wire" configuration. Bias is supplied by DAC and current/voltage response is measured based on electron flow between V^{+}_{drive} and V^{-}_{drive}. Ohmic losses for the PPF lead and the metal lead are corrected by V^{+}_{sense} and V^{-}_{sense} respectively. The corrected applied voltage is $V^{+}_{sense} - V^{-}_{sense}$.

used to compensate for ohmic losses in the PPF and the Au lead respectively. In this study, all the voltages are stated as PPF relative to Au. For instance, when a positive bias is applied, the PPF lead serves as the positive electrode and as a result, the electron flows from the Au electrode through the molecular layers to the PPF electrode.

4.2 Results and Discussion

4.2.1 Electronic Properties of PPF/Styrene/Cu/Au Junctions

PPF/Styrene/Cu/Au is a notation used here to describe a molecular junction which is obtained through modifying PPF stripes with styrene and then depositing metal contacts on top of the styrene-modified surfaces. The styrene layers were modified on PPF stripes through CPE at -500 mV for 4 min and 8 min, which are notated as Styrene_4 min and Styrene_8 min respectively. Figure 4.3 shows J-V curves of both PPF/Styrene_4 min/Cu/Au and PPF/Styrene_8 min/Cu/Au molecular junctions. J is the current density, which is obtained through dividing currents by the area of the junction, 0.09 mm^2, and V is the applied bias. The J-V curve of a control junction, where the bottom contact and the top contact are connected up without a "bridging" molecular layer between them, is also shown in Figure 4.3(A). A short circuit was observed for the control junction. The J-V responses of eight molecular junctions on one PPF sample show variation for the

PPF/Styrene_4 min/Cu/Au junctions, and this variation is more significant for the PPF/Styrene_8 min/Cu/Au junction. The variability of J-V curves is possibly caused by the variation of metal penetration from junction to junction. And the reason why J-V curves of PPF/Styrene_8 min/Cu/Au junctions are more variable might be attributed to a more variable packing density of the styrene layer in the PPF/Styrene_8 min/Cu/Au junctions. In addition, it is possible that the longer electrolysis time resulted in parasitic or cross-linking reactions which increased the disorder of the film. Continued generation of phenyl radicals by reduction of diazonium ions through the styrene layer might cause partial degradation of the molecular layer, leading to greater variability in the final devices.

In order to determine if PPF/Styrene_4 min/Cu/Au and PPF/Styrene_8 min/Cu/Au junctions are statistically different from each other, low-voltage resistance (R_{low}) was determined for each junction and Student's t-test was applied for the two sets of data. R_{low} was calculated by taking the reciprocal of the slope of a current-voltage curve ranging from +0.1 to -0.1V. Table 4.1 lists all the observed R_{low} values for both PPF/Styrene_4 min/Cu/Au and PPF/Styrene_8 min/Cu/Au junctions. And through calculation from Student's t-test, it was found that there is no statistical difference between these two types of junctions at 99.9% confidence level.

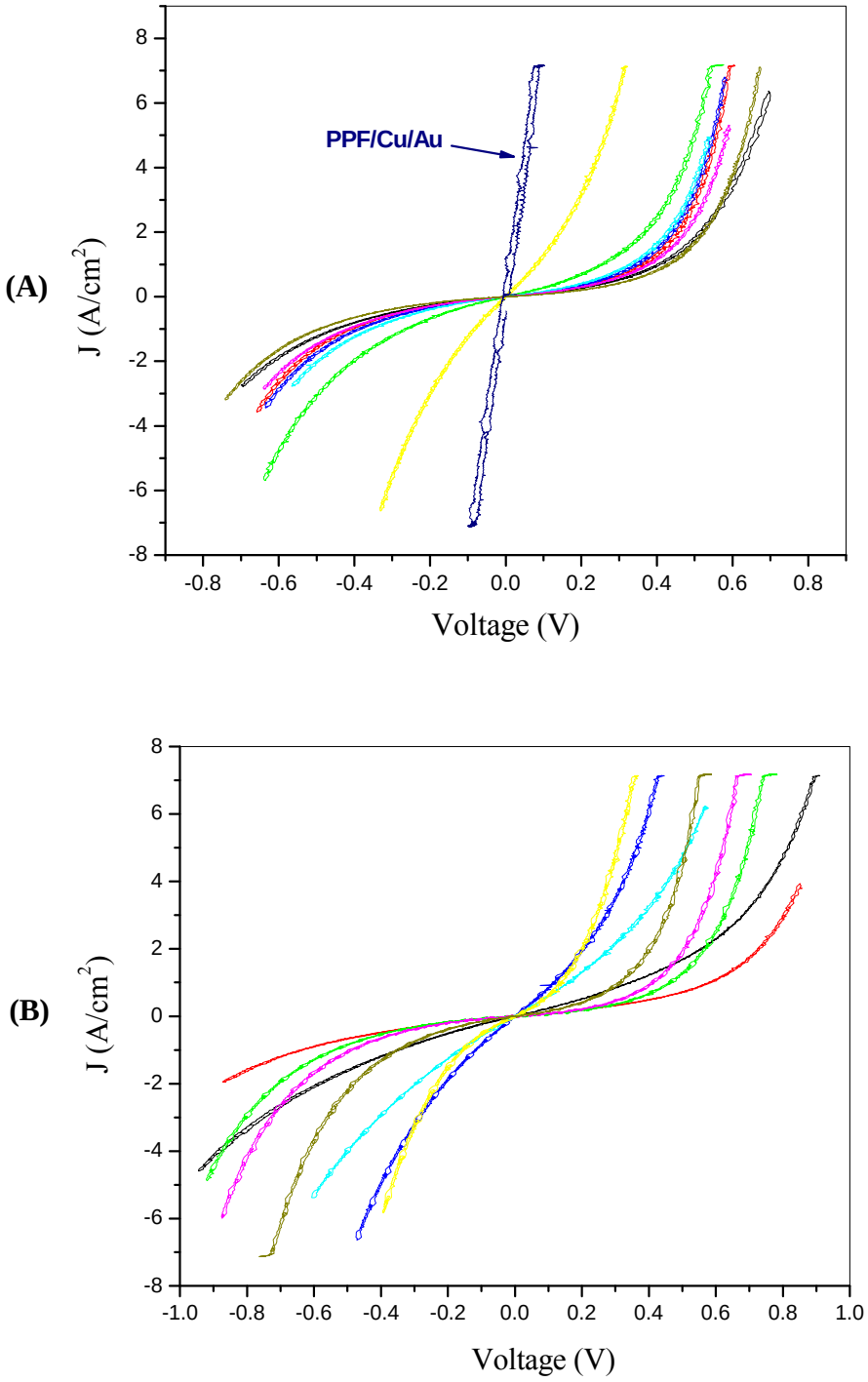

Figure 4.3 J-V curves of (A) PPF/Styrene_4 min/Cu/Au junctions and (B) PPF/Styrene_8 min/Cu/Au junctions. The J-V curve of a control junction is also shown in the top panel (pointed by an arrow). Sweep rate = 1000 mV/s.

Table 4.1 Low-voltage resistance (R_{low}) of PPF/Styrene_4 min/Cu/Au and PPF/Styrene_8 min/Cu/Au junctions.

	Low-voltage resistance (R_{low}) (ohms)	
	PPF/Styrene_4 min/Cu/Au	PPF/Styrene_8 min/Cu/Au
1	91	135
2	402	190
3	714	204
4	827	481
5	941	746
6	963	1296
7	1043	1316
8	1399	1546
Mean ± Std dev	**787 ± 402**	**739 ± 574**

4.2.2 Electronic Properties of PPF/Styrene/Fc/Cu/Au Junctions

Modification of the molecular layer in PPF/Styrene/Fc/Cu/Au junctions was achieved by attaching a layer of Fc-thiol on top of the styrene layer through the thiol-ene reaction, as described in Chapter 3. Figure 4.4 shows J-V curves for both PPF/Styrene_4 min/Fc/Cu/Au and PPF/Styrene_8 min/Fc/Cu/Au junctions. Figure 4.4A also includes the J-V curve of a PPF/Fc/Cu/Au junction, the molecular layer of which was achieved by modifying Fc-thiol directly on the PPF surface. A short circuit was observed for the junction, indicating that there are so many pinholes on the PPF/Fc surface that metal can penetrate through the molecular layer to form filaments and connect with the bottom contact. This result is highly consistent with the catechol test result, described in Chapter 3. J-V curves of eight junctions on the same PPF sample vary significantly in magnitude, which might be attributed to the variance of metal penetration from junction to junction.

4.2.3 Comparison between Styrene-Only and Styrene/Fc Junctions

Figure 4.5(A) shows an overlay of J-V curves for the PPF/Styrene/Cu/Au junctions and PPF/Styrene/Fc/Cu/Au junctions. Each curve is an average of J-V responses for eight junctions of the same PPF sample. The corresponding ln(J) vs. V curves are shown in Figure 4.5(B). By comparing J-V curves of the PPF/Styrene/Cu/Au junctions with those of the PPF/Styrene/Fc/Cu/Au junctions,

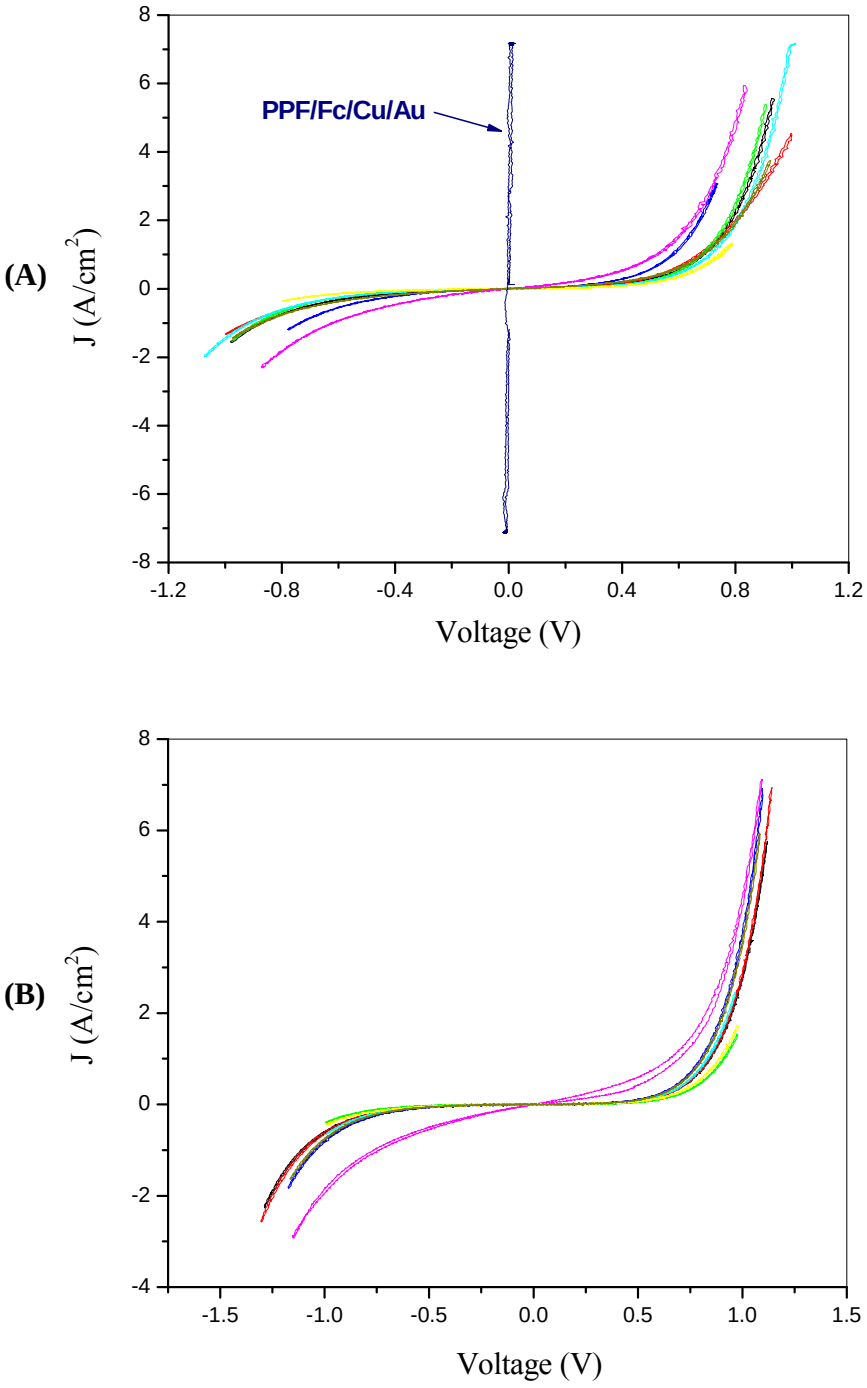

Figure 4.4 J-V curves of (A) PPF/Styrene_4 min/Fc/Cu/Au junctions and (B) PPF/Styrene_8 min/Fc/Cu/Au junctions. The J-V curve of a PPF/Fc/Cu/Au junction is also shown in the top panel. Sweep rate = 1000 mV/s.

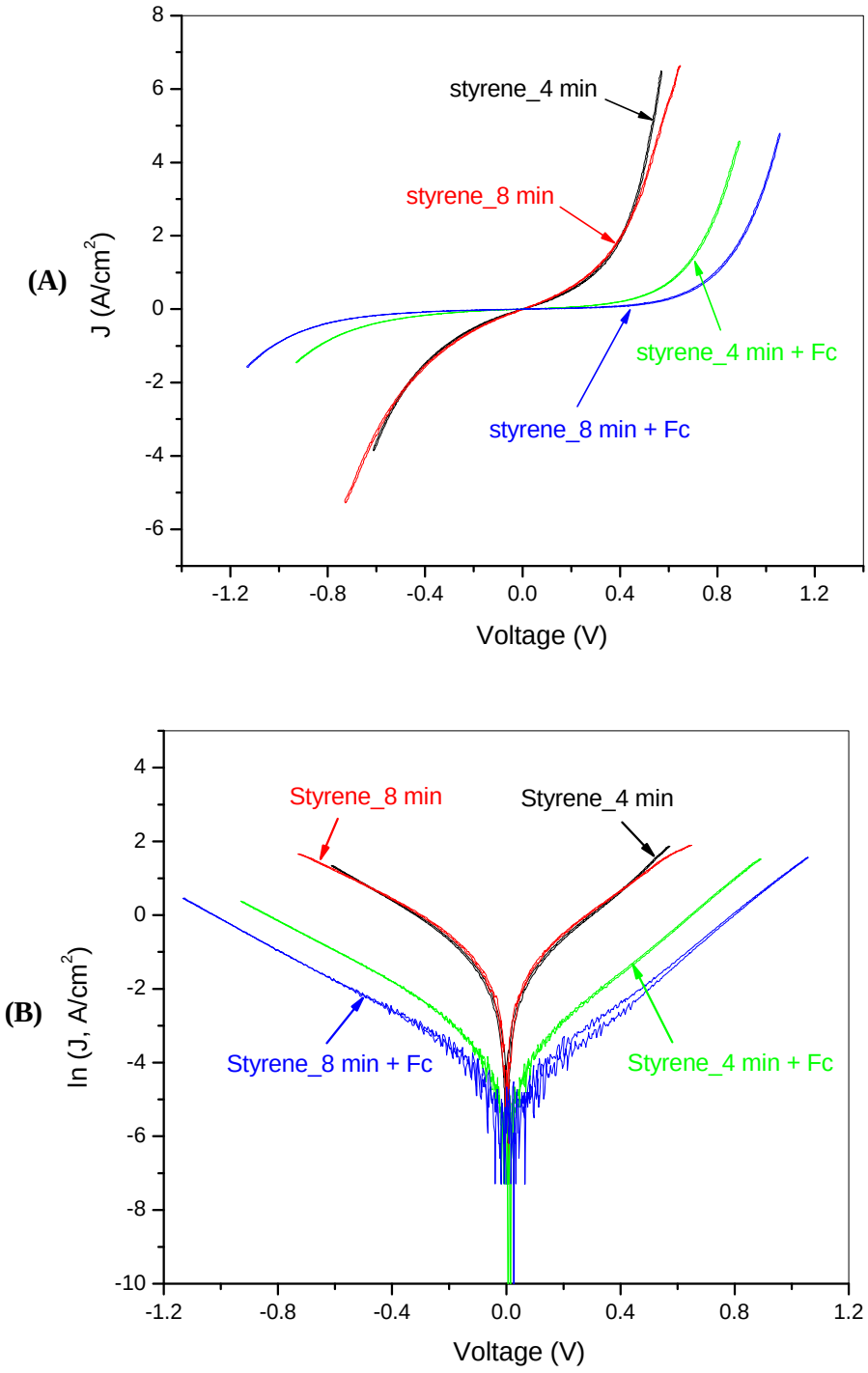

Figure 4.5 (A) Overlay of J-V curves for the PPF/Styrene/Cu/Au junctions and the PPF/Styrene/Fc/Cu/Au junctions and (B) the corresponding ln(J) vs. V curves. Each curve is an average of J-V responses for eight junctions of the same PPF sample.

it is found that curves are basically symmetric for the PPF/Styrene/Cu/Au junctions but asymmetric for the PPF/Styrene/ Fc/Cu/Au junctions. This asymmetry of J-V curves with higher current density at one bias polarity than the other is called rectification.[126] Rectification ratio is obtained by division of |J(+V)| over |J(-V)|. A rectification ratio equal to one indicates a symmetric J-V curve, whereas a higher value of the rectification ratio indicates a larger rectification effect. Rectification ratios should be insensitive to junction area, and may show less variation than the absolute magnitudes of the current densities.

Table 4.2 lists rectification ratios, which are calculated based on the average J-V curves as shown in Figure 4.5(A), for the PPF/Styrene/Cu/Au junctions and the PPF/Styrene/Fc/Cu/Au junctions at different selected voltages. The J-V curves at lower bias (less than 0.4 V) are nearly symmetric for all the junctions and at 0.6 V, a slight rectification effect is observed for both styrene-only junctions and styrene/Fc junctions. However, the styrene/Fc junctions show greater rectification effects at higher bias. The reason why the rectification effects are observed for the styrene/Fc junctions will be discussed in detail in the following section.

Table 4.2 Rectification ratios of the PPF/Styrene/Cu/Au junctions and the PPF/Styrene/Fc/Cu/Au junctions at different selected voltages.

	Rectification Ratio, |J(+V)| / |J(-V)|			
	Styrene_ 4 min	Styrene_8 min	Styrene_4 min + Fc	Styrene_8 min + Fc
± 0.2 V	1.12	1.09	1.07	1.00
± 0.4 V	1.32	1.29	1.31	1.09
± 0.6 V	1.68	1.71	1.95	1.76
± 0.8 V			3.24	2.68
± 1.0 V				3.97

4.2.4 Electron Transfer Mechanism of Molecular Junctions

The electron transfer (ET) mechanisms for both PPF/Styrene/Cu/Au and PPF/Styrene/Fc/Cu/Au molecular junctions are considered here in the context of the experimental results on molecular junctions. The McCreery group has considered many carbon/molecule/metal molecular junctions, and recently proposed a mechanism based on interactions between the contact Fermi levels and the molecular orbitals inside the junction.[127] A similar mechanism should apply to the PPF/Styrene/Cu/Au junction studied here, so the mechanism will be reviewed.

A "resonant" electron transfer model is considered as the mechanism for electron transport in the styrene incorporated molecular junctions. Molecular energy levels (HOMOs and LUMOs) of styrene should be broadened by

intermolecular interactions between neighboring styrene molecules and electronic interactions between the styrene molecules and the contacts (PPF and Cu). Other studies, focusing on the effect of contact-molecule coupling,[128,129] intermolecular interactions[130,131] and disordering of molecular multilayers,[132,133] reported the same phenomenon of broadening of molecular energy levels. As molecular orbital levels are broadened, orbitals with varying energy will be generated and discretely distributed around the center energy level. When a portion of these energy states overlap with the Fermi level of the contacts, they are in resonance with the contacts and consequently, resonant electron transport from one of the contacts through the styrene molecular layer to the other contact can take place.

Figure 4.6 illustrates proposed energy level diagrams for the PPF/Styrene/ Cu/Au junction before and after applying bias. Broadened electronic states are randomly distributed around the center energy levels (-6.7 eV for HOMO and 0.1 eV for LUMO, relative to vacuum). The values of HOMO and LUMO energy levels were calculated through density functional theory utilizing Gaussian software for isolated styrene molecules. The work functions of PPF and Cu contacts as shown in Figure 4.6 were measured with a Kelvin probe.[134] When a positive voltage is applied (Figure 4.6b), the energy level of the positively biased contact, PPF, will be lowered, which allows the electron to transfer from the HOMO energy level of the styrene molecular orbital to the PPF contact. Then, the

HOMO molecular orbital will be refilled by the electron transferred from the negatively biased contact, Cu. When a negative voltage is applied (i.e. PPF is negative), the electron on the HOMO orbital will first transfer to the Cu contact and then the HOMO orbital is refilled by the electron from the PPF contact (Figure 4.6c). Since electron transport undergoes the same mechanism for both polarities, J-V responses of the PPF/Styrene/Cu/Au junctions are nearly symmetric.

For the PPF/Styrene/Fc/Cu/Au junction, the molecular component lying between two contacts consists of three molecular layers: styrene, alkane and ferrocene. Thus, the electron will transmit through the molecular component following a series of steps. Since the electron is liable to transmit through the molecular layers from one contact to the other, but having difficulties to tunnel through in the opposite direction, the phenomenon of rectification is observed.

Figure 4.7 shows proposed energy level diagrams for the PPF/Styrene/ Fc/Cu/Au junction before and after applying voltage. The HOMO and LUMO energy levels for both alkane and ferrocene were obtained from density functional theory of Gaussian software. As illustrated in Figure 4.7(b), after applying a positive voltage (i.e. PPF is positive), the energy level of the PPF contact is lower than the HOMO level of Fc, which allows electron transfer from the HOMO energy level of Fc, tunneling through the alkane layer and the styrene layer

sequentially, to the PPF contact. When a negative bias is applied (Figure 4.7c), the electron will transmit in the reverse direction (from PPF to Cu). An electron will be ejected from the PPF contact and tunnel through the styrene layer, the alkane layer and the Fc layer to the Cu contact. Since the electron needs to tunnel through a thicker molecular layer (three layers) as compared with the reverse transport direction (two layers), the electron transport rate from PPF to Cu is reduced. Therefore, rectification effects, with larger current density at the positive voltage than at the negative voltage, were observed in the PPF/Styrene/Fc/Cu/Au junctions.

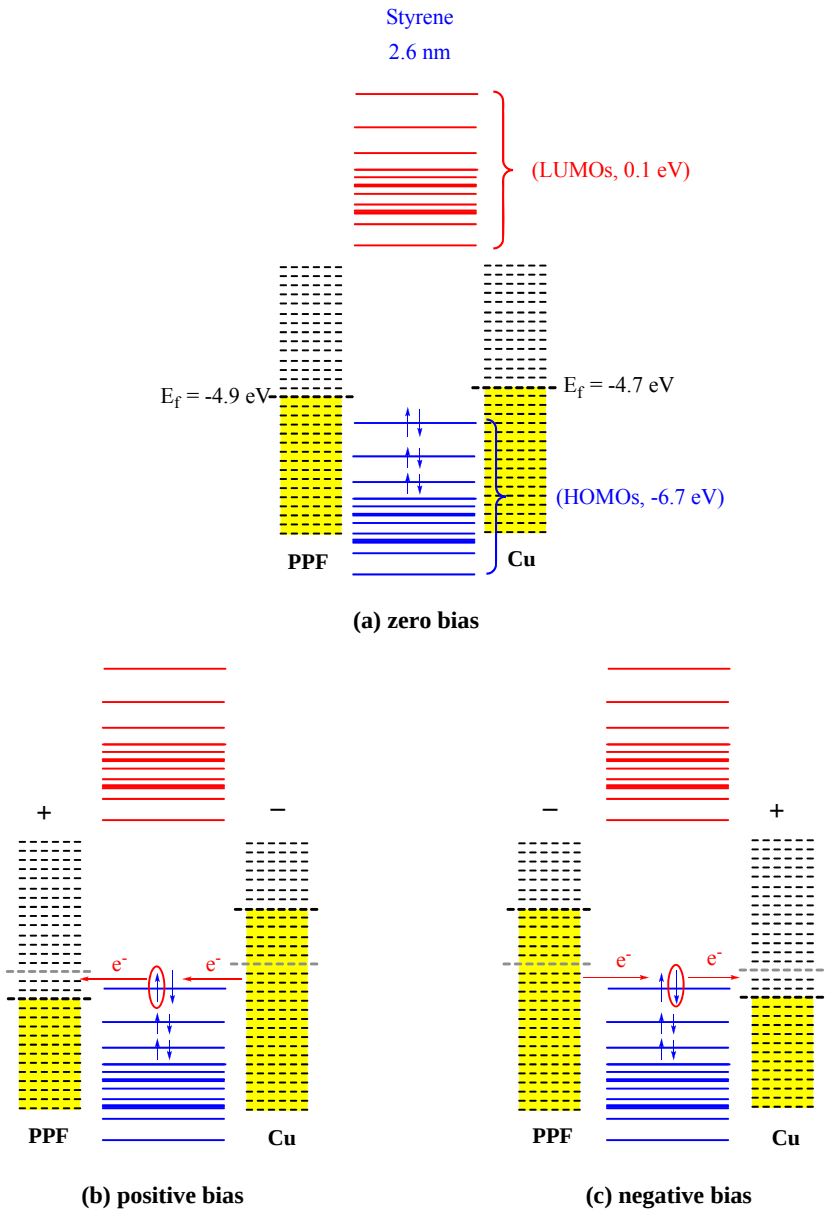

Figure 4.6 Proposed energy level diagrams of the PPF/Styrene/Cu/Au junction (a) before applying bias and (b) after applying positive bias and (c) negative bias. A distribution of broadened electronic states is scattered around the center energy levels (HOMO, -6.7 eV and LUMO, 0.1 eV). The HOMO and LUMO values were calculated through density functional theory using Gaussian software. The work functions of PPF and Cu were measured through a Kelvin probe. E_f represents the Fermi levels of the contacts and the yellow shading in the PPF and Cu contacts indicates the filled electronic states.

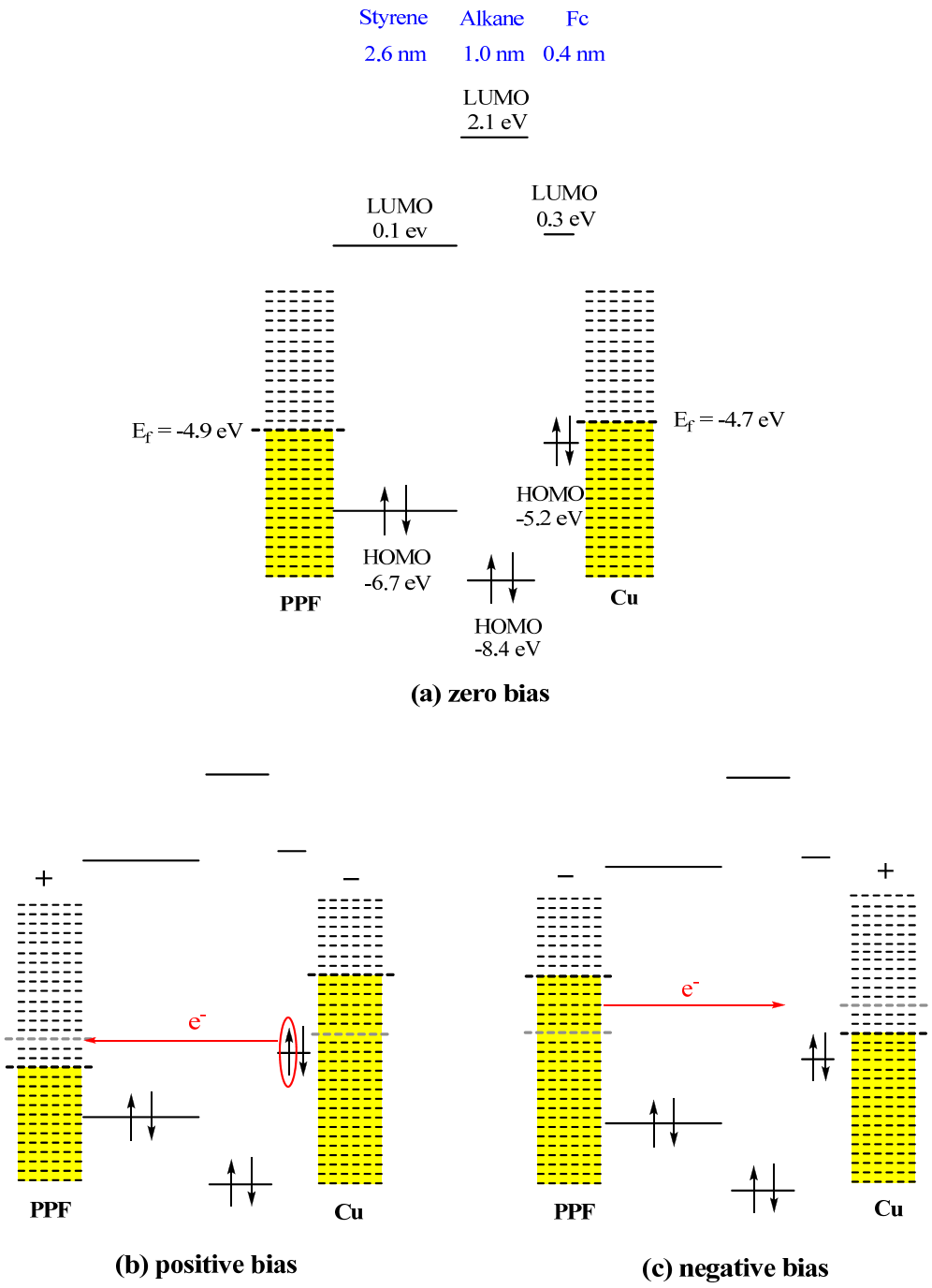

Figure 4.7 Proposed energy level diagrams of the PPF/Styrene/Fc/Cu/Au junction before (a) and after applying positive bias (b) and negative bias (c).

4.3 Conclusion

In this study, “crossbar” molecular electronic junctions have been fabricated by depositing metal top contacts through e-beam evaporation on top of the molecule-modified PPF surfaces. J-V responses of the resulting molecular junctions were measured in a “4-wire” configuration and the electronic behaviors of these junctions were investigated. It was found that J-V curves of different junctions on the same PPF sample show significant variation, which could be attributed to the variance of metal penetration from junction to junction. In addition, symmetric J-V responses were observed for the PPF/Styrene/Cu/Au junctions, while J-V curves of the PPF/Styrene/Fc/Cu/Au junctions were asymmetric. The difference in J-V responses for these two kinds of junctions is ascribed to the different electron transfer processes, which were defined by the proposed energy level diagrams. Similar electron transport mechanisms for both polarities for the PPF/Styrene/Cu/Au junctions result in the symmetric J-V responses. However, for the PPF/Styrene/Fc/Cu/Au junctions, the electron is facile to transfer from one contact to the other but difficult to transmit in the reverse direction and consequently, the rectification effects occur.

Summary

The molecular signature in microelectronic devices has been an active topic of research in the field of molecular electronics. By incorporating molecules with different structures and conformation in electronic devices, a diversity of molecular junctions with intriguing electronic behaviors could be fabricated, at least in principle. In this thesis, modification of molecular layers on PPF surfaces was achieved through two independent steps, which were described in Chapter 2 and Chapter 3 respectively. Molecular junctions involving the molecular layers in electric contact with two conductors were fabricated and the electronic properties of these junctions were studied and investigated in Chapter 4.

Chapter 2 describes the modification of the first molecular layer (styrene) on PPF surfaces utilizing the method of reduction of *in situ* generated diazonium salts. It was shown that the thickness and roughness of the resulting styrene layers increased gradually when more voltammetric scans and longer electrolysis time were applied during surface derivatization. The film growth of the styrene layers undergoes a process that an initial styrene layer formed rapidly on the PPF surface and then it was slowly thickened with increased voltammetric scans and electrolysis times; meanwhile, pinholes on the surface were gradually removed. In addition, this *in situ* method, which is less common than direct reduction of

diazonium salts, has been proved to be as efficient as the direct diazonium ion reduction.

Fc-thiol was covalently attached on top of the styrene layer through the thiol-ene reaction, as shown in Chapter 3. The quantitative surface coverage, which was determined from the amount of surface-bound Fc through electrochemical measurements, was found to vary from sample to sample. The discrepancy in surface coverage is attributed to the variability of UV-Vis absorption of Fc-thiol from sample to sample due to variation of the Fc-thiol solution thickness. By comparing with the theoretical surface coverage, which was calculated based on a closely packed model, the amount of Fc anchored on the PPF surfaces was found to be about half of the theoretical value.

In Chapter 4, two kinds of molecular junctions, PPF/Styrene/Cu/Au and PPF/Styrene/Fc/Cu/Au were constructed and their corresponding electronic properties were investigated. Symmetric J-V curves were observed for the PPF/Styrene/Cu/Au junctions, implying that electron transfer is equally efficient for both bias polarities. However, for the PPF/Styrene/Fc/Cu/Au junctions, larger current densities at positive bias than those at negative bias were observed and these rectification effects are attributed to a more facile electron transfer process from the Cu contact to the PPF contact than the reverse direction.

Bibliography

(1) Gracias, D. H.; Tien, J.; Breen, T. L.; Hsu, C.; Whitesides, G. M. *Science* **2000**, *289*, 1170-1172.

(2) Wong, E. W.; Collier, C. P.; Behloradsky, M.; Raymo, F. M.; Stoddart, J. F.; Heath, J. R. *J. Am. Chem. Soc.* **2000**, *122*, 5831-5840.

(3) Liu, Z.; Yasseri, A. A.; Lindsey, J. S.; Bocian, D. F. *Science* **2003**, *302*, 1543-1545.

(4) Ranganathan, S.; Steidel, I.; Anariba, F.; McCreery, R. L. *Nano Lett.* **2001**, *1*, 491-494.

(5) Ho Choi, S.; Kim, B.; Frisbie, C. D. *Science* **2008**, *320*, 1482-1486.

(6) Kinoshita, K. *Carbon: Electrochemical and Physicochemical Properties*; Wiley: New York, **1988**.

(7) Ranganathan, S.; McCreery, R.; Majji, S. M.; Madou, M. *J Electrochem. Soc.* **2000**, *147*, 277-282.

(8) McCreery, R. L.; Cline, K. K.; McDermott, C. A.; McDermott, M. T. *Colloids Surf., A* **1994**, *93*, 211-219.

(9) Brooksby, P. A.; Downard, A. J. *Langmuir* **2005**, *21*, 1672-1675.

(10) Ssenyange, S.; Anariba, F.; Bocian, D. F.; McCreery, R. L. *Langmuir* **2005**, *21*, 11105-11112.

(11) Ranganathan, S.; McCreery, R. L. *Anal. Chem.* **2001**, *73*, 893-900.

(12) McCreery, R. L. *Chem. Rev.* **2008**, *108*, 2646-2687.

(13) Barbier, B.; Pinson, J.; Desarmot, G.; Sanchez, M. *J. Electrochem. Soc.* **1990**, *137*, 1757-1764.

(14) Delamar, M.; Hitmi, R.; Pinson, J.; Saveant, J. M. *J. Am. Chem. Soc.* **1992**, *114*, 5883-5884.

(15) Vila, N.; Brussel, M. V.; D'Amours, M.; Marwan, J.; Buess-Herman, C.; Belanger, D. *J. Electroanal. Chem.* **2007**, *609*, 85-93.

(16) Corgier, B. P.; Marquette, C. A.; Blum, L. J. *J. Am. Chem. Soc.* **2005**, *127*, 18328-18332.

(17) Toupin, M.; Belanger, D. *Langmuir* **2008**, *24*, 1910-1917.

(18) Toupin, M.; Belanger, D. *J. Phys. Chem. C* **2007**, *111*, 5394-5401.

(19) Baranton, S.; Belanger, D. *J. Phys. Chem. B* **2005**, *109*, 24401-24410.

(20) Baranton, S.; Belanger, D. *Electrochim. Acta* **2008**, *53*, 6961-6967.

(21) Kullapere, M.; Seinberg, J.-M.; Maeorg, U.; Maia, G.; Schiffrin, D. J.; Tammeveski, K. *Electrochim. Acta* **2009**, *54*, 1961-1969.

(22) Pinson, J.; Podvorica, F. *Chem. Soc. Rev.* **2005**, *34*, 369-460.

(23) Allongue, P.; Delamar, M.; Desbat, B.; Fagebaume, O.; Hitmi, R.; Pinson, J.; Saveant, J.-M. *J. Am. Chem. Soc.* **1997**, *119*, 201-207.

(24) Brooksby, P. A.; Downard, A. J. *J. Phys. Chem. B* **2005**, *109*, 8791-8798.

(25) Downard, A. J. *Langmuir* **2000**, *16*, 9680-9682.

(26) Anariba, F.; DuVall, S. H.; McCreery, R. L. *Anal. Chem.* **2003**, *75*, 3837-3844.

(27) Harnisch, J. A.; Gazda, D. B.; Anderegg, J. W.; Porter, M. D. *Anal. Chem.* **2001**, *73*, 3954-3959.

(28) Lyskawa, J.; Belanger, D. *Chem. Mater.* **2006**, *18*, 4755-4763.

(29) Chamoulaud, G.; Belanger, D. *J. Phys. Chem. C* **2007**, *111*, 7501-7507.

(30) Bahr, J. L.; Tour, J. M. *Chem. Mater.* **2001**, *13*, 3823-3824.

(31) Deinhammer, R. S.; Ho, M.; Anderegg, J. W.; Porter, M. D. *Langmuir* **1994**, *10*, 1306-1313.

(32) Gallardo, I.; Pinson, J.; Vila, N. *J. Phys. Chem. B* **2006**, *110*, 19521-19529.

(33) Cruickshank, A. C.; Tan, E. S. Q.; Brooksby, P. A.; Downard, A. J. *Electrochem. Commun.* **2007**, *9*, 1456-1462.

(34) Adenier, A.; Chehimi, M. M.; Gallardo, I.; Pinson, J.; Vila, N. *Langmuir* **2004**, *20*, 8243-8253.

(35) Kraeutler, B.; Jaeger, C. D.; Bard, A. J. *J. Am. Chem. Soc.* **1978**, *100*, 4903-4905.

(36) Vassiliev, Y. B.; Grinberg, V. A. *J. Electroanal. Chem.* **1991**, *308*, 1-16.

(37) Vijh, A. K.; Conway, B. E. *Chem. Rev.* **1967**, *67*, 623-664.

(38) Brooksby, P. A.; Downard, A. J.; Yu, S. S. C. *Langmuir* **2005**, *21*, 11304-11311.

(39) Cicero, R. L.; Linford, M. R.; Chidsey, C. E. D. *Langmuir* **2000**, *16*, 5688-5695.

(40) Sun, Q.-Y.; de Smet, L. C. P. M.; van Lagen, B.; Giesbers, M.; Thune, P. C.; van Engelenburg, J.; de Wolf, F. A.; Zuilhof, H.; Sudholter, E. J. R. *J. Am. Chem. Soc.* **2005**, *127*, 2514-2523.

(41) Buriak, J. M. *Chem. Rev.* **2002**, *102*, 1271-1308.

(42) Lasseter, T. L.; Clare, B. H.; Abbott, N. L.; Hamers, R. J. *J. Am. Chem. Soc.* **2004**, *126*, 10220-10221.

(43) Nichols, B. M.; Butler, J. E.; Russell, J. N.; Hamers, R. J. *J. Phys. Chem. B* **2005**, *109*, 20938-20947.

(44) Tse, K.-Y.; Nichols, B. M.; Yang, W.; Butler, J. E.; Russell, J. N.; Hamers, R. J. *J. Phys. Chem. B* **2005**, *109*, 8523-8532.

(45) Yang, W.; Auciello, O.; Butler, J. E.; Cai, W.; Carlisle, J. A.; Gerbi, J. E.; Gruen, D. M.; Knickerbocker, T.; Lasseter, T. L.; Russell, J. N.; Smith, L. M.; Hamers, R. J. *Nat. Mater.* **2002**, *1*, 253-257.

(46) Yu, S. S. C.; Downard, A. J. *Langmuir* **2007**, *23*, 4662-4668.

(47) Knickerbocker, T.; Strother, T.; Schwartz, M. P.; Russell, J. N., Jr.; Butler, J.; Smith, L. M.; Hamers, R. J. *Langmuir* **2003**, *19*, 1938-1942.

(48) Sánchez-González, J.; Ruiz-García, J.; Gálvez-Ruiz, M. J. *J. Colloid Interface Sci.* **2003**, *267*, 286-293.

(49) Dronov, R.; Kurth, D. G.; Mohwald, H.; Spricigo, R.; Leimkuhler, S.; Wollenberger, U.; Rajagopalan, K. V.; Scheller, F. W.; Lisdat, F. *J. Am. Chem. Soc.* **2008**, *130*, 1122-1123.

(50) Yokoyama, S.; Goto, H.; Miyamoto, T.; Ikeda, N.; Shibahara, K. *Appl. Surf. Sci.* **1997**, *112*, 75-81.

(51) Yoshimura, T.; Tatsuura, S.; Sotoyama, W. *Appl. Phys. Lett.* **1991**, *59*, 482-484.

(52) Bitzer, T.; Richardson, N. V. *Appl. Phys. Lett.* **1997**, *71*, 1890-1892.

(53) Du, Y.; George, S. M. *J. Phys. Chem. C* **2007**, *111*, 8509-8517.

(54) Dameron, A. A.; Seghete, D.; Burton, B. B.; Davidson, S. D.; Cavanagh, A. S.; Bertrand, J. A.; George, S. M. *Chem. Mater.* **2008**, *20*, 3315-3326.

(55) Zhang, X.; Chen, H.; Zhang, H. *Chem. Commun.* **2007**, *14*, 1395-1405.

(56) Iler, R. K. *J. Colloid Interface Sci.* **1966**, *21*, 569-594.

(57) Stockton, W. B.; Rubner, M. F. *Macromolecules* **1997**, *30*, 2717-2725.

(58) Wang, L.; Wang, Z.; Zhang, X.; Shen, J.; Chi, L.; Fuchs, H. *Macromol. Rapid Commun.* **1997**, *18*, 509-514.

(59) Jiao, J.; Anariba, F.; Tiznado, H.; Schmidt, I.; Lindsey, J. S.; Zaera, F.; Bocian, D. F. *J. Am. Chem. Soc.* **2006**, *128*, 6965-6974.

(60) Kohli, P.; Blanchard, G. J. *Langmuir* **2000**, *16*, 4655-4661.

(61) Katz, H. E.; Scheller, G.; Putvinski, T. M.; Schilling, M. L.; Wilson, W. L.; Chidsey, C. E. D. *Science* **1991**, *254*, 1485-1487.

(62) Altman, M.; Shukla, A. D.; Zubkov, T.; Evmenenko, G.; Dutta, P.; van der Boom, M. E. *J. Am. Chem. Soc.* **2006**, *128*, 7374-7382.

(63) Kim, A.; Filler, M. A.; Kim, S.; Bent, S. F. *J. Am. Chem. Soc.* **2005**, *127*, 6123-6132.

(64) Walling, C.; Helmreich, W. *J. Am. Chem. Soc.* **1959**, *81*, 1144-1148.

(65) Chiou, B.-S.; English, R. J.; Khan, S. A. *Macromolecules* **1996**, *29*, 5368-5374.

(66) Cramer, N. B.; Reddy, S. K.; Cole, M.; Hoyle, C.; Bowman, C. N. *J. Polym. Sci., Part A: Polym. Chem.* **2004**, *42*, 5817-5826.

(67) Hoyle, C., E; Lee, T. Y.; Roper, T. *J. Polym. Sci., Part A: Polym. Chem.* **2004**, *42*, 5301-5338.

(68) Cramer, N. B.; Reddy, S. K.; O'Brien, A. K.; Bowman, C. N. *Macromolecules* **2003**, *36*, 7964-7969.

(69) Morgan, C. R.; Magnotta, F.; Ketley, A. D. *J Polymer Sci. Polymer Chem. Ed.* **1977**, *15*, 627-645.

(70) Okay, O.; Bowman, C., N *Macromol. Theory and Simul.* **2005**, *14*, 267-277.

(71) Samuelsson, J.; Mats, J.; Tore, B.; Mats, J. *J. Polym. Sci., Part A: Polym. Chem.* **2004**, *42*, 6346-6352.

(72) Roper, T. M.; Guymon, C. A.; Jonsson, E. S.; Hoyle, C. E. *J. Polym. Sci., Part A: Polym. Chem.* **2004**, *42*, 6283-6298.

(73) Cramer, N. B.; Scott, J. P.; Bowman, C. N. *Macromolecules* **2002**, *35*, 5361-5365.

(74) Khire, V. S.; Harant, A. W.; Watkins, A. W.; Anseth, K. S.; Bowman, C. N. *Macromolecules* **2006**, *39*, 5081-5086.

(75) Cramer, N. B.; Bowman, C. N. *J. Polym. Sci., Part A: Polym. Chem.* **2001**, *39*, 3311-3319.

(76) Chiou, B.-S.; Khan, S. A. *Macromolecules* **1997**, *30*, 7322-7328.

(77) Reddy, S. K.; Sebra, R. P.; Anseth, K. S.; Bowman, C. N. *J. Polym. Sci., Part A: Polym. Chem.* **2005**, *43*, 2134-2144.

(78) Hagberg, E. C.; Malkoch, M.; Ling, Y.; Hawker, C. J.; Carter, K. R. *Nano Lett.* **2007**, *7*, 233-237.

(79) Besson, E.; Gue, A.-M.; Sudor, J.; Korri-Youssoufi, H.; Jaffrezic, N.; Tardy, J. *Langmuir* **2006**, *22*, 8346-8352.

(80) Sangermano, M.; Bongiovanni, R.; Malucelli, G.; Priola, A.; Harden, A.; Rehnberg, N. *J. Polym. Sci., Part A: Polym. Chem.* **2002**, *40*, 2583-2590.

(81) Reddy, S. K.; Cramer, N. B.; Cross, T.; Raj, R.; Bowman, C. N. *Chem. Mater.* **2003**, *15*, 4257-4261.

(82) Davis, W. B.; Svec, W. A.; Ratner, M. A.; Wasielewski, M. R. *Nature* **1998**, *396*, 60-63.

(83) Helms, A.; Heiler, D.; McLendon, G. *J. Am. Chem. Soc.* **2002**, *114*, 6227-6238.

(84) Krider, E. S.; Meade, T. J. *J. Biol. Inorg. Chem.* **1998**, *3*, 222-225.

(85) Aviram, A.; Ratner, M. A. *Chem. Phys. Lett.* **1974**, *29*, 277-283.

(86) McCreery, R. L. *Chem. Mater.* **2004**, *16*, 4477-4496.

(87) Anariba, F.; Steach, J. K.; McCreery, R. L. *J. Phys. Chem. B* **2005**, *109*, 11163-11172.

(88) Nuzzo, R. G.; Allara, D. L. *J. Am. Chem. Soc.* **1983**, *105*, 4481-4483.

(89) Porter, M. D.; Bright, T. B.; Allara, D. L.; Chidsey, C. E. D. *J. Am. Chem. Soc.* **1987**, *109*, 3559-3568.

(90) Love, J. C.; Estroff, L. A.; Kriebel, J. K.; Nuzzo, R. G.; Whitesides, G. M. *Chem. Rev.* **2005**, *105*, 1103-1170.

(91) Metzger, R. M. *Chem. Rev.* **2003**, *103*, 3803-3834.

(92) Pease, A. R.; Jeppesen, J. O.; Stoddart, J. F.; Luo, Y.; Collier, C. P.; Heath, J. R. *Acc. Chem. Res.* **2001**, *34*, 433-444.

(93) Balakumar, A.; Lysenko, A. B.; Carcel, C.; Malinovskii, V. L.; Gryko, D. T.; Schweikart, K.-H.; Loewe, R. S.; Yasseri, A. A.; Liu, Z.; Bocian, D. F.; Lindsey, J. S. *J. Org. Chem.* **2004**, *69*, 1435-1443.

(94) Hurley, P. T.; Ribbe, A. E.; Buriak, J. M. *J. Am. Chem. Soc.* **2003**, *125*, 11334-11339.

(95) Liu, Y.-C.; McCreery, R. L. *J. Am. Chem. Soc.* **1995**, *117*, 11254-11259.

(96) McCreery, R. L.; Bergren, A. J. *Adv. Mater.* **2009**, *21*, 4303-4322.

(97) Lamb, D. R. *Electrical Conduction Mechanisms in Thin Insulating Films*; Methuen and Co.: London, **1968**.

(98) Simmons, J. G. *DC Conduction in Thin Films*; Mills and Boon Ltd.: London, **1971**.

(99) Segal, D.; Nitzan, A.; Davis, W. B.; Wasielewski, M. R.; Ratner, M. A. *J. Phys. Chem. B* **2000**, *104*, 3817-3829.

(100) Newton, M. D. *Theor. Chem. Acc.* **2003**, *110*, 307-321.

(101) Skourtis, S. S.; Archontis, G.; Xie, Q. *J. Chem. Phys.* **2001**, *115*, 9444-9462.

(102) Abu-Hilu, M.; Peskin, U. *Chem. Phys.* **2004**, *296*, 231-241.

(103) Selzer, Y.; Cabassi, M. A.; Mayer, T. S.; Allara, D. L. *J. Am. Chem. Soc.* **2004**, *126*, 4052-4053.

(104) McCreery, R. L.; Wu, J.; Kalakodimi, R. P. *Phys. Chem. Chem. Phys.* **2006**, *8*, 2572-2590.

(105) Murphy, C. J.; Arkin, M. R.; Jenkins, Y.; Ghatlia, N. D.; Bossmann, S. H.; Turro, N. J.; Barton, J. K. *Science* **1993**, *262*, 1025-1029.

(106) Cullis, P. M.; McClymont, J. D.; Symons, M. C. R. *J. Chem. Soc., Faraday Trans.* **1990**, *86*, 591-592.

(107) Thomas, J. M.; Jon, F. K. *Angew. Chem. Int. Ed.* **1995**, *34*, 352-354.

(108) Mujica, V.; Ratner, M. A. *Chem. Phys.* **2001**, *264*, 365-370.

(109) Segal, D.; Nitzan, A.; Ratner, M.; Davis, W. B. *J. Phys. Chem. B* **2000**, *104*, 2790-2793.

(110) Bixon, M.; Jortner, J. *J. Am. Chem. Soc.* **2001**, *123*, 12556-12567.

(111) Renger, T.; Marcus, R. A. *J. Phys. Chem. A* **2003**, *107*, 8404-8419.

(112) Li, X.-Q.; Zhang, H.; Yan, Y. *J. Phys. Chem. A* **2001**, *105*, 9563-9567.

(113) Terrill, R. H.; Murray, R. W. Electron Hopping Transport in Electrochemically Active, Molecular Mixed Valent Materials. In *Molecular Electronics*; Jortner, J., Ratner, M., Eds.; Blackwell Science Ltd.: Oxford, U.K., **1997**; pp. 215-239.

(114) Cline, K. K.; Baxter, L.; Lockwood, D.; Saylor, R.; Stalzer, A. *J. Electroanal. Chem.* **2009**, *633*, 283-290.

(115) Breton, T.; Belanger, D. *Langmuir* **2008**, *24*, 8711-8718.

(116) Bard, A. J.; Faulkner, L. R. *Electrochemical Methods,* 2nd ed.; Wiley: New York, **2001**.

(117) DuVall, S. H.; McCreery, R. L. *Anal. Chem.* **1999**, *71*, 4594-4602.

(118) DuVall, S. H.; McCreery, R. L. *J. Am. Chem. Soc.* **2000**, *122*, 6759-6764.

(119) Haaland, A.; Nilsson, J. E. *Acta Chem. Scand.* **1968**, *22*, 2653-2670.

(120) Elihn, K.; Larsson, K. *Thin Solid Films* **2004**, *458*, 325-329.

(121) Nitzan, A.; Ratner, M. A. *Science* **2003**, *300*, 1384-1389.

(122) Kitagawa, K.; Morita, T.; Kimura, S. *Langmuir* **2005**, *21*, 10624-10631.

(123) Kitagawa, K.; Morita, T.; Kimura, S. *J. Phys. Chem. B* **2005**, *109*, 13906-13911.

(124) Wang, Y. Z.; Epstein, A. J. *Acc. Chem. Res.* **1999**, *32*, 217-224.

(125) Epstein, A. J.; Lee, W. P.; Prigodin, V. N. *Synth. Met.* **2001**, *117*, 9-13.

(126) Nijhuis, C. A.; Reus, W. F.; Whitesides, G. M. *J. Am. Chem. Soc.* **2009**, *131*, 17814-17827.

(127) Bergren, A. J.; Jimenez-Sandoval, S. J.; McCreery, R. L.; Stoyanov, S. R.; Gusarov, S.; Kovalenko, A. *Submitted paper "Molecular Energy Level Broadening in Ensemble Molecular Electronic Junctions: Resonant Charge Transport".*

(128) Moth-Poulsen, K.; Bjornholm, T. *Nat. Nanotechnol.* **2009**, *4*, 551-556.

(129) Vondrak, T.; Cramer, C. J.; Zhu, X.-Y. *J. Phys. Chem. B* **1999**, *103*, 8915-8919.

(130) Landau, A.; Nitzan, A.; Kronik, L. *J. Phys. Chem. A* **2009**, *113*, 7451-7460.

(131) Wu, S.; Gonzalez, M. T.; Huber, R.; Grunder, S.; Mayor, M.; Schonenberger, C.; Calame, M. *Nat. Nanotechnol.* **2008**, *3*, 569-574.

(132) Haming, M.; Ziroff, J.; Salomon, E.; Seitz, O.; Cahen, D.; Kahn, A.; Scholl, A.; Reinert, F.; Umbach, E. *Phys. Rev. B* **2009**, *79*, 155418.

(133) Yu, L. H.; Gergel-Hackett, N.; Zangmeister, C. D.; Hacker, C. A.; Richter, C. A.; Kushmerick, J. G. *J. Phys.: Condens. Matter* **2008**, *20*, 374114.

(134) Yan, H.; McCreery, R. L. *ACS Appl. Mater. Interfaces* **2009**, *1*, 443-451.